Engineering of Oncolytic Adenoviruses for Intratumoral Delivery of Novel T-Cell Engagers for Dual-Antigen-Targeting

Martin Alexander Boos

2025

Inaugural dissertation

for

obtaining the doctoral degree

of the

Combined Faculty of Mathematics, Engineering and Natural Sciences

of the

Ruprecht - Karls - University

Heidelberg

Presented by

M.Sc. Martin Alexander Boos

born in: Würzburg

Oral examination: 31.03.25

Engineering of Oncolytic Adenoviruses for Intratumoral Delivery of Novel T-Cell Engagers for Dual-Antigen-Targeting

Referees: Prof. Dr. Martin Müller

PD. Dr. Dirk M. Nettelbeck

Table of Contents

List of Abbreviations

%	percent
°C	degrees Celsius
Ad	Adenovirus
ADC	antibody-drug conjugate
ADCC	antibody-dependent cell-mediated cytotoxicity
ADP	adenovirus death protein
ALL	acute lymphoblastic leukemia
approx.	approximately
BCMA	B-cell maturation antigen
BiTE	bispecific T-cell engager
bp	base pair
BsAb	bispecific antibody
CAG	CMV early enhancer/chicken β actin
CAR	chimeric antigen receptor
CAR	coxsackie/adenovirus receptor
CDR	complementarity determining region
c-MET	cellular mesenchymal epithelial transition factor
CMV	cytomegalovirus
CPE	cytopathic effect
CRC	colorectal cancer
CRS	cytokine release syndrome
DAMP	damage-associated molecular pattern
DAPI	4′,6-diamidino-2-phenylindole
DMSO	dimethyl sulfoxide
DNA	desoxyribonucleic acid
DPBS	dulbecco's phophate based saline
dpi	days post infection
e.g.	example given
E1-E4	early transcription region 1-4
EC50	half maximal effective concentration
EGFR	epidermal growth factor receptor
ELISA	enzyme-linked immunosorbent assay
EpCAM	epithelial cell adhesion molecule
Fab	antigen binding fragment
FR-a	folate receptor alpha
g	gravitational constant
GBM	glioblastoma
GFP	green fluorescent protein
GPRC5D	G protein-coupled receptor calls C group-5 member-D
h	hours
HAMA	human anti-mouse antibody
HER2	human EGFR2
HGFR	hepatocyte growth factor receptor
HMWS	high molecular weight species
HNSCC	head and neck squamous cell carcinoma
hPGK	human phosphoglycerate kinase
HPLC	high performance liquid chromatography
HSV	herpes simplex virus
hTERT	human telomerase reverse transcriptase
i.e.	id est
ICD	immunogenic cell death
ICI	immune checkpoint inhibitor
IFNγ	interferon gamma
Ig	Immunoglobulin
IL13Rα2	Interleukin-13 receptor subunit alpha-2
IL-2	interleukine 2
IMAC	immobilized metal ion affinity chromatography
IRES	internal ribosome entry site
ITR	inverted terminal repeat
kb	kilobase pair
l	liter
L1-L5	late transcription region 1-5
LITR	left inverted terminal repeat
LU	light unit
mAb	monoclonal antibody
mCMV	minimal CMV
MFI	mean fluorescent intensity
mg	milligram

FACS	fluorescence-activated cell sorting	**MHC**	major histocompatibility complex
FAP	fibroblast associated protein	**min**	minutes
Fc	crystallizable fragment	**ml**	milliliter
FCS	fetal calf serum	**MLP**	major late promoter
MM	multiple myeloma	**SEC**	size-exclusion chromatography
mM	millimolar	**S-phase**	synthesis phase
MOI	multiplicity of infection	**TAA**	tumor-associated antigen
mol	mole	**TBE**	Tris/Borate/EDTA
ng	nanogram	**TCE**	T-cell engager
NKCE	NK-cell engager	**TCID50**	tissue culture infectious dose 50
nM	nanomolar	**TCR**	T-cell receptor
NSCLC	non-small cell lung cancer	**TE**	Tris/EDTA
oAd	oncolytic Adenovirus	**TGF-β**	transforming growth factor beta
OV	oncolytic virus	**TIL**	tumor inflitrating lymphocyte
P/S	penicillin / streptomycin	**TKI**	tyrosine kinase inhibitor
PAMP	pathogen-associated molecular pattern	**TME**	tumor microenvironment
PBS	phosphate based saline	**TNBC**	triple negative breast cancer
PCR	polymerase chain reaction	**Treg**	regulatory T-cell
PFA	paraformaldehyde	**TSA**	tumor-specific antigen
pM	picomolar	**v/v**	volume to volume
pRb	retinoblastoma protein	**VEGF**	vascular endothelial growth factor
rel.	relative	**VH**	heavy chain
RGD	Arginylglycylaspartic acid	**VHH**	heavy-chain-only antibody
RITR	right inverted terminal repeat	**VL**	light chain
RSV	Rous sarcoma virus	**VP**	viral particle
RT	room temperature	**w/v**	weight to volume
RTK	receptor tyrosine kinase	**wt**	wild type
SA	splice acceptor	**Δ24**	Delta-24, describing mutation of 24 base pairs in the CR2 region of the E1A gene
scDb	single-chain Diabody	**µg**	microgram
scDb-scFv	single-chain Diabody-single-chain variable fragment	**µl**	microliter
scFv	single-chain variable fragment	**ρ**	density
SDS	sodium dodecyl sulfate	**ψ**	packaging signal
SDS-PAGE	sodium dodecyl sulfate–polyacrylamide gel electrophoresis		

List of Tables

List of Figures

Abstract

The field of immunotherapy has advanced greatly in the past decades and brought forward numerous treatment modalities, including antibody therapy and oncolytic virus (OV) therapy. Different antibody formats have been engineered for more potent anti-tumor effects, such as T-cell engagers (TCEs) that simultaneously bind to tumor-associated antigens (TAAs) and the T-cell receptor, redirecting T-cells to kill cancer cells. Numerous viruses have been explored for OV therapy, including oncolytic Adenoviruses (oAds), the most commonly used OVs in clinical development and an attractive platform for delivery of transgenes to tumors. Tumor heterogeneity, immune evasion and systemic toxicity pose challenges for effective TCE therapy, which could be overcome by local delivery of TCEs targeting multiple antigens via oAds. Here, I generated different TCE formats, bispecific T-cell engagers (BiTEs), bispecific single-chain Diabodies (scDbs) and trispecific scDb single-chain variable fragments (scDb-scFvs) for multitargeting of four TAAs, focusing on the epidermal growth factor receptor (EGFR) and the cellular mesenchymal epithelial transition factor (c-MET). I conducted a first of its kind comparison of scDbs and BiTEs directed at the chosen targets, analyzing binding properties and induction of T-cell mediated cytotoxicity. My results showed equal efficacies of the scDb-cMET and the BiTE-cMET, allowing for the generation of a scDb-cMET-based trispecific scDb-scFv, which was more favorable for genetic delivery by oAds due to its smaller size and fewer repetitive sequences than two distinct TCEs. I could show equal binding and induction of cytotoxicity on single target-positive cells compared to corresponding bispecifics and superior efficacy on double target-positive cells for the scDb-cMET-scFv-EGFR. I therefore produced a panel of oAds expressing one or two TCEs to characterize dual-targeting strategies of EGFR and c-MET. I was able to identify an expression strategy that retained oncolytic activity of oAds while driving expression of functional TCEs. My T-cell activation data revealed secretion of IL-2 and IFNγ and upregulation of CD69 on T-cells in cocultures of oAd-infected tumor cells with PBMCs only when cross-linking TCEs were produced. In addition, tumor cell killing was enhanced by TCEs when PBMCs were present. Ad5/3-CMV-scDb-cMET-scFv-EGFR, encoding the trispecific TCE, exhibited the highest potency regarding T-cell activation and killing throughout all tested cell lines compared to other dual-targeting strategies with bispecific TCEs via co-expression or co-infection approaches. This oAd showed efficacy in both single and double target-positive cell lines, indicating potential in treatment of heterogeneous tumors and reducing the risk of immune evasion of tumor cells. In summary, I generated and showed the efficacy of the novel scDb-cMET-scFv-EGFR and successfully incorporated it into a viro-antibody-therapy approach. Future experiments have to be conducted to elucidate the therapeutic potential of the Ad5/3-CMV-scDb-cMET-scFv-EGFR for different tumor entities *in vivo*.

Zusammenfassung

Das Feld der Immuntherapie hat in den letzten Jahrzehnten große Fortschritte gemacht und zahlreiche Behandlungsmodalitäten hervorgebracht, einschließlich Antikörpertherapie und Therapie mit onkolytischen Viren (OVs). Verschiedene Antikörperformate wurden für effektivere Anti-Tumor-Wirkungen entwickelt, wie zum Beispiel T-cell Engager (TCEs), die gleichzeitig an tumorassoziierte Antigene (TAAs) und den T-Zell-Rezeptor binden und dadurch T-Zellen umleiten, um Krebszellen abzutöten. Zahlreiche Viren wurden für die OV-Therapie erforscht, darunter onkolytische Adenoviren (oAds), die am häufigsten in der klinischen Entwicklung verwendeten OVs und eine attraktive Plattform für die Übertragung von Transgenen in Tumore. Tumorheterogenität, Immunevasion und systemische Toxizität stellen Herausforderungen für eine effektive TCE-Therapie dar, die durch von oAds getriebener lokaler Produktion von TCEs mit unterschiedlichen Spezifitäten, überwunden werden könnten. Hier habe ich verschiedene TCE-Formate generiert: bispezifische T-cell Engager (BiTEs), bispezifische single-chain-Diabodies (scDbs) und trispezifische scDb single-chain-variable-Fragments (scDb-scFvs) für das Multitargeting von vier TAAs, wobei der Fokus auf dem epidermalen Wachstumsfaktor-Rezeptor (EGFR) und dem zellulären mesenchymal-epithelialen Übergangsfaktor (c-MET) lag. Ich führte einen ersten Vergleich von scDbs und BiTEs durch, die auf die ausgewählten Ziele gerichtet waren und analysierte die Bindungseigenschaften und die Induktion der T-Zell-vermittelten Zytotoxizität. Meine Ergebnisse zeigten gleiche Wirksamkeiten des scDb-cMET und des BiTE-cMET, was die Entwicklung eines scDb-cMET-basierten trispezifischen scDb-scFv ermöglichte, welches aufgrund seiner geringeren Größe und weniger repetitiven Sequenzen im Vergleich zu zwei unterschiedlichen TCEs für die genetische Übertragung durch oAds vorteilhafter war. Ich konnte eine gleiche Bindung und Induktion der Zytotoxizität an Einzelziel-positiven Zellen im Vergleich zu korrespondierenden bispezifischen TCEs und eine überlegene Wirksamkeit an Doppelziel-positiven Zellen für den scDb-cMET-scFv-EGFR zeigen. Daher habe ich eine Reihe von oAds produziert, die ein oder zwei TCEs exprimieren, um duale Targeting-Strategien von EGFR und c-MET zu charakterisieren. Ich konnte eine Expressionsstrategie identifizieren, die die onkolytische Aktivität von oAds beibehielt und gleichzeitig die Expression funktioneller TCEs antrieb. Meine T-Zell-Aktivierungsdaten zeigten die Sekretion von IL-2 und IFNγ sowie die Hochregulierung von CD69 auf T-Zellen in Kokulturen von oAd-infizierten Tumorzellen mit PBMCs nur dann, wenn vernetzende TCEs produziert wurden. Zusätzlich wurde die TCE-vermittelte Zytotoxizität verstärkt, wenn PBMCs anwesend waren. Ad5/3-CMV-scDb-cMET-scFv-EGFR, das den trispezifischen TCE kodiert, zeigte die höchste Wirksamkeit hinsichtlich T-Zell-Aktivierung und Abtötung von Tumorzellen in allen getesteten Zelllinien im Vergleich

zu anderen dualen Targeting-Strategien mit bispezifischen TCEs durch Ko-Expressions- oder Ko-Infektionsansätze. Dieses oAd zeigte Wirksamkeit sowohl in Einzel- als auch in Doppelziel-positiven Zelllinien, was auf ein Potenzial in der Behandlung heterogener Tumore und eine Verringerung des Risikos der Immunevasion von Tumorzellen hinweist. Zusammenfassend habe ich den neuartigen scDb-cMET-scFv-EGFR generiert und seine Wirksamkeit gezeigt und ihn erfolgreich in einen Viro-Antikörper-Therapie-Ansatz integriert. Zukünftige Experimente müssen durchgeführt werden, um das Potenzial des Ad5/3-CMV-scDb-cMET-scFv-EGFR für verschiedene Tumorentitäten *in vivo* zu untersuchen.

Acknowledgements

First and foremost, I want to thank Dirk Nettelbeck, without whom this thesis would not have been possible. He supported me even before I started my PhD, helping me secure a fellowship. His committed and agreeable supervision created a pleasant work environment and I worked on my projects gladly and learned a lot.

I also want to thank Guy Ungerechts, who welcomed me in his department. I want to thank Roland Kontermann and Oliver Seifert, who were great collaborators for this project and gave helpful input for my work. I greatly enjoyed my two lab visits in Stuttgart and all of our videoconferences. I want to thank all the lab members of the CCU who helped create a great work environment that I was lucky to enjoy, in addition to always being ready to help with experiments. I would also like to thank Joshua Hesse and Martin Uerlich, who were great interns and helped contribute to some of the work presented in this thesis. I want to thank Martin Müller, who agreed to examine this thesis, gave valuable input during our TAC meetings and has a great ability of choosing his lab members. The Antibody Core Facility headed by Ilse Hofmann was also a great help throughout my thesis and I am very thankful for the great work of the team that contributed to my project.

A special thanks goes to my family and my wife, whom I married during my time as a PhD student, for their constant support. Danke, köszönöm e grazie.

1. Introduction

1.1 Cancer Therapy

In 2020, close to 10 million cancer deaths and approximately 19.3 million new cases were reported worldwide. The cancer burden is estimated to increase to an estimated 28.4 million new cases by 2040.[1] This high number of cancer cases calls for effective treatment options. In the past decades, several breakthroughs have been made with therapies including small molecule inhibitors, peptide drugs and radiation therapy.[2-4] Since chemotherapy is generally unspecific and radiation therapy is usually combined with chemotherapy, there is a need for more targeted treatment strategies.[5, 6]

1.2 Cancer Immunotherapy Approaches

Cancer immunotherapy is a treatment approach that harnesses the immune system to combat cancer, including treatment approaches such as monoclonal antibodies (mAbs), immune checkpoint inhibitors (ICIs), oncolytic viruses (OVs), cancer vaccines, and adoptive cell therapies. It exhibits promising efficacy for various tumors, where conventional therapy has proven ineffective or not durable.[7] Still, cancer immunotherapy has to overcome challenges including homing to and persistence of therapeutics in the tumor, the immunosuppressive tumor microenvironment (TME) and tumor heterogeneity, especially in solid tumors. The challenges constituted by the TME have driven the development of different treatment modalities.[8]

T-cells are most commonly used in cellular immunotherapy approaches, with three major treatment modalities: tumor-infiltrating lymphocyte (TIL) therapy, genetically engineered T-cell receptor T-cell (TCR-T) therapy and chimeric antigen receptor (CAR) T-cell therapy.[9] TIL therapy involves harvesting T-cells from a patient's tumor, expanding them *in vitro* and reinfusing them back into the patient. TIL therapy is especially effective if the TME is already rich in TILs.[10] In TCR-T-cell therapy, T-cells with genetically encoded TCRs targeting specific antigens are expanded.[11] CAR-T cells are equipped with genetically engineered, synthetic receptors that recognize specific antigens independent of major histocompatibility complex (MHC) restriction and possess costimulatory and T-cell activation domains.[12] There are currently six CAR molecules approved for therapy of hematological malignancies, but efficacy in solid tumors has so far been limited.[13, 14] CAR-T cells can be engineered to target more than one antigen, reducing the risk of immune evasion.[15] Here, antibody therapy and OVs will be highlighted.

1.2.1 Antibody Therapy

Antibody therapy allows for a targeted treatment approach, with increasing importance in clinical practice. Nearly 200 antibody therapeutics were under regulatory review or had market approval as of November 2023, mAbs making up the largest part.[16]

1.2.1.1 Monoclonal Antibodies

Monoclonal antibodies are produced from a single clone of B-cells, targeting a specific antigen.[17] Therapeutic applications of mAbs comprise their use for treatment of infectious diseases, autoimmune diseases and cancer.[18] The first murine mAb used in clinical practice was Muromonab (αCD3) in 1986, for the prevention of organ transplant rejection, realized through the hybridoma technology, which allowed for production of mAbs in large amounts.[19, 20] The disadvantage of murine antibodies is the development of human anti-mouse antibodies (HAMAs) that pose a risk of eliciting neurotoxic responses in patients.[21] Methods like phage display and transgenic mice have allowed development of humanized and fully human antibodies, greatly reducing immunogenicity, while retaining their antigen specificity.[17] Chimeric antibodies retain their murine variable regions, while the constant region is exchanged by a human sequence. This modification lowered the immunogenicity of the chimeric antibodies and importantly, the human Fc-region enhanced cell killing via antibody-dependent cell-mediated cytotoxicity (ADCC) and complement activation.[22, 23] Antibodies with humanization of the variable regions, where only the complementarity determining regions (CDRs) are of murine origin, showed an improved immunogenicity profile compared to murine or chimeric counterparts.[24] Transgenic mice and phage display technology drove the development of fully human antibodies, completely eradicating the risk of HAMAs.[25]

Antibody-drug conjugates (ADCs) are novel drugs that take advantage of the specificity of mAbs for a targeted delivery of a potent cytotoxic payload linked to the mAbs. This approach allows the use of highly cytotoxic therapeutics while minimizing damage to healthy tissue. As of 2020, nine ADCs were approved for clinical use by the FDA and more than 80 others were in clinical development. The most commonly used payloads target tubulins or DNA.[26]

ICIs are mAbs that inhibit regulatory mechanisms of immune activation. Under healthy conditions, immune checkpoints limit immune responses, inhibition of these checkpoints can therefore restore T-cell activity in an immunosuppressive TME.[27] ICIs have exhibited strong tumor controlling effects in advanced metastatic and highly immunogenic tumors, including

melanoma and Merkel cell carcinoma, with 11 ICIs having received FDA approval as of 2024, targeting four different immune checkpoint proteins.[28]

1.2.1.2 Recombinant Antibodies

While the treatment strategies described above mainly employ immunoglobulin (Ig) formats, especially IgG, advances in antibody engineering have led to the development of numerous other antibody formats. IgG molecules, schematically shown in Figure 1, consist of two heavy and two light chains, connected by disulfide bonds. The heavy chains form the crystallizable fragment (Fc) part of the antibody, responsible for the effector functions of the IgG, such as ADCC. The antigen binding fragments (Fabs) are made up of the light chains and the fragments of the heavy chains associated with the light chains, forming two heterodimers that form the monospecific, bivalent IgG molecule.[29] The Fabs contain the variable regions with the CDRs.

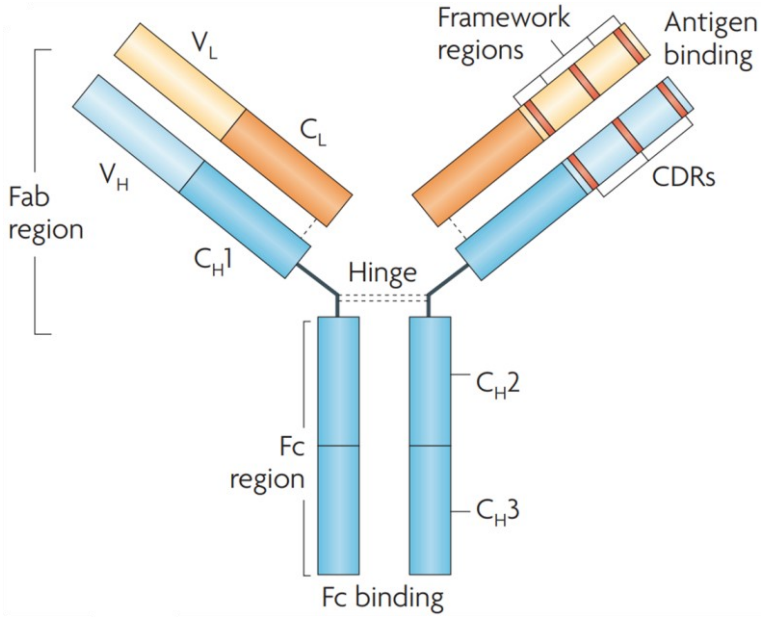

Figure 1 Schematic structure of an IgG antibody. Fab – antigen binding fragment; V_H – variable heavy chain; V_L – variable light chain; C_H – constant heavy chain; C_L – constant light chain; Fc – crystallizable fragment; CDR – complementarity-determining region. Adapted from Hansel et al. 2010.[30]

As only the Fab is involved in antigen binding, the genetic sequences of the variable heavy (V_H) and variable light (V_L) chains can be used to produce single-chain variable fragments (scFvs) without the constant region of the Fabs or the Fc region, retaining antigen affinity.[31] Different approaches have been pursued to create different antibody formats incorporating scFvs.

Bispecific antibodies (BsAbs) have been developed to target two distinct antigens with a single molecule. Different formats of BsAbs have been developed, a selection is shown in Figure 2. The earliest employed formats of BsAbs were chimeric forms of two monospecific IgGs.[32].

Importantly, scFvs have been used to create Fc-less BsAbs. These BsAbs can be used to engage immune cells, as in the case of T-cell engagers (TCEs) or NK-cell engagers (NKCEs).[33, 34]

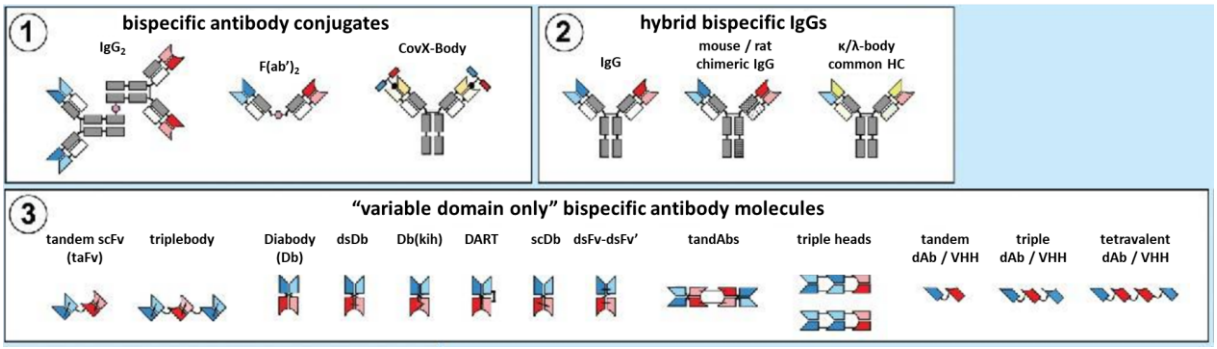

Figure 2 Excerpt of bispecific antibody landscape. Adapted from Brinkmann & Kontermann, 2017.[35]

NKCEs retarget NK-cells to cancer cells by binding activating receptors on NK-cells, most commonly CD16a, and a tumor antigen.[36] In addition to promoting tumor cell killing through direct cytotoxicity, activated NK-cells produce chemokines and cytokines, initiating an immune response involving multiple immune cell types.[33] Compared to TCEs, NKCEs have a shorter research history, but show better safety profiles with lower risk of cytokine release syndrome (CRS) and neurotoxicity. Furthermore, they represent a better treatment option for patients with impaired T-cell function, but have shown overall lower response rates compared to TCEs in some indications.[37]

TCEs cross-link T-cells and cancer cells, typically by binding to CD3 on T-cells and to antigens present on cancer cells. The advantage of TCEs is their ability to retarget T-cells to malignant cells irrespective of their MHC status. Furthermore, induction of T-cell mediated cytotoxicity is possible without costimulation. Simultaneous binding of target cell and T-cell creates a synapse resembling an immunological synapse, importantly resulting in the exclusion of the inhibitory CD45 molecule.[38] After formation of the synapse, cancer cells are killed via release of perforin and granzymes or via bystander mechanisms, more precisely via expression of TNF superfamily ligands on the T cell surface that bind to and crosslink cell surface death receptors on target cells.[39, 40] The distance between T-cell and target cell plays a crucial role for cytotoxicity, more so than antigen density.[41]

Compared to CAR-T cells, TCEs have shown a lower complete response rate in multiple myeloma (MM), but a significantly better safety profile.[42] The first TCE to be approved clinically was Blinatumomab, a bispecific T-cell engager (BiTE®) targeting CD3 and CD19 for the treatment of acute lymphoblastic leukemia (ALL). It is a tandem-scFv consisting of two scFvs covalently linked by a short linker peptide.[43] Although BiTEs have shown promise in

various immunotherapy applications, they face important limitations. The small size leads to rapid systemic clearance, therefore therapies often require continuous infusions.[44] Several adverse effects are also associated with BiTE therapy, including on-target, off-tumor toxicity when targeting TAAs, CRS and neurotoxicity.[45, 46] Furthermore, BiTEs have shown only limited efficacy in the treatment of solid tumors due to the complex TME, higher efficacies have been reported for hematological malignancies.[44]

Different formats of bispecific TCEs have been engineered, the BiTE being the most prominent in ongoing clinical trials.[36]. A novel BsAb format that has been employed as a TCE, the single-chain Diabody (scDb), is structurally very similar to the tandem-scFv, as schematically depicted in Figure 3. It consists of the same V_H and V_L fragments as the tandem-scFv, the difference lies within the linking of the different domains. While tandem-scFvs follow a structure of $V_{H/L}A$-$V_{L/H}A$-$V_{H/L}B$-$V_{L/H}B$ (scFv-scFv), scDbs are structured as $V_{H/L}A$-$V_{L/H}B$-$V_{H/L}B$-$V_{L/H}A$. This difference in linking makes the scDb more rigid and stable than the tandem-scFv, the performance in antigen binding remains identical.[47] A novel trivalent antibody format was generated using the scDb format and fusing an additional scFv to the antigen binding scFv. The described scDb-scFv molecule is a trivalent, bispecific antibody and showed superior binding, T-cell activation and target cell killing compared to the bivalent scDb.[48]

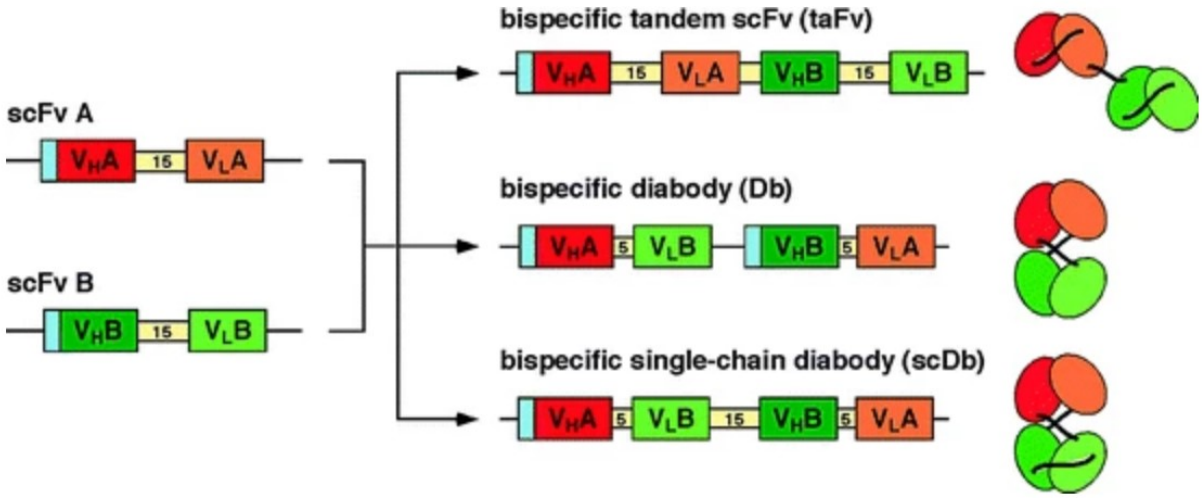

Figure 3 Formation of tandem-scFv, Diabody and scDb from two scFvs. Adapted from Müller et al.2011.[49]

1.2.2 Oncolytic Viruses

OVs are viruses that preferentially infect, replicate and spread through tumor cells, which is facilitated by intrinsic properties of malignant cells.[50] The general mechanism of OV therapy is outlined in Figure 4.

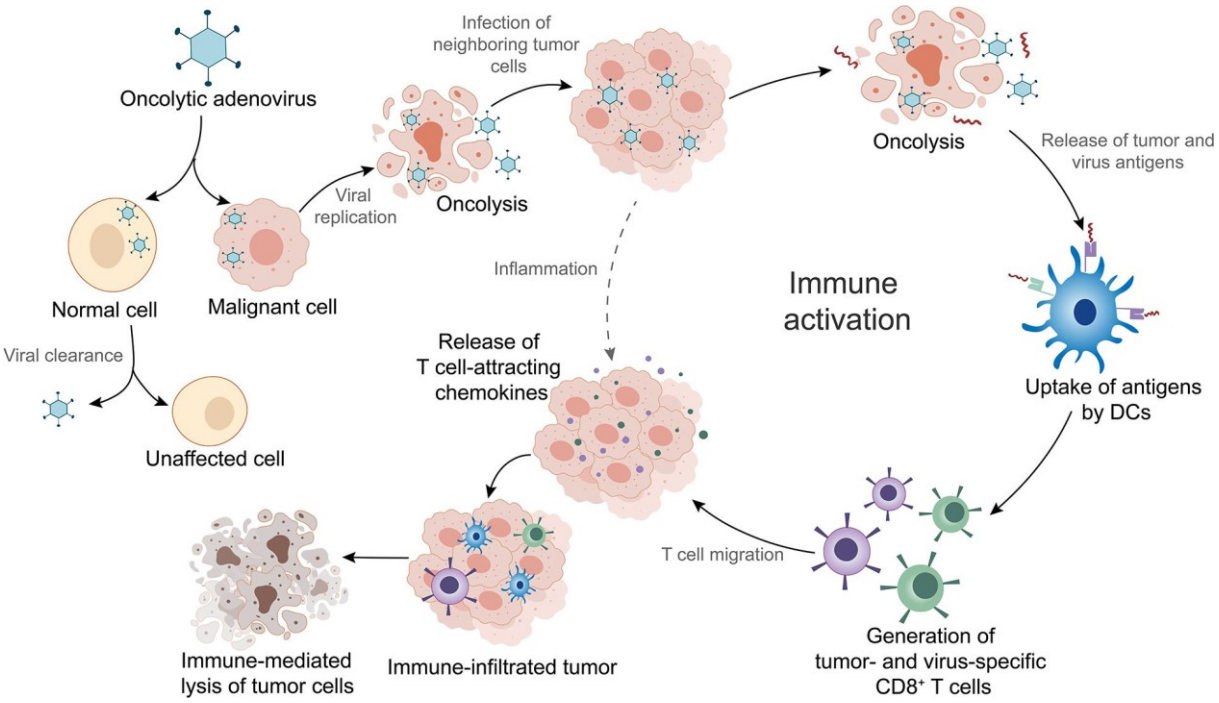

Figure 4 Mechanism of oncolytic adenoviruses in cancer immunotherapy. Adapted from Zhao et al. 2021.[51]

For certain viruses, deregulation of pathways that convey antiviral protection under healthy conditions confer their selectivity. Tumor cells proliferate more rapidly and possess a more active metabolism compared to healthy cells. Furthermore, the type I interferon response to viral infection is oftentimes dysfunctional in malignant cells.[52] Other viruses are genetically engineered to restrict their replication to tumor cells, putting genes under control of tumor-specific promoters or enhancers, as described for oAds and herpes simplex virus (HSV).[53] Alternatively, tumor surface markers can be exploited as entry receptors or essential cofactors for viral gene expression by engineered OVs.[54]

The spread of OVs to surrounding cells depends on multiple factors. Expression of cell surface receptors that mediate viral entry, the type of virus and the form of cell death undergone by the infected cells are important factors.[55] Lysis of tumor cells by OVs is inherently immunogenic, showing characteristics of immunogenic cell death (ICD). Upon cell lysis, pathogen-associated molecular patterns (PAMPs) and damage-associated molecular patterns (DAMPs) are released, as well as tumor-associated antigens (TAAs). The molecules attract immune cells and cytotoxic $CD8^+$ T-cells are activated following TAA peptide presentation by dendritic cells.[56, 57]

A first OV, T-VEC, an HSV, has been approved for treatment of advanced melanoma in the US and EU in 2015. Three others (H101, an adenovirus (Ad), ECHO-7, an echovirus, Teserpaturev, a herpes virus) have been approved in other countries.[58, 59] As of June 2023, 31 different OV products were being used in clinical trials. Clinical trials have shown that virotherapy is well

tolerated, but the efficacy is often not yet sufficient.[60] The outcomes of these clinical trials highlight the need for more potent OVs or OV-based therapies.

1.3 Adenoviruses

The most abundantly represented OV in clinical trials are oncolytic adenoviruses (oAds), making up over 40% in 2022, serotype 5 being the most frequently used.[61, 62] To date, 116 human Ads have been identified.[63]

The properties of Ads make them particularly suitable as OVs. Wild type Ads exhibit low pathogenicity for immunocompetent humans, are stable and easy to produce at high titers. Furthermore, adenoviral gene functions are well described, thus facilitating genomic modifications.[64] Especially the possibility of modifying oAds at multiple levels, e.g. tropism-modifications, tumor cell-restricted replication and expression of therapeutic genes, makes oAds an attractive candidate for cancer treatment, as described in the following.[65]

1.3.1 Adenovirus Structure and Genome

Ads are non-enveloped icosahedral viruses with a double-stranded DNA genome, schematically shown in Figure 5.[66] They are about 65-90 nm in size and possess a complex structural organization. The non-segmented genome can be categorized into early, intermediate and late regions.[67] Structural and non-structural proteins involved in capsid formation, DNA encapsidation and maturation of virions are encoded by the late region.[68] The main structural capsid protein is the hexon, lining the faces and edges of the capsids. The other major components, the penton bases and fibers, are found on the vertices. Minor components associated with the capsid are pIIIa, VI, VIII and IX.[69] The core is made up of the DNA and the core proteins, which are involved in DNA replication and condensation, as well as cleavage of precursor proteins.[68]

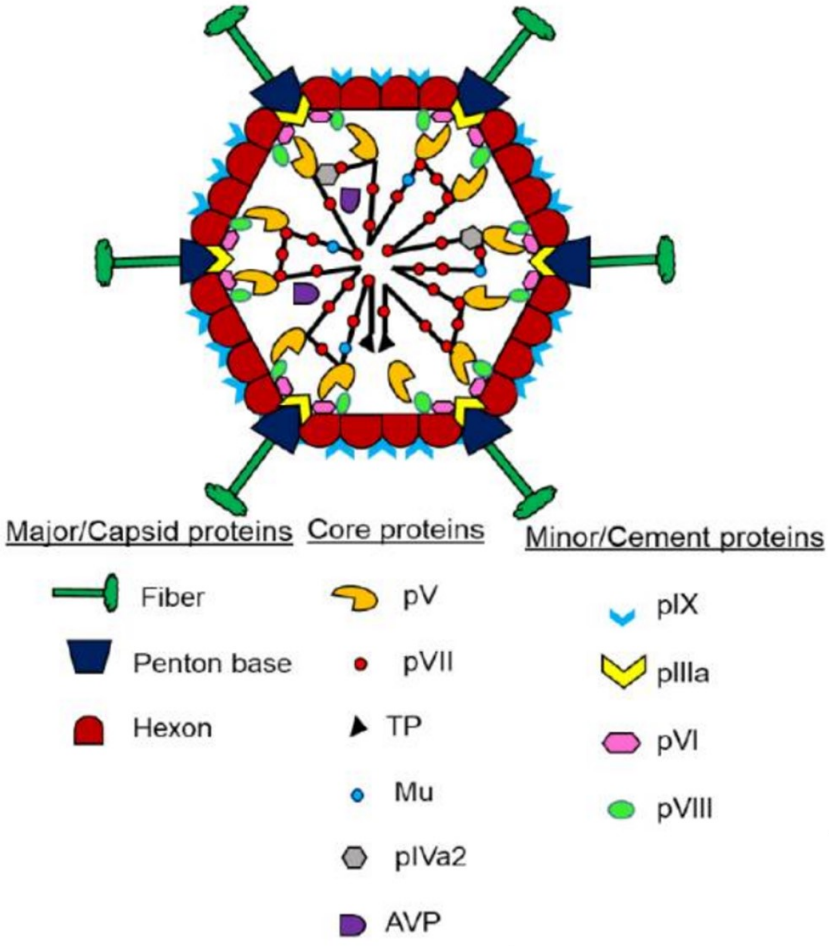

Figure 5 Schematic depiction of Adenovirus structure. AVP-adenovirus protease; TP-terminal protease; p-protein. Adapted from Kulanayake & Tikoo, 2021.[68]

The adenovirus serotype 5 (Ad5) genome is a linear, double-stranded DNA genome with a size of approximately 36 kb. A schematic depiction of the Ad5 genome is shown in Figure 6. It is organized into early (E1, E2, E3, and E4) and late (L1, L2, L3, L4, and L5) transcriptional regions. Inverted terminal repeats (ITRs) make up the ends of the genome, the packaging signal (ψ) is located at the left end.[70]

1.3.2 Replication Cycle

The infectious cycle of Ads starts with host cell entry, mediated by high-affinity binding to cell surface receptors via the fiber knob.[71] The main entry receptor for Ad5 is the coxsackie/adenovirus receptor (CAR).[72] Following the interaction of the fiber knob with the CAR, clathrin-mediated endocytosis is driven by interaction of the penton base with integrins.[73] The virus-encoded protease then disrupts the capsid and the genome is passaged into the nucleus.[74] Transcription starts with the E1 genes E1A and E1B. E1A proteins interfere with various cell cycle and apoptosis regulators, pushing infected cells into the synthesis phase (S-phase) and subduing the transcription of host cell genes in favor of viral

genes while promoting apoptosis.[75] E1B proteins then counteract the proapoptotic effects of E1A activation by inhibition of p53-mediated apoptosis and mimicking the function of Bcl-2 to inhibit the pro-apoptotic Bak and Bax proteins.[76] E1 gene products transactivate E2 genes which in turn convey viral DNA replication and transcription.[77] The E3-genes are dispensable for replication.[66] The E3 protein gp19k downregulates expression of MHCI molecules, promoting immune evasion of Ads.[78] Another E3 protein, the adenovirus death protein (ADP) promotes the release of viral particles via cell lysis, but is only present in one species of human Ads.[79] Products of the E4 region are involved mainly in shutting down protein production of the host cells, replication of viral DNA, expression of late proteins and prevention of concatenation of viral genomes.[80, 81] Transcription of the late genes L1-L5 is driven by the major late promoter (MLP), which shows low activity in the early infection phase and is fully activated following viral DNA replication.[82] The proteins encoded by the late genes are mainly structural proteins of the viral capsid and encapsidation of the viral DNA is triggered by the packaging signal located at the left end of the genome.[83] After successful assembly, viral particles are released into the cytoplasm following permeabilization of the nuclear membrane. Finally, the plasma membrane disintegrates, releasing the viral progeny to spread to neighboring cells.[66, 79]

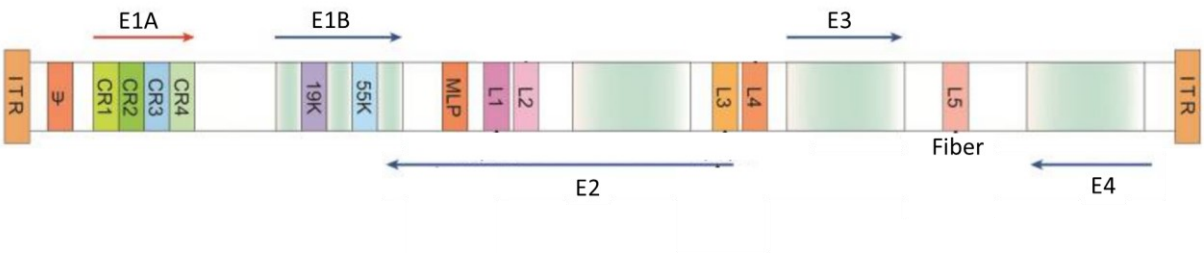

Figure 6 Schematic depiction of the wild-type Ad5 genome structure. ITR - inverted terminal repeat; ψ - packaging element; E - early transcription element; CR - conserved region; 19K - 19 kDa protein; 55K - 55 kDa protein; MLP - major late promoter; L - late transcription element. Adapted from Bulcha et al., 2021.

1.3.3 Modifying Adenoviruses for Oncolytic Virotherapy

Virions have a tight constraint on the genome size that can stably be packaged inside of them. Viruses with genomes exceeding 105% of the wild-type (wt) size show very poor replication and fast genome rearrangement resulting in loss of excessive genes.[84] This limitation only allows stable insertion of about 1.8 kilobases (kb) into otherwise intact Ad5 genomes. Therefore, deletions of non-essential regions in the Ad5 genome are necessary for insertion of larger inserts. As mentioned in 1.3.2, the E3 region encodes for proteins involved in immune evasion, but the genes are not essential for viral replication.[66] This finding has led to the E3-region being deleted completely or partially in most armed oAds.[85]

While oAds inherently exhibit a good safety profile, a stringent tumor specific replication is highly desirable. Tumor specificity can be achieved through modifications on numerous levels. The E1A region encodes proteins essential for viral replication, it is therefore an attractive target for modulation of viral replication. Replacing the E1A promoter with a cancer specific promoter, e.g. the survivin or human telomerase reverse transcriptase (hTERT) promoter, represents an effective strategy.[86, 87] Modification of E1 genes to achieve tumor specificity is also pursued. In delta-24 (Δ24) oAds, 24 base pairs (bps) in the CR2 region of E1A are deleted, leading to a loss of the ability to sequestrate the retinoblastoma protein (pRb), which negatively regulates cell cycle progression in non-malignant cells by binding the transcription factor E2F. Consequently, viruses with a Δ24 deletion cannot free pRb-bound E2F in healthy cells and replicate.[88] Deregulation of the pRb pathway in many cancers leads to abundantly available E2F for viral replication, which is crucial for transition into S-phase.[89]

Ad5 has a natural tropism for epithelial cells of the respiratory tract, using the CAR as the main entry receptor.[90] To increase tropism to tumor entities of different tissues, modifications of the Ad5 fiber have been investigated. The fiber consists of a tail, attaching the fiber to the penton base, a central shaft and a knob, the knob initiating viral entry into the host cell.[91] Therefore, knob modifications and serotype switching of the fiber shaft and knob or just the knob are used to increase infectivity of tumor cells.[92, 93] Incorporation of an Arg-Gly-Asp (Arginylglycylaspartic acid or RGD) containing peptide in the HI-loop domain of the fiber knob has been shown to increase the tropism of Ad5 to otherwise refractory cells by allowing binding to cellular integrins.[94] Switching the Ad5 knob to the knob of Ad3 switches the entry receptors to mainly desmoglein 2 and CD46, which are more highly expressed on cancer cells.[95]

There are multiple possible insertion sites for transgenes in the oAd genome. The late transcriptional unit is more active than the early units after replication of the viral DNA, therefore placing transgenes under control of the late gene promoter leads to a higher transgene expression.[96] In addition to the insertion site, the strategy for control of transgene transcription is also crucial. Transcription can be driven by endogenous adenoviral promoters, by usage of internal ribosome entry sites (IRES), 2A sequences and splice acceptors (SAs).[85, 97] Different SAs have been explored for transgene insertion into oAds, e.g. the SA of the Ad5 protein IIIa[98] and the SAs of the Ad40[99] and Ad41[100] long fibers. Exogenous promoters have also been employed for transgene expression, such as the cytomegalovirus immediate-early (CMV) or Rous sarcoma virus long terminal repeat (RSV) promoter.[101, 102] Arming

of oAds with genes for multiple therapeutic proteins has also been shown.[103-105] A challenge with insertion of transgenes in Ads is posed by the inherent ability of genetic recombination, which leads to new viral variants in nature.[106] Recombination events have to be considered when planning structure and location of transgenes, i.e. repeats of identical sequences should be avoided.[107]

1.3.4 Viro-Antibody-Therapy

To enhance therapeutic efficacy of oAds, transgenes with anti-tumor activity can be inserted into the Ad5 genome. As described in chapter 1.2.1, antibody therapy represents a potent strategy for cancer treatment with numerous ongoing developments. Combining virotherapy with antibody therapy via genetic delivery of antibody-based therapeutics has therefore been investigated with numerous different antibody formats and targets. Genetic delivery of therapeutic antibodies holds the advantage of higher tumor-blood ratios of antibody concentrations compared to systemic antibody application.[108, 109] Therapeutic antibodies genetically delivered by OVs have also been shown to enhance tumor cell killing and prolong survival, complementary to viral oncolysis.[110] Armed oAds have been equipped with genes for mAbs, scFvs, Fabs, antibody-fusion proteins (e.g. immunocytokines), nanobodies and BiTEs.[110] Expression of Trastuzumab via an Ad5 with a serotype 3 knob (Ad5/3) with heavy and light chains linked via IRES has been shown to induce ADCC and exhibit enhanced antitumor efficacy in a gastric cancer xenograft model compared to Trastuzumab or the unarmed virus alone, showing the potential of targeting TAAs with OV-encoded mAbs.[111] OV-encoded ICIs have shown enhanced treatment efficacy, while reducing systemic side effects associated with standard ICI therapy. This approach has been pursued with numerous OVs and antibody formats, including mAbs, nanobodies and scFvs.[110] Furthermore, different OVs have been developed for delivery of antibodies to tumors for inhibition of the vascular endothelial growth factor (VEGF) to counteract tumor angiogenesis. Vaccinia viruses with anti-VEGF scFvs have been employed in several studies, demonstrating augmented inhibition of tumor growth and reduced blood vessel density in infected areas.[112-115]

BiTE-encoding oAds are especially interesting, as various challenges of conventional TCE therapies can be overcome. Due to their small size, BiTEs have a short half-life and require continuous infusion. oAd-encoded BiTEs are secreted as long as viral replication is ongoing. Furthermore, TCEs are ineffective in solid tumors with low T-cell infiltration and an immunosuppressive TME. The immunogenic process of oncolysis aids in increasing the presence of TILs and therefore enhances TCE efficacy. Lastly, a major limitation of TCEs is

potential on-target, off-tumor toxicity. Local expression of TCEs leads to retention of the antibodies within the tumor, with little systemic leakage.[116-118] oAds armed with BiTEs targeting fibroblast associated protein (FAP) have shown specific depletion of FAP^+ fibroblasts in an *ex vivo* ascites model and an increase of inflammatory markers.[119] In another study with FAP-targeting BiTEs, genetic delivery via oAds increased T-cell infiltration into oAd-injected tumors accompanied by stronger inhibition of tumor growth and prolonged survival compared to treatment with the unarmed oAd in *in vivo* models of pancreatic and alveolar adenocarcinoma.[120] EnAdenotucirev (EnAd), a chimeric oAd of serotypes 11 and 3, has been armed with a BiTE targeting the epithelial cell adhesion molecule (EpCAM). In primary peritoneal ascites and pleural effusion samples, infection with the EpCAM-BiTE armed oAds lead to potent T-cell activation, despite an immunosuppressive TME.[121] An armed oAd overcoming the immunosuppressive TME was also shown for an Ad5 armed with a MUC16-BiTE, which showed enhanced tumor cell killing in both *ex vivo* and *in vivo* xenograft models of ovarian cancer compared to the parental virus.[122] An Ad5 based virus, ICOVIR-15K-cBiTE, armed with an EGFR-BiTE, has been described in multiple studies. Compared to the parental virus, it increased accumulation and persistence of TILs and enhanced tumor cell killing in *in vivo* models of alveolar adenocarcinoma and colorectal cancer.[123] In combination with folate receptor alpha (FR-α) specific CAR-T cells, ICOVIR-15K-cBiTE was able to redirect CAR-T cells to $FR\text{-}\alpha^-/EGFR^+$ tumor cells, addressing the problem of tumor heterogeneity and significantly increasing CAR-T cell activation and proliferation *in vitro*. In a murine *in vivo* model, the combination therapy enhanced antitumor efficacy and prolonged survival compared to either monotherapy.[124] A single OV addressing the problem of heterogeneity by co-expression of multiple TCEs or expression of multispecific TCEs has not been described to date.

Apart from antibodies, other transgenes have been explored for oAd therapy, such as cytokines, including IL-2, IL-12, TNFα, GM-CSF and IFNα.[125-128]

1.4 Tumor Targets

For more selective tumor cell killing, efforts have been made to identify potential tumor cell targets. These targets can be divided into tumor-specific antigens (TSAs) and TAAs. While TSAs are only present on tumor cells and not on healthy cells, TAAs are also present on non-malignant cells, but are often upregulated in tumors. Unfortunately, TSAs are very rare and not present for all tumor entities.[129] TAAs are more prevalent, but targeting TAAs poses a higher risk of on-target, off-tumor toxicity. This makes targeting TAAs more challenging and calls for

strict controllability of therapeutics. The form in which TSAs or TAAs are present on tumor cells is also of note. Surface antigens can be detected by antibodies, antibody-based therapeutics or CAR-T cells, whereas intracellular proteins, which are processed and presented via MHCI molecules, require detection by T-cells via their TCR.[130, 131] Here, four different TAAs, all surface antigens, were chosen as therapeutic targets, namely EGFR, HER2, c-MET and IL13Rα2.

1.4.1 EGFR

The epidermal growth factor receptor (EGFR) belongs to the erbB family of receptor tyrosine kinases (RTKs). RTKs are cell surface receptors that consist of an extracellular, ligand-binding domain, a transmembrane domain and an intracellular domain containing the tyrosine kinase and other regulatory regions.[132] Phosphorylation of tyrosine residues on intracellular proteins occurs after ligand binding and subsequent receptor dimerization. The downstream effects of TRK signaling include activation of pathways that promote cell proliferation, survival, differentiation, angiogenesis, migration, metabolism and cell cycle progression.[133] High levels of RTK activity in tumor cells are correlated with increased aggressiveness, progression and poor prognosis of tumors.[134] The involvement of EGFR in this variety of tumor promoting mechanisms makes it an attractive target for cancer therapy. EGFR is overexpressed in various cancers, including non-small cell lung cancer (NSCLC), colorectal cancer (CRC), gliomas and head and neck cancer.[135] Two classes of drugs are currently on the market for anti-EGFR therapy, tyrosine kinase inhibitors (TKIs) and monoclonal antibodies (mAbs). TKIs are a group of small molecules that bind to intracellular domains of RTKs, including EGFR, disrupting the downstream signaling cascade.[136] Acquired and intrinsic resistance to TKI therapy are an important limitation to their efficacy. Resistances can occur due to receptor mutations, amplification of alternative receptors or due to populations of drug-tolerant persister cells.[137] mAbs that are currently approved for anti-EGFR therapy, such as Cetuximab[138], unfold their efficacy through various mechanisms described in chapter 1.2.1. They face similar challenges as TKIs by development of resistances, which include upregulation of alternative receptors, such as c-MET, receptor mutations and mutations in mediators of the downstream signaling cascade, but also unique mechanisms such as impaired ADCC and reduced degradation of internalized mAb-receptor complexes.[139]

1.4.2 HER2

Human EGFR2 (HER2) belongs to the same family of receptors (erbB) as EGFR and is a common dimerization partner of EGFR. HER2 is typically amplified in e.g. breast, ovarian, gastric and esophageal cancers, but is also increasingly investigated as a target in glioblastoma (GBM).[140-142] Existing HER2-targeting therapeutics include TKIs, mAbs and ADCs. Trastuzumab, a humanized IgG1 antibody, binds to the extracellular domain of HER2 and is able to inhibit dimerization with other receptors and furthermore triggers ADCC.[135] The only two ADCs targeting HER2 are based on Trastuzumab.[139]

1.4.3 c-MET

Cellular mesenchymal epithelial transition factor (c-MET), like EGFR and HER2, is an RTK encoded by the MET gene, it is also known as hepatocyte growth factor receptor (HGFR). In cancer, c-MET is involved in tumor invasion, growth, angiogenesis, resistance to TKI or antibody therapy and the generation and maintenance of cancer stem cells in a variety of solid tumors.[143-145] As for EGFR and HER2, treatment modalities include TKIs and mAbs. Interestingly, c-MET amplification has been described as an escape mechanism following EGFR inhibition.[146, 147] Amivantamab is a bispecific EGFR/c-MET antibody approved for the treatment of NSCLC. It prevents ligand binding to either receptor and mediates ADCC.[148]

1.4.4 IL13Rα2

Interleukin-13 receptor subunit alpha-2 (IL13Rα2) is a high-affinity receptor for IL-13 and has been believed to be a decoy receptor for IL-13 without any downstream signaling domains. Recent studies have shown the involvement of IL13Ra2 in tumorigenesis and progression.[149, 150] Overexpression of IL13Rα2 has been correlated with poorer prognosis of gliomas, breast cancer and pancreatic cancer.[151] Compared to the RTKs described above, IL13Rα2 is primarily expressed in cancer cells, making it a prime target for therapy. In healthy tissue IL13Rα2 is found exclusively in spermatocytes.[152] Current efforts of targeting IL13Rα2 include CAR-T cell therapy and antibody therapy.[153]

1.5 Tumor Heterogeneity and Combination Therapy

With growing efforts of more targeted therapy approaches, tumor heterogeneity poses an additional challenge. Solid tumors have been characterized as generally heterogeneous, consisting of different subpopulations.[154] Monotherapy targeting only a single target can therefore lead to survival of a small fraction of tumor cells or to development of resistant

subpopulations that in case of relapse are completely resistant to the original therapy, as schematically outlined in Figure 7.[155, 156] Approaches of dual- or multitargeting have been undertaken to circumvent the problem of immune evasion.[157] Such approaches include dual-CAR-T cell therapies, multispecific antibodies or antibody combinations.[158, 159]

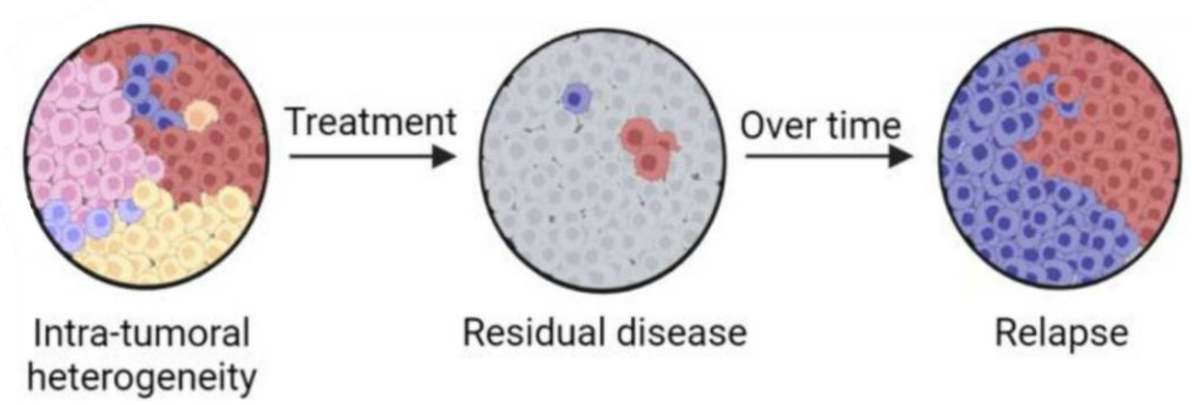

Figure 7 Schematic depiction of tumor relapse following treatment of heterogeneous tumor. Adapted from Al-Hamaly et al., 2023.[160]

The chosen targets (chapters 1.4.1-1.4.4) have also been involved in dual-targeting approaches. As mentioned in chapter 1.4.3, a dual-targeting antibody for EGFR and c-MET, Amivantamab, has been FDA approved. Different small molecules have also been investigated for EGFR/c-MET dual inhibition, inducing apoptosis in TKI-resistant EGFR-mutated NSCLC cells and suppressing xenograft tumor formation.[161] Similarly, another EGFR/c-MET dual-targeting agent suppressed growth of a triple-negative breast cancer (TNBC) tumor model accompanied by reduced angiogenesis.[162] In a head and neck squamous cell carcinoma (HNSCC) model, combined EGFR/c-MET targeting was reported to reduce tumor growth compared to treatment with the single agents.[163]

Dual-targeting of EGFR and HER2 has been investigated in the form of combining Cetuximab and Trastuzumab. In an HNSCC *in vivo* model, anti-EGFR/HER2 therapy resulted in decreased tumor hypoxia compared to single agent therapy.[164] A study combining Cetuximab and Trastuzumab therapy in a human pancreatic carcinoma xenograft model demonstrated prolonged survival with the dual-targeting approach compared to standard of care, gemcitabine chemotherapy.[165]

In GBM, dual-targeting of EGFR and IL13Rα2 is currently being investigated in a phase 1 clinical trial with CAR T-cells, co-expressing two different CARs.[15] Preclinical studies have investigated EGFR and IL13Rα2 dual-targeting by BiTE-secreting T-cells and bivalent CAR-T cells, expressing two different CARs via a 2A sequence. BiTE-T cells demonstrated superior T-

cell activation, cytokine production and cytotoxicity compared to the bivalent CAR-T cells *in vitro*, whereas the bivalent CAR-T cells outperformed the BiTE-T cells in regards to long term tumor control and survival.[166]

Similarly, co-targeting of HER2 and IL13Rα2 has also been pursued in GBM, employing CAR-T cells equipped with a dual-targeting CAR, its extracellular domains consisting of a HER2-binding scFv and a mutated IL-13 molecule, in a murine tumor model. The approach showed promising results with the CAR T-cell therapy being able to overcome antigen escape, enhanced tumor control, elimination and increased time until tumor progression.[167]

1.6 Aim of Thesis

The aim of this thesis was to generate oAds equipped with genes for scDbs, BiTEs and scDb-scFvs for dual-targeting of TAAs, addressing the problem of tumor heterogeneity.

In the first part of this thesis, I aimed to generate a panel of bispecific TCEs that could be used in dual-targeting approaches. To this end, I chose EGFR, HER2, c-MET and IL13Rα2 as targets. I conducted a first of its kind comparison of the BiTE and scDb format regarding target binding and induction of T-cell mediated cytotoxicity in order to identify efficacious scDb and BiTE molecules for genetic delivery via oAds. In addition, I aimed to identify suitable scDbs to be used as bases for the novel, trispecific scDb-based scDb-scFv format. This antibody format has only been described as a trivalent, bispecific molecule to date, but the format holds the potential to be employed as a trivalent, trispecific antibody and could therefore be used to target two tumor antigens at the same time with a single molecule. Characterization of the trispecific scDb-scFvs in regard to antigen binding and induction of T-cell mediated cytotoxicity was hypothesized to identify scDb-scFvs that perform on par with corresponding bispecific TCEs on single target-positive cells and show superior binding and induction of T-cell mediated cytotoxicity on double target-positive cells.

In the second part of the thesis, I aimed to generate and characterize a TCE-encoding virus panel for a dual-antigen-targeting approach. In order to identify the most promising expression strategy, I explored two different insertion sites with different expression mechanisms including endogenous and exogenous promoters, as well as co-expression strategies employing synthetic, bidirectional promoter cassettes and T2A peptides. Characterization of the virus panel in terms of oncolytic activity, TCE production, T-cell activation and cytotoxicity in cocultures of oAd-infected tumor cells with PBMCs was aimed to identify an expression strategy that exhibited little to no attenuation of oAds compared to the parental virus, while maintaining genomic

stability and driving expression of functional TCEs in amounts that effectively induce T-cell activation and T-cell mediated cytotoxicity. By comparing different dual-targeting strategies, i.e. co-expression of two bispecific TCEs with one oAd, co-infection of two oAds encoding two different, single TCEs and expression of a trispecific scDb-scFv, I aimed to identify the most potent dual-antigen-targeting strategy. This implied equal production of two bispecific TCEs or effective production of the trispecific TCE, potent T-cell activation and T-cell mediated cytotoxicity in cocultures with single target-positive and double target-positive cells, but importantly, T-cell activation and effector functions only in settings where TCE targets were expressed. I aimed to utilize these analyses to validate the feasibility of a dual-targeting approach and to conclude whether the expression strategy using an scDb-scFv holds possible advantages over co-expression of two bispecific TCEs due to smaller transgene size and fewer repetitive sequences, considering the limited genomic capacity of oAds and the risk of homologous recombination. The *in vitro* studies were intended to identify the oAd with the most potent dual-targeting properties for future *in vivo* translation. A graphical abstract showing the viro-antibody-therapy approach is shown in Figure 8.

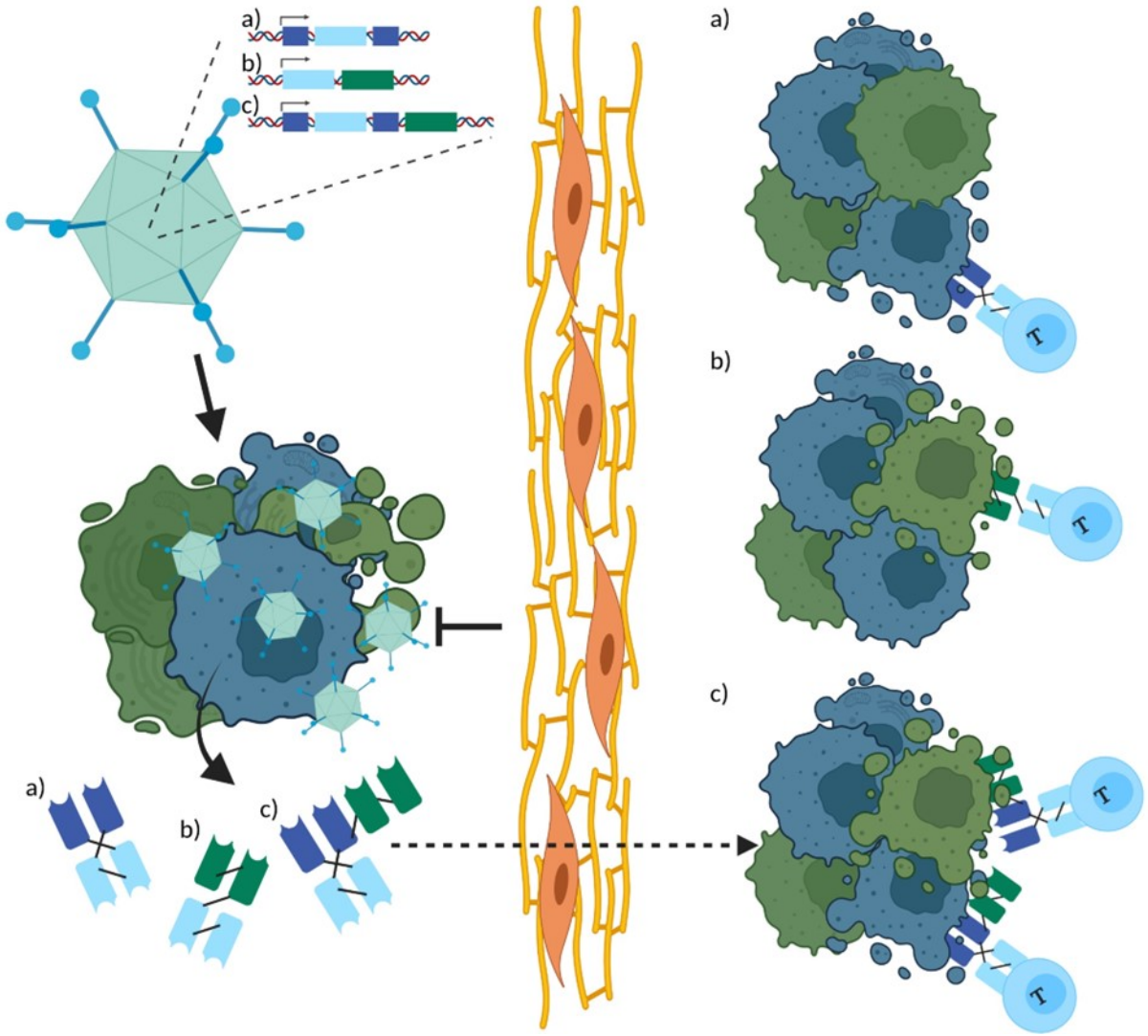

Figure 8 Viro-antibody-therapy with trispecific T-cell engagers. Schematic depiction of the principle of a combination therapy with oncolytic adenoviruses and encoded T-cell engagers. oAds infect and lyse tumor cells, while at the same time directing the production of T-cell engagers, i.e. bispecific a) scDbs, b) BiTEs or c) trispecific scDb-scFvs. Virus spread is limited by anatomical barriers like connective tissue. The small T-cell engagers are able to perfuse the tumor and reach tumor cells inaccessible to the virus, mediating their destruction through T-cells. Trispecific T-cell engagers can bind two different targets to address the problem of tumor heterogeneity and immune editing-based treatment resistance.

2. Materials and Methods

2.1 Materials

2.1.1 General Consumables

Laboratory plastics were purchased from Greiner Bio-One, Corning and Thermo Fisher Scientific, unless otherwise specified.

Table 1 List of consumables.

1.5 mL, 2 mL, 5 mL Safe-lock reaction tube	Eppendorf SE
13.2 mL, Thinwall Polypropylene Tubes	Beckman Coulter
2 mL 5PRIME Phase Lock GelTM	Quantabio
Mini-PROTEAN TGX Stain Free Gel (12 %)	Bio-Rad
PD-10 desalting column	Cytiva
Poly-Prep® Chromatography Column	Bio-Rad

2.1.2 Chemicals

Table 2 List of chemicals.

Acetic Acid	Supelco
Agarose	Sigma-Aldrich
Ampicillin	Carl Roth
ATP	New England Biolabs
CsCl	AppliChem
D-glucose	Gibco
DMSO	Sigma-Aldrich
Ethanol	VWR
HCl	Thermo Fisher
Imidazole	Sigma-Aldrich
Isopropanol	Carl Roth
Kanamycin	Sigma-Aldrich
KCl	Carl Roth
KH_2PO_4	Carl Roth
LiCl	Carl Roth
Lipofectamine 2000	Thermo Fisher Scientific
Lipofectamine 3000	Thermo Fisher Scientific
$Na_2HPO_4 \cdot 2\ H_2O$	Carl Roth
NaCl	Fisher Scientific
NaH_2PO_4	Carl Roth
Ni-NTA Agarose	Protino
Penicillin-Streptomycin	Gibco
SDS (20%)	AppliChem
Tween 20	Merck

β-mercaptoethanol	Sigma-Aldrich

2.1.3 Antibodies

Table 3 List of antibodies.

Name/Target	Fluorophore	Isotype	Working Dilution	Manufacturer
5D5 / anti c-MET	-	Chimeric IgG1	0.4 nM	Kontermann lab
anti CD3	AF700	Mouse IgG2a, κ	1:200	Biolegend
anti CD4	PE	Mouse IgG1, κ	1:200	Biolegend
anti CD69	AF488	Mouse IgG1, κ	1:200	Biolegend
anti CD8	APC	Mouse IgG1, κ	1:200	BD Pharmingen
anti c-Myc	AF647	Mouse IgG1, κ	1:200	Biolegend
anti HA	PE	Mouse IgG1	1:200	Miltenyi
anti His	PE	Mouse IgG1	1:200	Miltenyi
anti IgG Fc	APC	Rat IgG2a, κ	1:200	Biolegend
Cetuximab	-	Chimeric IgG1	0.4 nM	Merck KGaA
IL13Rα2	-	Humanized IgG1	0.4 nM	Kontermann lab
Trastuzumab	-	Humanized IgG1	0.4 nM	Genentech

2.1.4 Buffers and Solutions

Table 4 List of buffers and solutions.

Bradford Reagent (5x)	Bio-Rad protein assay (Bio-Rad)
Coommassie Blue	0.008 % Coommasie Blue (w/v), 35 mM HCl
Crystal Violet	0.5 % (w/v) crystal violet, 20 % (v/v) methanol
CutSmart (10x)	New England Biolabs, used as 1x
DPBS (1x)	GIBCO® Dulbecco's phosphate-buffered saline (Thermo Fisher Scientific)
ELISA Stop Buffer	2N H_2SO_4
ELISA wash buffer	0.005 % (v/v) TWEEN 20 in DPBS
FACS Buffer	2 % FCS, 2 mM EDTA in DPBS
Fixation Buffer	1 % PFA in FACS buffer
Histopaque®-1077	Sigma-Aldrich
IMAC Elution Buffer	250 mM Imidazole in 1x sodium phosphate buffer
IMAC Wash Buffer	25 mM Imidazole in 1x sodium phosphate buffer
Laemmli Loading Buffer (4x)	Bio-Rad, used as 1x reducing buffer, 10 % (v/v) β-mercaptoethanol
Loading Dye (6x)	New England Biolabs, used as 1x
PBS (10x)	80.6 mM Na_2HPO_4, 14.7 mM KH_2PO_4, 1.37 M NaCl, 26.7 mM KCl; used as 1x PBS
PFA	4 % PFA in PBS (Thermo Fisher Scientific)
Q5 reaction buffer (5x)	New England Biolabs, used as 1x
r3.1 reaction buffer (10x)	New England Biolabs, used as 1x
SDS-PAGE Running buffer (10x)	Bio-Rad, used as 1x

Sodium phosphate buffer (5x)	210 mM Na_2HPO_4, 40 mM NaH_2PO_4, 1.25 M NaCl, pH 7.5
T4 Ligase buffer (10x)	New England Biolabs, used as 1x
TBE buffer (10x)	SERVA Electrophoresis GmbH, used as 1x
TE (10x)	Tris-EDTA, Fisher Scientific, used as 1x
Virus Lysis Buffer	0.5 % SDS in TE

2.1.5 Enzymes

Table 5 List of enzymes.

AgeI	New England Biolabs
BbsI	New England Biolabs
ClaI	New England Biolabs
KpnI	New England Biolabs
MluI	New England Biolabs
NcoI	New England Biolabs
PacI	New England Biolabs
Platinum II Taq Hot-Start DNA Polymerase	Thermo Fisher Scientific
PmeI	New England Biolabs
Q5 High-Fidelity DNA Polymerase	New England Biolabs
rSAP	New England Biolabs
SalI	New England Biolabs
SwaI	New England Biolabs
T4 Ligase	New England Biolabs
XbaI	New England Biolabs
XhoI	New England Biolabs

2.1.6 Kits

Table 6 List of kits.

Dual-Glo® Luciferase Assay System	Promega
ELISA MAX™ Deluxe Set Human IL-2	Biolegend
ELISA MAX™ Standard Set Human IFN-γ	Biolegend
QIAGEN Plasmid Maxi Kit	QIAGEN
QIAGEN Plasmid Midi Kit	QIAGEN
QIAprep Spin Miniprep Kit	QIAGEN
QIAquick Gel Extraction Kit	QIAGEN
QIAquick PCR Purification Kit	QIAGEN

2.1.7 Prokaryotic and Eukaryotic Cell Lines

Table 7 List of prokaryotic and eukaryotic cell lines.

A172	Glioblastoma
A549	Lung adenocarcinoma

BJ5183	Electrocompetent, recombination proficient E.coli (Agilent)
BT474	Breast ductal carcinoma
H1650	Lung adenocarcinoma
HeLa	Cervical Adenocarcinoma
Jurkat	T-cell leukemia
NEB 10-beta	Chemically or electrocompetent E.coli (New England Biolabs)
SK-Mel-23	Melanoma
SKOV3	Ovarian serous cystadenocarcinoma
SW480	Colorectal Cancer
U215	Glioblastoma
U87	Glioblastoma

2.1.8 Media and Supplements for Cell Culture

Table 8 List of media and supplements for cell culture.

DMEM	Gibco
FCS	
LB-Medium (Lennox)	Roth
Opti-MEM	Gibco
RPMI 1640	Gibco
SOC	LB-Medium, 1 % glucose

2.1.9 Plasmids

Table 9 List of plasmids.

Name	Description
pAd5/3-(CMV-BiTE-EGFR-HA-His)r	Ad5/3Δ24ΔE3 genome with post E4 insertion of CMV-BiTE-EGFR-HA-His in reverse orientation
pAd5/3-(CMV-scDb-cMET-Myc-His)r	Ad5/3Δ24ΔE3 genome with post E4 insertion of CMV-scDb-cMET-Myc-His in reverse orientation
pAd5/3-(CMV-scDb-cMET-scFv-EGFR)r	Ad5/3Δ24ΔE3 genome with post E4 insertion of CMV-scDb-cMET-scFv-EGFR in reverse orientation
pAd5/3-(scDb-HER2-Myc-His-CMV-mCMV-BiTE-EGFR-HA-His)r	Ad5/3Δ24ΔE3 genome with post E4 insertion of scDb-HER2-Myc-His-CMV-mCMV-BiTE-EGFR-HA-His in reverse orientation
pAd5/3-CMV-BiTE-EGFR-HA-His	Ad5/3Δ24ΔE3 genome with post E4 insertion of CMV-BiTE-EGFR-HA-His
pAd5/3-CMV-scDb-cMET-Myc-His	Ad5/3Δ24ΔE3 genome with post E4 insertion of CMV-scDb-cMET-Myc-His
pAd5/3-CMV-scDb-cMET-scFv-EGFR	Ad5/3Δ24ΔE3 genome with post E4 insertion of CMV-scDb-cMET-scFv-EGFR

pAd5/3-CMV-scDb-cMET-T2A-BiTE-EGFR	Ad5/3Δ24ΔE3 genome with post E4 insertion of CMV-scDb-cMET-T2A-BiTE-EGFR
pAd5/3d24-DE3	Ad5/3Δ24ΔE3 genome
pAd5/3-FSA-BiTE-EGFR-HA-His	Ad5/3Δ24ΔE3 genome with post fiber insertion of Ad40SA-BiTE-EGFR-HA-His
pAd5/3-scDb-HER2-Myc-His-CMV-mCMV-BiTE-EGFR-HA-His	Ad5/3Δ24ΔE3 genome with post E4 insertion of scDb-HER2-Myc-His-CMV-mCMV-BiTE-EGFR-HA-His
pBOMcheck2	Modified psicheck2 vector for Golden Gate cloning of bidirectional promoter expression cassettes
pBOMcheck2-hRluc-CMV-mCMV-Fluc	pBOMcheck2 with bidirectional CMV-mCMV promoter driving expression of Renilla and firefly luciferase
pBOMcheck2-hRluc-hPGK1-mCMV-Fluc	pBOMcheck2 with bidirectional hPGK1-mCMV promoter driving expression of Renilla and firefly luciferase
pBOMcheck2-hRluc-mCMV-CMV-Fluc	pBOMcheck2 with bidirectional mCMV-CMV promoter driving expression of Renilla and firefly luciferase
pBOMcheck2-hRluc-mCMV-hPGK1-Fluc	pBOMcheck2 with bidirectional mCMV-hPGK1 promoter driving expression of Renilla and firefly luciferase
pBOMcheck2-scDb-HER2-Myc-His-CMV-mCMV-BiTE-EGFR-HA-His	pBOMcheck2 with bidirectional CMV-mCMV promoter driving expression of scDb-HER2-Myc-His and BiTE-EGFR-HA-His
pF5/3-Ad40SA-BiTE-EGFR-HA-His	Fiber shuttle with Ad40SA-BiTE-EGFR-HA-His for homologous recombination with pVK500Δ24
pF5/3-Ad40SA-Luc	Fiber shuttle with Ad40SA-Luc, used here as cloning template for other fiber shuttles
pGL3-Ad40SA-BiTE-EGFR-HA-His	pGL3 vector with insertion of Ad40SA-BiTE-EGFR-HA-His for cloning into fiber shuttle
pGL3-Ad40SA-Luc	pGL3 vector with insertion of Ad40SA-Luc, used here as template for other pGL3-Ad40SA vectors
pGL3-CMV-BiTE-EGFR-HA-His	pGL3 vector with insertion of CMV-BiTE-EGFR-HA-His for cloning into pSD24
pGL3-CMV-scDb-cMET-Myc-His	pGL3 vector with insertion of CMV-scDb-cMET-Myc-His for cloning into pSD24
pGL3-CMV-scDb-cMET-scFv-EGFR	pGL3 vector with insertion of CMV-scDb-cMET-BiTE-EGFR for cloning into pSD24
pGL3-CMV-synthPA	pGL3 vector with CMV promoter and synthetic PolyA tail, used here as template for other pGL3-CMV vectors
pSD24-(CMV-BiTE-EGFR-HA-His)r	E1AΔ24 shuttle with insertion of CMV-BiTE-EGFR-HA-His in reverse orientation for homologous recombination with pVK500F5/3ΔE3
pSD24-(CMV-BiTE-EGFR-HA-His-T2A-scDb-cMET-Myc-His)r	E1AΔ24 shuttle with insertion of CMV-BiTE-EGFR-HA-His-T2A-scDb-cMET-Myc-His in

	reverse orientation for homologous recombination with pVK500F5/3ΔE3
pSD24-(CMV-scDb-cMET-Myc-His)r	E1AΔ24 shuttle with insertion of CMV-scDb-cMET-Myc-His in reverse orientation for homologous recombination with pVK500F5/3ΔE3
pSD24-(CMV-scDb-cMET-scFv-EGFR)r	E1AΔ24 shuttle with insertion of CMV-scDb-cMET-scFv-EGFR in reverse orientation for homologous recombination with pVK500F5/3ΔE3
pSD24-(CMV-scDb-cMET-T2A-BiTE-EGFR)r	E1AΔ24 shuttle with insertion of CMV-scDb-cMET-T2A-BiTE-EGFR in reverse orientation for homologous recombination with pVK500F5/3ΔE3
pSD24-(scDb-HER2-Myc-His-CMV-mCMV-BiTE-EGFR-HA-His)r	E1AΔ24 shuttle with insertion of scDb-HER2-Myc-His-CMV-mCMV-BiTE-EGFR-HA-His in reverse orientation for homologous recombination with pVK500F5/3ΔE3
pSD24-CMV-BiTE-EGFR-HA-His	E1AΔ24 shuttle with insertion of CMV-BiTE-EGFR-HA-His for homologous recombination with pVK500F5/3ΔE3
pSD24-CMV-BiTE-EGFR-HA-His-T2A-scDb-cMET-Myc-His	E1AΔ24 shuttle with insertion of CMV-BiTE-EGFR-HA-His-T2A-scDb-cMET-Myc-His for homologous recombination with pVK500F5/3ΔE3
pSD24-CMV-scDb-cMET-Myc-His	E1AΔ24 shuttle with insertion of CMV-scDb-cMET-Myc-His for homologous recombination with pVK500F5/3ΔE3
pSD24-CMV-scDb-cMET-Myc-His-T2A-BiTE-EGFR-HA-His	E1AΔ24 shuttle with insertion of CMV-scDb-cMET-Myc-His-T2A-BiTE-EGFR-HA-His for homologous recombination with pVK500F5/3ΔE3
pSD24-CMV-scDb-cMET-scFv-EGFR	E1AΔ24 shuttle with insertion of CMV-scDb-cMET-scFv-EGFR for homologous recombination with pVK500F5/3ΔE3
pSD24-Mlu-Sal	E1AΔ24 shuttle for homologous recombination with pVK500F5/3ΔE3 for transgene insertion between E4 and RITR featuring MluI-SalI cloning site
pSD24-Sal-Mlu	Modified pSD24-Mlu-Sal with cloning site switched to SalI-MluI for reverse insertions
pSD24-scDb-HER2-Myc-His-CMV-mCMV-BiTE-EGFR-HA-His	E1AΔ24 shuttle with insertion of scDb-HER2-Myc-His-CMV-mCMV-BiTE-EGFR-HA-His for homologous recombination with pVK500F5/3ΔE3
pSE1wt	Plasmid encoding Ad5 wildtype E1 region
pSecTag-BiTE-EGFR-HA-His	Expression plasmid of BiTE-EGFR-HA-His
pSecTag-BiTE-IL13Rα2-HA-His	Expression plasmid of BiTE-IL13Rα2-HA-His
pSecTag-cMET BiTE	Expression plasmid of BiTE-cMET
pSecTag-EGFR BiTE	Expression plasmid of BiTE-EGFR

pSecTag-HER2 BiTE	Expression plasmid of BiTE-HER2
pSecTag-IL13Rα2 BiTE	Expression plasmid of BiTE-IL13Rα2
pSecTag-scDbCD3xcMET	Expression plasmid of scDb-cMET
pSecTag-scDbCD3xEGFR	Expression plasmid of scDb-EGFR, used here as template for V_H and V_L amplification
pSecTag-scDbCD3xHER2	Expression plasmid of scDb-HER2
pSecTag-scDbCD3xIL13Rα2	Expression plasmid of scDb-IL13Rα2
pSecTag-scDb-cMET-Myc-His	Expression plasmid of scDb-cMET-Myc-His
pSecTag-scDb-HER2-Myc-His	Expression plasmid of scDb-HER2-Myc-His
pSecTag-scDb-scFvCD3xcMETxEGFR	Expression plasmid of scDb-cMET-scFv-EGFR
pSecTag-scDb-scFvCD3xHER2xEGFR	Expression plasmid of scDb-HER2-scFv-EGFR
pSecTag-scDb-scFvCD3xHER2xIL13Rα2	Expression plasmid of scDb-HER2-scFv-IL13Rα2
pSecTag-scDbXxCD3	Backbone of expression plasmid for Golden Gate cloning of scDbs
pSecTag-scDbXxCD3xX-scFvX	Backbone of expression plasmid for Golden Gate cloning of scDb-scFvs
pSecTag-scFv-EGFR-scDb-HER2	Expression plasmid of scFv-EGFR-scDb-HER2
pSecTag-scFvhuU3-scFvGG-His	Backbone of expression plasmid for Golden Gate cloning of BiTEs
pSecTag-scFv-IL13Ra2-scDb-HER2	Expression plasmid of scFv-IL13Rα2-scDb-HER2
pSecTag-V_H4D5	Expression plasmid carrying V_H HER2 for cloning
pSecTag-V_H5D5	Expression plasmid carrying V_H c-MET for cloning
pSecTag-V_HIL13Rα2	Expression plasmid carrying V_H IL13Rα2 for cloning
pSecTag-V_L4D5	Expression plasmid carrying V_L HER2 for cloning
pSecTag-V_L5D5	Expression plasmid carrying V_L c-MET for cloning
pSecTag-V_LIL13Rα2	Expression plasmid carrying V_L IL13Rα2 for cloning
psiCheck2	Vector for dual expression of Renilla and firefly luciferase (Promega)
pTG3602	Ad5 wildtype genome plasmid
pVK5/3-d24-SAGFP	Control plasmid for 5/3 chimeric fiber
pVK500F5/3ΔE3	Ad5/3 backbone for homologous recombination with pSD24 shuttles
pVK500d24	Ad5/3 backbone for homologous recombination with pF5/3 shuttles

2.1.10 Primers

Table 10 List of primers.

#	Name	Sequence 5' → 3'	Application
19	VH5D5 fwd	AAAAAGAAGACGGACCGGTGAAGTGC AGCTGGTGGAATC	Golden Gate cloning primer
20	VH5D5 rev	AAAAAGAAGACGGCACCACTCGAGAC GGTAACCAATG	Golden Gate cloning primer
21	VL5D5 fwd	AAAAAGAAGACGGGGATCCGACATCCA GATGACCCAGAG	Golden Gate cloning primer
22	VL5D5 rev	AAAAAGAAGACGGCCGCCTTGATTTCC ACCTTGGTGC	Golden Gate cloning primer
23	VH4D5 fwd	AAAAAGAAGACGGACCGGTGAAGTGC AGCTCGTCGAAAG	Golden Gate cloning primer
24	VH4D5 rev	AAAAAGAAGACGGCACCACTCGAGAC GGTCACCAGTG	Golden Gate cloning primer
39	VL4D5 fwd_2	AAAAAGAAGACGGGGATCCGACATCCA GATGACCCAG	Golden Gate cloning primer
26	VL4D5 rev	AAAAAGAAGACGGCCGCCTTGATCTCG ACCTTCGTTC	Golden Gate cloning primer
37	T7 fwd	TAATACGACTCACTATAGG	Sequencing primers for pSecTag
38	BGH rev	TAGAAGGCACAGTCGAGG	Sequencing primers for pSecTag
43	VHIL13Ra2 fwd	AAAAAGAAGACGGACCGGTCAAGTCC AGCTGGTGCAG	Golden Gate cloning primer
47	VHIL13Ra2 rev2	AAAAAGAAGACGGCACCAGAGCTAAC GGTCACGG	Golden Gate cloning primer
45	VLIL13Ra2 fwd	AAAAAGAAGACGGGGATCCGACATCCA GATGACACAGAG	Golden Gate cloning primer
46	VLIL13Ra2 rev	AAAAAGAAGACGGCCGCCTTGATTTCC ACCTTGGTGC	Golden Gate cloning primer
48	scDb_fwd	AGCCACCATGGAGACAGACAC	general fwd primer for scDbs
49	cMET/IL13Ra2_ Myc-His_rev	AAAAATCTAGATTAGTGATGGTGATGAT GGTGGTCGACGGCGCTATTCAGATCCTC TTCTGAGATGAGTTTTTGTTCGGCGGCC GCCTTGATTTCC	rev primer for Myc-His Tag for scDbCD3xcMET & scDbCD3xIL13Ra2
50	HER2_Myc-His_rev	AAAAATCTAGATTAGTGATGGTGATGAT GGTGGTCGACGGCGCTATTCAGATCCTC TTCTGAGATGAGTTTTTGTTCGGCGGCC GCCTTGATCTCG	rev primer for Myc-His Tag for scDbCD3xHER2
51	VHcMET_BiTE_ fwd	AAAAAGAAGACGGGGATCCGAAGTGC AGCTGGTGGAATC	BiTE GG Cloning primer
52	VHcMET_BiTE_ rev	AAAAAGAAGACGGCTCCACTCGAGAC GGTAACCAATG	BiTE GG Cloning primer
53	VLcMET_BiTE_f wd	AAAAAGAAGACGGTTCAGACATCCAG ATGACCCAGAG	BiTE GG Cloning primer
54	VLcMET/IL13Ra 2_BiTE_rev	AAAAAGAAGACTTCCGCCTTGATTTCC ACCTTGGTGC	BiTE GG Cloning primer
55	VHHER2_BiTE_ fwd	AAAAAGAAGACGGGGATCCGAAGTGC AGCTCGTCGAAAG	BiTE GG Cloning primer
56	VHHER2_BiTE_ rev	AAAAAGAAGACGGCTCCACTCGAGAC GGTCACCAGTG	BiTE GG Cloning primer
57	VLHER2_BiTE_f wd	AAAAAGAAGACGGTTCAGACATCCAG ATGACCCAGTC	BiTE GG Cloning primer
58	VLHER2_BiTE_r ev	AAAAAGAAGACTTCCGCCTTGATCTCG ACCTTCGTTC	BiTE GG Cloning primer
59	VHEGFR_BiTE_ fwd	AAAAAGAAGACGGGGATCCGAAGTGC AGCTGGTTGAAAG	BiTE GG Cloning primer

60	VHEGFR_BiTE_rev	AAAAAGAAGACGGCTCCACTCGAGACCGTAACGGTG	BiTE GG Cloning primer
61	VLEGFR_BiTE_fwd	AAAAAGAAGACGGTTCAGATATTCAGCTGACCCAG	BiTE GG Cloning primer
62	VLEGFR_BiTE_rev	AAAAAGAAGACTTCCGCTTTAATTTCCAGTTTGGTGC	BiTE GG Cloning primer
63	VHIL13Ra2_BiTE_fwd	AAAAAGAAGACGGGGATCCCAAGTCCAGCTGGTGCAGTC	BiTE GG Cloning primer
64	VHIL13Ra2_BiTE_rev	AAAAAGAAGACGGCTCCAGAGCTAACGGTCACGGTTG	BiTE GG Cloning primer
65	VLIL13Ra2_BiTE_fwd	AAAAAGAAGACGGTTCAGACATCCAGATGACACAGC	BiTE GG Cloning primer
93	pGL3-Ad40SA fwd	GCAAAATAGGCTGTCCCCAG	Sequencing primer for pGL3-Ad40SA vector
94	pGL3-Ad40SA rev	CAGTCATAAGTGCGGCGAC	Sequencing primer for pGL3-Ad40SA vector
105	PolyAfwd	TTTTTTCTAGAATCCAAGTCTTCAGAGATGCATGAAGACCGGCCGCCGAAATAAAATATCTTTATTTTC	Multifragment GG cloning of BOMcheck
106	PolyArev	AAAAAGGTACCCACACAAAAAACCAACACAC	Multifragment GG cloning of BOMcheck
107	hRluc GG fwd	AAAAAGAAGACGGAGCTATGGCTTCCAAGGTGTACG	Multifragment GG cloning of BOMcheck
108	hRluc GG rev	AAAAAGAAGACGGCGGCTTACTGCTCGTTCTTCAGCAC	Multifragment GG cloning of BOMcheck
109	Ffluc GG fwd	AAAAAGAAGACGGAGCTATGGCCGATGCTAAGAAC	Multifragment GG cloning of BOMcheck
110	Ffluc GG fev	AAAAAGAAGACGGATCCTTACACGGCGATCTTGCC	Multifragment GG cloning of BOMcheck
113	BOMcheck fwd	TTTGCTCACATGGCTCGACAG	Sequencing Primer for BOMcheck
114	BOMcheck rev	TCTAGTTGTGGTTTGTCCAAACTC	Sequencing Primer for BOMcheck
143	cMET/IL13Ra2_HA_His_rev	AAAAATCTAGATTAGTGATGGTGATGATGGTGGCCGCTGCTGCCGGCGTAGTCGGGCACGTCGTAGGGGTAGGCGGCCGCCTTGATTTCCAC	Cloning primers for changing scDb Tag from His to HA-His
144	HER2_HA_His_rev	AAAAATCTAGATTAGTGATGGTGATGATGGTGGCCGCTGCTGCCGGCGTAGTCGGGCACGTCGTAGGGGTAGGCGGCCGCCTTGATCTCGAC	Cloning primers for changing scDb Tag from His to HA-His
192	EGFR VH fwd	AAAAAGAAGACAAGGGAGCGAAGTGCAGCTGGTTGAAAG	scDb-scFv cloning primer
193	EGFR VH rev	AAAAAGAAGACAACTCCACTCGAGACCGTAACGGTGG	scDb-scFv cloning primer
194	EGFR VL fwd	AAAAAGAAGACGGTTCAGATATTCAGCTGACCCAGAG	scDb-scFv cloning primer
195	EGFR VL rev	AAAAAGAAGACGGTACCTTTAATTTCCAGTTTGGTGC	scDb-scFv cloning primer
196	HER2 VH fwd	AAAAAGAAGACAAGGGAGCGAAGTGCAGCTCGTCGAAAG	scDb-scFv cloning primer
197	HER2 VH rev	AAAAAGAAGACAACTCCACTCGAGACGGTCACCAGTG	scDb-scFv cloning primer
198	HER2 VL fwd	AAAAAGAAGACGGTTCAGACATCCAGATGACCCAGTC	scDb-scFv cloning primer
199	HER2 VL rev	AAAAAGAAGACGGTACCCTTGATCTCGACCTTCGTTC	scDb-scFv cloning primer
200	scDb fwd seq	GCAGTACATCAATGGGCGTG	sequencing primer
221	EGFR HA His rev	AAAAATCTAGATTAGTGATGGTGATGATGGTGGCCGCTGCTGCCGGCGTAGTCGG	Editing of BiTE-EGFR to HA-His Tag

		GCACGTCGTAGGGGTAGGCGGCCGCTTTAATTTCCAG	
222	Il13ra2_vh_fwd	AAAAAGAAGACAAGGGAGCCAAGTCCAGCTGGTGCAG	scDb-scFv cloning primer
223	Il13ra2_vh_rv	AAAAAGAAGACAACGCCAGAGCTAACGGTCACG	scDb-scFv cloning primer
224	Il13ra2_vl_fwd	AAAAAGAAGACGGATCAGACATCCAGATGACACAGAGC	scDb-scFv cloning primer
225	Il13ra2_vl_rv	AAAAAGAAGACGGTACCCTTGATTTCCACCTTGGTGC	scDb-scFv cloning primer
244	BGH Poly A fwd	AAAAATCTAGAATCCAAGTCTTCAGAGATGCATGAAGACCGGCCGGGGCCCGAACAAAAACTCATC	Cloning of BOMcheck
245	BGH Poly A rev	AAAAAGGTACCCCATAGAGCCCACCGCATC	Cloning of BOMcheck
258	IL13_VH_fwd_2	AAAAAGAAGACAAGGGAGCCAAGTCCAGCTGGTGCAGTC	scDb-scFv cloning primer
259	IL13_VH_rev_2	AAAAAGAAGACAACGCCAGAGCTAACGGTCACGGTTG	scDb-scFv cloning primer
260	IL13_VL_fwd_2	AAAAAGAAGACGGATCAGACATCCAGATGACACAGAG	scDb-scFv cloning primer
261	IL13_VL_rev_2	AAAAAGAAGACGGTACCCTTGATTTCCACCTTGGTG	scDb-scFv cloning primer
264	His-Tag_XbaI_rev	AAAAATCTAGATTAGTGATGGTGATGATGGTGG	scDb-scFv to pGL3 insertion
265	BC2_Igk_fwd	AAAAAGAAGACGGAGCTGCCACCATGGAGACAGAC	Cloning primer for Golden Gate Insertion of TCEs into BOMcheck plasmid
266	BC2_His-Tag_rev1	AAAAAGAAGACGGCGGCTTAGTGATGGTGATGATGGTGG	Cloning primer for Golden Gate Insertion of TCEs into BOMcheck plasmid
267	BC2_His-Tag_rev2	AAAAAGAAGACGGATCCTTAGTGATGGTGATGATGGTGG	Cloning primer for Golden Gate Insertion of TCEs into BOMcheck plasmid
276	BOMcheck2_BGH_fwd	GGCAAACAACAGATGGCTGG	Sequencing primer
277	BOMcheck2_SV40_rev	TCACTGCATTCTAGTTGTGGTTTG	Sequencing primer
278	BOMcheck2_CMVe_rev	ATGGAAAGTCCCTATTGGCG	Sequencing primer
279	BOMcheck2_CMV_fwd	AAATGTCGTAACAACTCCGCC	Sequencing primer
280	BOMcheck2_PGK_fwd	TCCCTCGTTGACCGAATCAC	Sequencing primer
281	BOMcheck2_PGK_rev	GGAATTCGATATCAAGCTTCTCG	Sequencing primer
326	SD24-SalI-MluI-rev	CTGTGCGGTATTTCACACC	Recloning of pSD24 MluI-SalI to pSD24 SalI-MluI
330	SD24-SalI-MluI-fwd_2	AAAAAGCGCGCGTCGACACGCGTCCCATTTTAAGAAAACTACAATTCCC	Recloning of pSD24 MluI-SalI to pSD24 SalI-MluI
462	T2A fwd	GCCGCCACCATGGAGACAGACACAC	Cloning primer for generation of T2A-coupled TCEs for insertion into pSD24 shuttle
463	T2A fwd_2	GCCGCCACCATGGAG	Cloning primer for generation of T2A-coupled TCEs for insertion into pSD24 shuttle
464	T2A rev_1	AGGTCCGGGGTTCTCTTCCACGTCGCCACATGTAAGCAGGCTGCCTCTGCCTTCGCCGCTGCCGTGATGGTGATGATGGTGG	Cloning primer for generation of T2A-coupled TCEs for insertion into pSD24 shuttle

465	T2A rev_2	AAAAAACCGGTGGAACCTGGAACCCA GAGCAGCAGTACCCATAGCAGGAGTGT GTCTGTCTCCATGCTGCCAGGTCCGGG GTTCTCTTC	Cloning primer for generation of T2A-coupled TCEs for insertion into pSD24 shuttle
497	BEHH_prox_rev	GCTGCCAGAGCCAGAAAA	sequencing primer for BEHH/SMMH T2A constructs
498	SMMH_prox_rev	CCAGTAGCTGGTGAAGGTGT	sequencing primer for BEHH/SMMH T2A constructs
520	CD3_fwd	CTTCACAATCAGCAGCCTCC	sequencing primer
521	scFv-EGFR fwd	AAAAAGAAGACGGACCGGTGAAGTGC AGCTGGTTGAAAG	recloning of scFv-scDbs
522	scFv-EGFR rev	AAAAAGAAGACGCTCCCGCCTCCACCT GAACCTCCGGCGGCCGCTTTAATTTCCA GTTTGGTGC	recloning of scFv-scDbs
523	Igk-leader rev	AAAAAGAAGACCGCGGTGGAACCTGG AACCCAG	recloning of scFv-scDbs
524	scDb-HER2 fwd	AAAAAGAAGACCCGGGAGCGAAGTGC AGCTCGTCGAAAG	recloning of scFv-scDbs
527	scFv-IL13Ra2 fwd_2	AAAAAGAAGACGGACCGGTCAAGTCC AGCTGGTGC	recloning of scFv-scDbs
528	scFV-IL13Ra2 rev_2	AAAAAGAAGACGCTCCCGCCTCCACCT GAACCTCCGGCGGCCGCCTTGATTTCC ACCTTGG	recloning of scFv-scDbs

2.1.11 Instruments

Table 11 List of instruments.

Centrifuges	Eppendorf 5910R, 5810R, 5430R and 5424R Thermo Fisher Scientific Sorvall Lynx 6000 with rotor FibreLite F12-6x500-Lex Thermo Fischer Scientific Sorvall xW80+ Ultra with rotor THP6-4660, Nippon genetics mini centrifuge
Cytometers	BD CantoII, BD Fortessa
Electroporator	Bio-Rad MicroPulser
Gel documentation	Bio-Rad ChemiDoc, Bio-Rad Gel Doc EZ, Herolab UVT-22 BE-LED
Gel electrophoresis	VWR PerfectBlue power supply, Bio-Rad PowerPac Basic
Incubators	Infors HT Minitron, Thermo Fisher Scientific Heracell 150i and 240i
Magnetic stirrer	Starlab
Microscopes	Zeiss Axiovert 40C and Axiovert A1
Nanodrop	DeNovix DS-11, Thermo Fisher Scientific ND 1000
Orbital shaker	Heidolph Unimax 1010
pH-Meter	ph50 Violab Benchmeter
Plate Readers	Thermo Fisher Scientific Multiskan SkyHigh Spectrophotometer, Perkin Elmer Victor3 1420 Multilabel Counter
Scale	OHAUS Scout™ SKX
Thermomixer	Starlab Mixer HC
Timer	Annoying lab timer
Vortex	Bender & Hobein

2.1.12 Software and Online Tools

Table 12 List of software and online tools.

ApE	Plasmid Editor
BD FACS Diva	Cytometer Operating Software
Benchling	Plasmid Editor
ClustalW	Multiple Alignment Tool
FlowJo	Flow cytometry analysis software
GraphPad Prism	Data analysis
NEB Tm Calculator	Primer melting temperature calculator
NEBioCalculator	Ligation calculator tool
Perplexity.ai	Conversational search engine
SkanIt	Plate reader operating software

2.2 Cloning Strategies

2.2.1 Polymerase chain reaction

2.2.2.1 Q5 High-Fidelity DNA Polymerase

Polymerase chain reaction (PCR) using Q5 polymerase was employed for all cloning steps. Reactions were set up following manufacturer's instructions for 25 µl reactions and 30 cycles. Annealing temperatures were calculated using NEB Tm Calculator.

2.2.2.2 Taq II Platinum Hot-Start DNA Polymerase

Analytical PCRs were performed with Taq II polymerase, following manufacturer's instructions for 20 µl reactions and 30 cycles.

2.2.3 Transformation of competent E. coli

2.2.3.1 Chemically Competent NEB10 beta

Chemically competent bacteria were thawed on ice for 10 minutes. DNA was added to bacteria, the volume of DNA not exceeding one third of volume of bacterial aliquot. Sample was stored on ice for 30 minutes before 45 second heat-shock at 42 ˚C. Following the heat-shock, bacteria were incubated 5 minutes on ice, then were filled to 1 ml with SOC medium and incubated at 37 ˚C for 45 minutes while shaking. Bacteria were then plated on LB-agar selection plates.

2.2.3.2 Electrocompetent Bacteria

Electrocompetent NEB10 beta or BJ5183 were thawed on ice for 10 minutes. DNA was added to bacteria, the volume of DNA not exceeding one third of volume of bacterial aliquot. Bacteria were then transferred to electroporation cuvettes and pulsed with Bio-Rad Micropulser.

Prewarmed SOC medium was added immediately after pulsing, then bacteria were incubated at 37 ˚C for 45 minutes while shaking. Bacteria were then plated on LB-agar selection plates.

2.2.4 DNA preparation

2.2.4.1 Miniprep

5 ml of LB-medium were inoculated with single bacterial colony and incubated at 37 ˚C for 16 h shaking at 200 rpm. After incubation, cultures were spun down for 5 min at 4300 g and subsequently processed using the QIAGEN QIAprep Spin Miniprep Kit following the manufacturer's instructions.

When processing bacteria carrying oAd plasmids, cultures were incubated at 30 ˚C for 24 h. The protocol of the QIAprep kit was adjusted, wherein twice the amount of buffer P2 was used and 1.5 times the amount of P3. Samples were not processed via spin columns, but supernatants of centrifugation after addition of P3 were mixed with 800 µl isopropanol and DNA was precipitated by centrifugation at 17900 g for 30 min at 4 ˚C. DNA pellet was subsequently washed with 500 µl 70 % ethanol. After aspiration of the 70 % ethanol, pellets were dried briefly and pellets were finally reconstituted in TE buffer.

2.2.4.2 Midiprep

100 ml of LB-medium were inoculated with single bacterial colony and incubated at 37 ˚C for 16 h shaking at 200 rpm. After incubation, cultures were spun down at 6000 g for 15 min and pellets were subsequently processed with QIAGEN Plasmid Midi Kit, following the manufacturer's instructions.

When processing bacteria carrying oAd plasmids, 3 ml precultures were inoculated and incubated at 30 ˚C for 8 h shaking at 200 rpm, before being transferred to 500 ml of LB-medium and further incubated as described for 16 h. Cultures were then processed with QIAGEN Plasmid Midi Kit, using twice the amount of P2 and 1.5 times the amount of P3.

2.2.4.3 Maxiprep

3 ml of LB-medium precultures were inoculated with single bacterial colony and incubated for 8 h at 37 ˚C shaking at 200 rpm. Precultures were then transferred to 250 ml of LB-medium and further incubated for 8 h. Cultures were pelleted at 6000 g for 15 min and subsequently processed using the QIAGEN Plasmid Maxi Kit, following the manufacturer's instructions.

2.2.5 Golden Gate Cloning

Golden Gate cloning was used for multifragment plasmid assembly. In a single PCR reaction tube, 2 µl of T4 reaction buffer, 0.5 µl of ATP (10 mM), 0.5 µl of T4 ligase, 1 µl of BbsI, 3 µl of backbone plasmid (75 ng) and insert DNA (3:1 molarity ratio to backbone, calculated with NEBio calculator) were mixed with water in a final volume of 20 µl. Reactions were incubated in PCR cyclers with following settings:

37 ˚C 2.5 - 8 min \
30 cycles
16 ˚C 2.5 - 8 min /
37 ˚C 5 min
65 ˚C 5 min

For scDbs, BiTEs and bidirectional promoters, digestion and ligation steps were set to 2:30 min, for scDb-scFvs the steps were extended to 8 min per cycle. After Golden Gate reaction, 2 µl of reactions were used for transformation of competent bacteria.

2.2.6 Cloning of scDbs

V_H and V_L sequences were amplified from plasmids via PCR using primers with overhangs for Golden Gate cloning (HER2: primers #23; 24; 39; 26, c-MET: primers #19-22, IL13Rα2: primers #43; 45-47). Golden Gate reactions for scDb generation were set up with plasmid pSecTag-scDbXxCD3 and compatible PCR fragments. Miniprep cultures of clones were analyzed via analytic restriction digest and subsequent sequencing of seemingly correct clones with primers #37 or 200 and 38.

For editing the His-Tag of scDbs to Myc-His double tags, primers #48-50 were used to add new tags via primer overhangs.

2.2.7 Cloning of BiTEs

V_H and V_L sequences were amplified from plasmids via PCR using primers with overhangs for Golden Gate cloning (EGFR: primers #59-62, HER2: primers #55-58, c-MET: primers #51-54, IL13Rα2: primers #54; 63-65). Golden Gate reactions for BiTE generation were set up with plasmid pSecTag-scFvhuU3-scFvGG-His and compatible PCR fragments. Miniprep cultures of clones were analyzed via analytic restriction digest and subsequent sequencing of seemingly correct clones with primers #37 or 200 and 38.

For editing the His-Tag of BiTEs to HA-His double tags, primers #48-50 were used to add new tags via primer overhangs.

2.2.8 Cloning of scDb-scFvs

V_H and V_L sequences were amplified from plasmids via PCR using primers with overhangs for Golden Gate cloning (scDb-HER2-scFv-EGFR: primers #23; 24; 39; 26, 192-195, scDb-HER2-scFv-IL13Rα2: primers #23; 24; 39; 26, 258-261, scDb-cMET-scFv-EGFR: primers #19-22, 192-195). Golden Gate reactions for BiTE generation were set up with plasmid pSecTag-scDbXxCD3xX-scFvX and compatible PCR fragments. Miniprep cultures of clones were analyzed via analytic restriction digest and subsequent sequencing of seemingly correct clones with primers #37 or 200 and 38.

2.2.9 Cloning of Bidirectional Promoter Constructs

BGH poly A tail was amplified from scDb expression plasmid with primers #244 and 245, introducing restriction sites for KpnI and XbaI for cloning into psiCheck2 vector and introducing BbsI sites for Golden Gate cloning. Modified psiCheck2 vector was named BOMcheck2 and the correct sequence was confirmed by sequencing with primers #113 and 114. Primers #107-110 were used to create Golden Gate compatible PCR fragments of Renilla and firefly luciferase. mCMV-CMV and mCMV-hPGK1 bidirectional promoter cassette sequences were ordered compatible with Golden Gate cloning.

For cloning of bidirectional promoter constructs with BiTE-EGFR-HA-His and scDb-HER2-Myc-His, TCEs were amplified with primers #265-267.

Golden Gate reactions were set up as described in 2.2.4, with an 8 minute cycler setting.

2.2.10 Cloning of T2A Constructs

Primers #462 and 464 were used to amplify BiTE-EGFR-HA-His and scDb-cMET-Myc-His from pGL3 plasmids. In a subsequent PCR, primers #463 and 465 were used to add T2A peptides and make fragments compatible for cloning into pSD24 shuttle plasmids. PCR fragments were digested with AgeI, as were pSD24-CMV-BiTE-EGFR-HA-His, pSD24-(CMV-BiTE-EGFR-HA-His)r, pSD24-CMV-scDb-cMET-Myc-His and pSD24-(CMV-scDb-cMET-Myc-His)r. AgeI-digested plasmids were treated with rSAP and ligations were set up with AgeI-digested PCR fragments. Sequence was confirmed via sequencing with primers #96; 104; 279; 497 and 498 (after homologous recombination with pVK500F5/3ΔE3).

2.2.11 Cloning of Fiber Viruses

TCEs were excised from expression plasmids with NcoI and XbaI and inserted into pGL3-Ad40SA. Next, Ad40SA-TCEs were excised with XhoI and ClaI and inserted into the pF5/3 vector. Finally, homologous recombination with the pVK500Δ24 vector was performed in BJ5183 bacteria. For homologous recombination, 4 µg of pF5/3 plasmids were linearized with PmeI and 1 µg of pVK500Δ24 was linearized with SwaI and incubated with rSAP after digest. DNA was precipitated using 500 mM LiCl. A 2.5 fold volume of EtOH was added and DNA was precipitated by centrifugation at max rpm at 4 °C for >20 min. Supernatant was aspirated and pellets were washed with 70% EtOH. DNA was reconstituted in ddH_2O. For recombination, 100 ng of pVK500 plasmid and 600 ng of pF5/3 plasmids were used.

2.2.12 Cloning of E4-Viruses

TCEs were excised from expression plasmids with NcoI and XbaI and inserted into pGL3-CMV. scDb-scFvs had to be amplified with primers #200 and 264 before insertion into the pGL3 plasmid. Next, CMV-TCEs were excised with MluI and SalI and inserted into either pSD24-MluI-SalI or pSD24-SalI-MluI. pSD24 plasmids were linearized with PmeI and pVK500F5/3ΔE3 was used undigested. DNA was processed as described in 2.2.10. For homologous recombination, 100 ng of pVK500 plasmid and 500 ng of pSD24 plasmids were used.

2.3 Cell Culture

2.3.1 General Cultivation Techniques

All cells were cultivated in a humidified atmosphere containing 5 % CO2 at 37 °C. All cell lines were cultivated in either RPMI 1640 or DMEM medium supplemented with 10 % FBS. Cell passaging was typically performed every three to four days depending on the confluence. Prior to detachment of the cells by addition of 1x Trypsin-EDTA (37 °C, up to 10 min depending on the cell line), cells were washed with DPBS. Detached cells were resuspended in medium and split as needed. In order to count cells using a Neubauer chamber, cell suspensions were mixed 1:2 with trypan blue staining solution to discriminate viable and dead cells. Cells were stored in FBS containing 10 % (v/v) dimethyl sulfoxide at -80 °C after gentle cooling in an isopropanol-filled cryobox. Frozen cells were thawed at 37 °C, resuspended in medium, centrifuged (500 g, 5 min), and cultivated in appropriate medium.

2.3.2 Transfection Techniques

For non-adenoviral plasmids, HeLa cells were transfected with Lipofectamine 2000, following the manufacturer's instructions. For plasmids containing oAd genomes, Lipofectamine 3000 was used to transfect A549 cells, following the manufacturer's instructions. 10 µg of DNA was used for transfection of oAd genomes in T25 flasks.

2.3.3 Eukaryotic Protein Production

For production of recombinant antibodies, 225 µg of expression plasmids were used to transfect HEK293 (FreeStyle293-F) cells in a final volume of 150 ml. Cultivation and transfection of HEK293 cells was performed by the Antibody Core Facility of the DKFZ.

For production of virally encoded antibodies, five 150 mm cell culture dishes were seeded with A549 cells in DMEM containing 2 % FCS. Cells were infected at an MOI of 1 and kept in culture until CPE was observed for all cells before removing the supernatant for purification.

2.4 Purification of Recombinant Antibodies

2.4.1 Immobilized Metal Ion Affinity Chromatography

Supernatants of transfected FreeStyle-293F cells were dialyzed overnight against PBS using a membrane with a 6-8 kDa molecular weight cut-off. Supernatants were then incubated with 0.5 ml of equilibrated Ni-NTA agarose beads rolling for 4 hours at 4 °C. The protein solution was then centrifuged at 2000 g for 5 min and approximately 3 ml of supernatant were left on the beads for resuspension. Resuspended beads were then loaded on polyprep columns. Beads were washed with IMAC wash buffer until Bradford test (90 µl 1x bradford solution + 10 µl flow-through) was no longer positive. Protein was eluted with IMAC elution buffer in fractions of 200 µl. The fractions with high protein concentration (Bradford test) were pooled and dialyzed overnight against PBS with a membrane with a 10 kDa molecular weight cut-off. Beads were then centrifuged at 11,000 g for 1 min and supernatant was transferred to a fresh tube. For antibodies with a low yield, the antibodies were concentrated on VivaSpin protein concentrator columns for 20 min at 12,000 g at room temperature. The retentate was then transferred to a fresh tube. For long term storage, aliquots of purified antibodies were stored at -20 °C and after thawing, aliquots were centrifuged at 11,000 g for 1 min and supernatant was used.

For purification of virally encoded antibodies, supernatants of infected A549 cells were used.

2.5 Biochemical Characterization of Recombinant Antibodies

2.5.1 Measurement of Protein Concentration

Protein concentration was determined via spectrophotometer measuring absorption at 280 nm, inputting molecular weight and extinction coefficient ε. Parameters were extracted using the online tool ProtParam by inputting the amino acid sequence without the Igκ leader sequence.

2.5.2 SDS-PAGE

For sodium dodecyl sulfate-polyacrylamide gel electrophoresis (SDS-PAGE), 1 µg of protein was used per sample. Proteins were incubated at 95 °C for 5 minutes in 1x Laemmli buffer containing 10 % β-mercaptoethanol. Proteins were subsequently loaded on 12 % Mini-PROTEAN TGX Stain-Free gels and electrophoresis was performed at 40 mA constant current for approximately 30 min. After electrophoresis, gel was boiled once in dH_2O and then stained with coomassie blue solution for approximately 1 h on an orbital shaker. Afterwards, excessive staining was removed by incubation in dH_2O with a laboratory wipe for 30-60 min. Gels were then imaged with Bio-Rad ChemiDoc.

2.5.3 Analytical Size-Exclusion Chromatography

Size-exclusion chromatography (SEC) was performed by the Kontermann group in Stuttgart via high performance liquid chromatography (HPLC).

2.6 Flow Cytometry

2.6.1 Determination of Antigen Expression on Tumor Cells

Cells were detached and counted using Neubauer chambers. $1*10^5$ cells were used per sample and resuspended in FACS buffer. They were seeded in V-bottom 96-well plates and pelleted at 500 g for 3 min at 4 °C. Supernatant was discarded by flicking. Cells were then incubated with dilutions of primary antibodies (0.4 nM in FACS buffer) for 45-60 min at 4 °C. Cells were then centrifuged as before and washed once with FACS buffer by addition of 150 µl FACS buffer, resuspension and centrifugation as before. Secondary antibody APC-anti-IgG Fc was added in a 1:200 dilution in 100 µl FACS buffer and cells were resuspended and incubated in the dark at 4 °C for 20-30 min. The cells were washed once as before and were then resuspended in 100 µl FACS buffer containing 4',6-diamidino-2-phenylindole (DAPI, at 5 µg/ml) and incubated in the dark for 5 min at 4 °C. The cells were then washed twice as before and resuspended in 100

µl FACS buffer. The cell suspensions were then transferred to 5 ml round-bottom tubes with cell strainer caps for analysis.

2.6.2 Binding Studies

TCE concentrations were measured and 5-fold dilution series starting with 20 nM were prepared. Cells were processed using TCEs as primary antibodies, the protocol is described in 2.6.1. When detecting TCEs in supernatants, the secondary antibodies were specific for His-tags when detecting a single TCE and specific for HA- and Myc-tags when detecting scDbs and BiTEs in a single sample. When virus supernatants were used, an additional fixation step was performed. After the DAPI staining, cells were washed once and then resuspended in FACS buffer containing 1 % paraformaldehyde (PFA) and incubated at 4°C for 10 min. The cells were then washed twice and resuspended in 100 µl FACS buffer.

2.7 Purification and Titration of Recombinant Oncolytic Adenoviruses

2.7.1 Purification of Viral Particles

A549 cells were transfected with plasmids encoding oAd genomes in T25 tissue culture flasks, as described in 2.3.2. Cells were harvested when most cells showed signs of cytopathic effect (CPE). Three freeze-thaw cycles were conducted with the cell suspensions and half of the cell suspension was used to infect three 150 mm dishes of A549 cells in DMEM with 2 % FCS. After three days, cells were harvested by resuspending the medium on the cells. The cell suspensions were centrifuged in 50 ml falcon tubes and the pellets were resuspended in 3 ml of the supernatant. The cell suspension was then frozen and thawed three times and centrifuged at 4000 g for 15 min at 4 °C. The supernatant was distributed to three tubes. One tube was used to infect A549 cells in 24 150 mm dishes in DMEM with 2 % FCS. After 48 h, cells were detached by pipetting and distributed to 8 50 ml falcon tubes. Cell suspensions were centrifuged for 5 min at 300 g, the supernatant was removed and pellets were resuspended in a total of 5 ml DPBS. Three freeze-thaw cycles were performed with the cell suspension and it was subsequently centrifuged at 4000 g for 15 min at 4 °C. The supernatant was taken and brought to a total volume of 8 ml with DPBS. Two ultracentrifuge tubes were prepared with 3 ml CsCl solution (ρ = 1.41 g/ml) overlayed with 5 ml CsCl solution (ρ = 1.27 g/ml). The virus-containing supernatant was pipetted on top of the gradients and ultracentrifugation was performed at 175,000 g for 1:30 h at 4 °C without deceleration. After centrifugation, bands containing viral particles were removed using a 5 ml syringe with a G20 needle (approximately 1 ml). The virus-

containing suspension was transferred to a new ultracentrifugation tube and filled up with CsCl solution (ρ = 1.34 g/ml). Ultracentrifugation was performed at 175,000 g, >18 h at 4 °C without deceleration. The band containing viral particles was removed as before and transferred to a fresh 5 ml Eppendorf tube. The volume was brought to a total of 2.5 ml with DPBS. A PD-10 desalting column was equilibrated with 25 ml DPBS and the virus suspension was loaded onto the column. Virus was eluted in 3 fractions with DPBS (0.5 ml, 2 ml, 0.5 ml). 200 µl of glycerol were added to the 2 ml fraction and aliquots were prepared and stored at -80 °C.

2.7.2 Physical Titer Measurement

Purified viruses were diluted with virus lysis buffer and blanks were prepared in parallel with DPBS and virus lysis buffer. Samples were then incubated at 56 °C for 10 min while shaking. After incubation, absorbance at 260 nm (DNA) was measured via spectrophotometer, measuring each sample with its corresponding blank. Physical virus titers were calculated based on oAd genome size, calculating the genome copies.

2.7.3 $TCID_{50}$ Assay

Tissue culture infective dose 50 assays were performed with purified viruses. A549 cells were seeded in 96-well plates in 100 µl DMEM containing 2 % FCS at 5 x 10^3 cells per well and incubated overnight. 10-fold dilutions were prepared of virus stocks in DMEM containing 2 % FCS. 10^{-6} to 10^{-13} dilutions were added to wells in 10 replicates per dilution. Two independent dilution series were performed for each virus. After 21 days, all wells with visible CPE were counted. TCID50/ml was calculated as $10x10^{1+1(S-0.5)}$, with S being the sum of ratios of positive wells for each dilution, starting at 10^{-1}.

2.8 Cytotoxicity Assays

2.8.1 Isolation of PBMCs from Buffy Coats

Blood from buffy coats was diluted with an equal volume of DPBS. 15 ml Histopaque®-1077 were pipetted in a 50 ml falcon tube and overlayed with 25 ml of the diluted blood. The samples were subsequently centrifuged at 800 g for 25 min at room temperature, with acceleration set to 3 and deceleration set to 1. After centrifugation, the layer containing the PBMCs was aspirated and transferred to fresh 50 ml tubes. The tubes were filled with DPBS and the cell suspension was centrifuged at 400 g for 10 min at room temperature, with normal acceleration and brake settings. The supernatant was discarded and cells were resuspended in DPBS, filling the tube after resuspension. Cells were centrifuged at 300 g for 5 min and wash step was

repeated a third time. Cells of all tubes were then resuspended and pooled in 50 ml DPBS, counted and adjusted to preferred density for freezing, typically 4 x 10^7 cells / ml in RPMI + 10 % FCS medium. 2x freezing medium was prepared, consisting of FCS with 20 % DMSO. Freezing medium was added dropwise to cell suspension (equal volume) while swirling. After addition of freezing medium, the cell suspension was rapidly distributed to cryovials and transferred to -80 °C in a freezing container overnight, before final storage in liquid nitrogen.

2.8.2 Cocultures of Tumor Cells with PBMCs and T-cell Engagers

Target cells were seeded in 96-well plates at 1.5-2 x 10^4 cells per well in medium containing 10 % FCS and incubated overnight. PBMCs were thawed and seeded in a 150 mm dish and incubated overnight. The next day, PBMCs were rinsed from the plate, counted and adjusted to a cell number corresponding to an effector to target cell ratio of 10:1 in medium containing 1 % penicillin / streptomycin (P/S). 4-fold dilution series were prepared for TCEs in 1 % P/S medium. Medium was removed from cells and replaced by 100 µl of TCE dilution. 100 µl of PBMC suspension were added on top. After 3 days of incubation, medium was removed from wells and replaced by 50 µl crystal violet solution. After incubation for approximately 30 min, crystal violet was removed and wells were washed by repeated immersion into dH_2O. Wells were dried and crystal violet was dissolved with 10 % acetic acid for measuring absorption at 570 nm for quantification.

2.8.3 Cytotoxicity Assays with Tumor Cells and oAds

Target cells were seeded in 48-well plates at 1.5-2.5 x 10^4 cells per well in medium containing 2 % FCS and incubated overnight. Serial dilutions of oAds were prepared in medium containing 2 % FCS and added on top of seeded cells. Dilutions were calculated based on $TCID_{50}$ titers. Cells were incubated until CPE could be observed in the lowest multiplicity of infection (MOI) for one virus. Wells were then stained with crystal violet as described in 2.8.2, but instead using 100 µl of crystal violet solution with prior fixation of cells in 4 % PFA.

2.8.4 Cocultures of Tumor Cells with PBMCs and oAds

Target cells were seeded in 96-well plates at 1.5-2 x 10^4 cells per well in medium containing 10 % FCS and incubated overnight. After incubation, medium was removed and replaced with serial dilutions of oAds (100 µl). Plates were then incubated overnight and PBMCs were thawed as described in 2.8.1. After incubation, PBMCs were counted and adjusted to the desired effector cell to target cell ratio and added on top of infected cells in 100 µl medium containing

1 % P/S. After five days of incubation, wells were stained with crystal violet as described in 2.8.2.

2.9 Enzyme-linked Immunosorbent Assay

Enzyme-linked immunosorbent assays (ELISAs) were performed for quantification of IL-2 and IFNγ. Cocultures were set up as described in 2.8.3. Supernatants were taken 24 h after PBMC addition to quantify IL-2 levels and 48 h after PBMC addition to quantify IFNγ levels from a respective 96-well plate. ELISAs were performed with the ELISA MAX™ Deluxe Set Human IL-2 and ELISA MAX™ Standard Set Human IFNγ, following the manufacturer's instructions.

2.10 Luciferase Assay

1.5 x 10^4 HeLa cells were seeded per well in flat-bottom 96-well plates. Transfection was performed with 200 ng DNA as described in 2.3.2 with Lipofectamine 2000. After 24 h, cells were processed with the Promega Dual-Glo® Luciferase Assay System, following the manufacturer's instructions. Luminescence was measured using a plate reader.

2.11 Statistics

Pairwise and multiple comparisons were performed by GraphPad Prism® implemented unpaired t test (two-tailed) and One-Way ANOVA. A p-value of <0.05 was considered statistically significant (*P<0.05; **P<0.01; ***P<0.001)

3. Results

3.1 Cloning, Production and Characterization of Bispecific T-cell Engagers

3.1.1 Biochemical Characterization

In the first part of this thesis, I aimed to generate a panel of scDbs and BiTEs in order to firstly perform an original comparison of the two formats regarding antigen binding and induction of T-cell mediated cytotoxicity, secondly identify scDbs that are suitable as bases for the scDb-based trispecific scDb-scFv and lastly select bispecific TCEs that promise efficacy in a viro-antibody-therapy approach. As targets, I chose EGFR, HER2, c-MET and IL13Rα2 due to their implication in various solid tumors, outlined in chapter 1.4. Initially, I designed scDbs in collaboration with the group of Roland Kontermann in Stuttgart. Sequences for V_Hs and V_Ls were based on publicly available IgG sequences.[168-171] Schematic depictions of the molecular structure of the scDb and BiTE format are shown in Figure 9. The scDb-EGFR was already designed and produced at that time by the Kontermann lab and found to be ineffective (data not shown, personal communication).

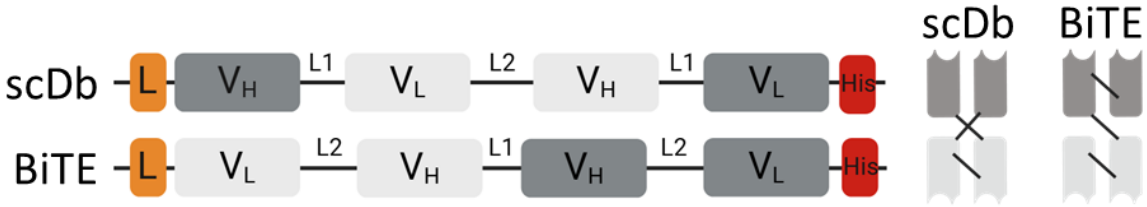

Figure 9 Composition schematic assembly of the scDb and BiTE format. L - Igκ leader; VH - heavy chain; VL - light chain; L1 – GGGGS; L2 - $(GGGGS)_3$; His - 6x Histidine-Tag.

In light of this result, I decided to design, clone and produce both scDbs and BiTEs for each TAA, with the exception of EGFR, where only the BiTE was produced. The final panel of bispecific TCEs is schematically shown in Figure 10.

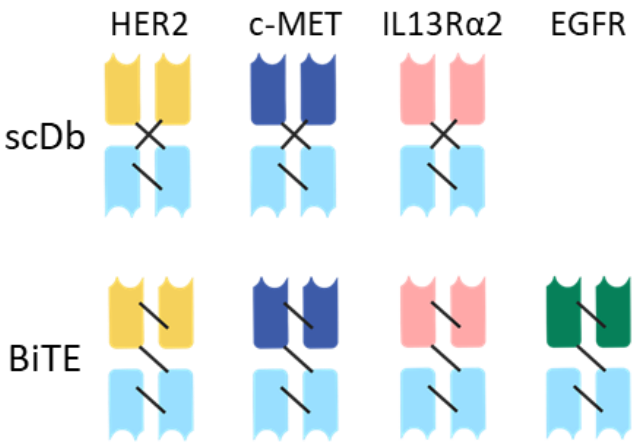

Figure 10 Panel of bispecific TCEs.

I cloned all expression plasmids encoding the bispecific TCEs using the Golden Gate method described in chapters 2.2.6 and 2.2.7 with plasmids for backbones and V_H/V_L inserts kindly provided by the Kontermann lab. I verified all plasmids by restriction digest and sequencing of seemingly correct clones. I amplified correctly sequenced plasmids by retransformation of correct clones into competent bacteria and preparation of DNA from maxiprep cultures. Transfection and cell culture of suspension FreeStyle293-F cell cultures for recombinant antibody production were performed by the Antibody Core Facility of the DKFZ. I purified all constructs from supernatants of transfected cells via immobilized metal ion affinity chromatography (IMAC), as described in chapter 2.4.1. For all bispecific TCEs, I obtained yields sufficient for all characterization assays and with 260/280 ratios between 0.48 and 0.56. The 260/280 ratios and concentrations of purified antibodies are listed in Table 13.

Table 13 Purity and concentration of purified scDbs and BiTEs.

		scDb-HER2	scDb-cMET	scDb-IL13Rα2
260/280		0,54	0,55	0,56
mg/ml		0,26	0,64	0,48
	BiTE-EGFR	**BiTE-HER2**	**BiTE-cMET**	**BiTE-IL13Rα2**
260/280	0,51	0,53	0,54	0,48
mg/ml	1,25	0,42	0,35	0,59

To further verify the purity of the constructs, I conducted an SDS-PAGE analysis. The results are shown in Figure 11. The SDS-PAGE showed clean bands at the expected sizes, with only very faint bands indicating a low degree of fragmentation or dimerization for all constructs.

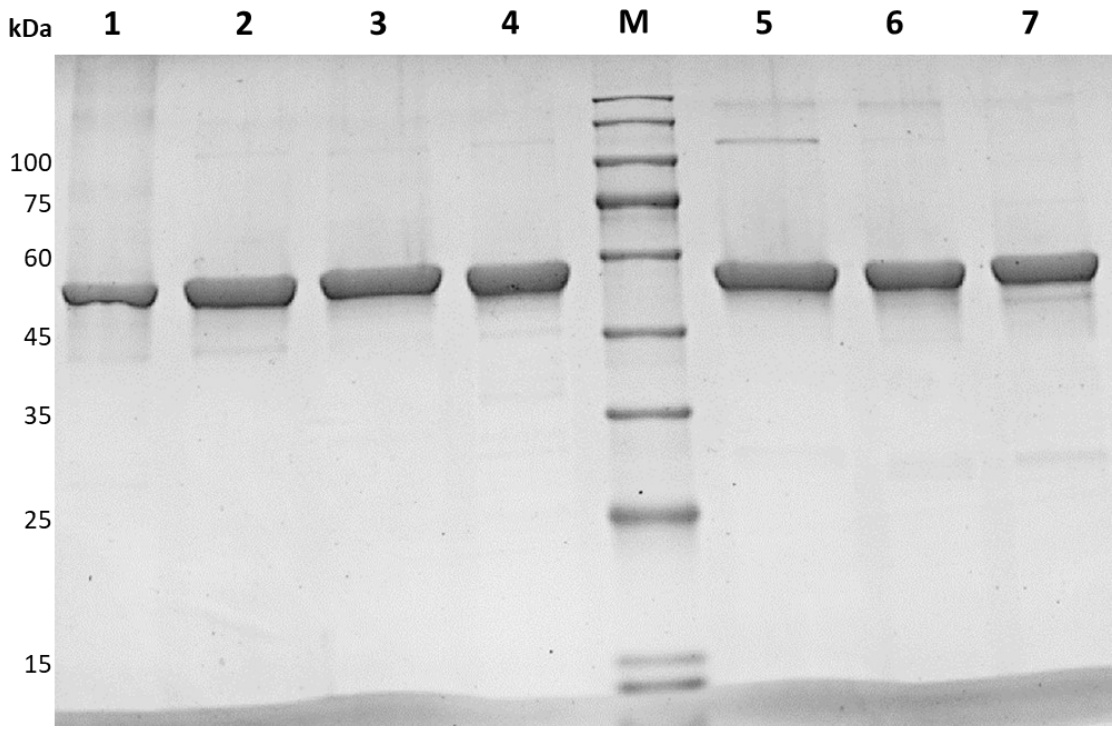

Figure 11 SDS-PAGE analysis of bispecific TCEs. 12% polyacrylamide, 1 µg/lane, Coomassie blue staining under reducing conditions. 1 – BiTE-EGFR; 2 – BiTE-HER2; 3 – BiTE-cMET; 4 – BiTE-IL13Rα2; 5 – scDb-HER2; 6 – scDb-cMET; 7 – scDb-IL13Rα2; M – marker.

3.1.2 Binding Analysis

After verifying the integrity of all bispecific TCEs, I conducted flow cytometric analysis to compare binding properties of scDbs and BiTEs. In order to find suitable cell lines for analysis, I screened various tumor cell lines with IgG antibodies for expression of EGFR, HER2, c-MET and IL13Rα2. The expression profiles of cell lines used for TCE characterization are shown in Figure 12.

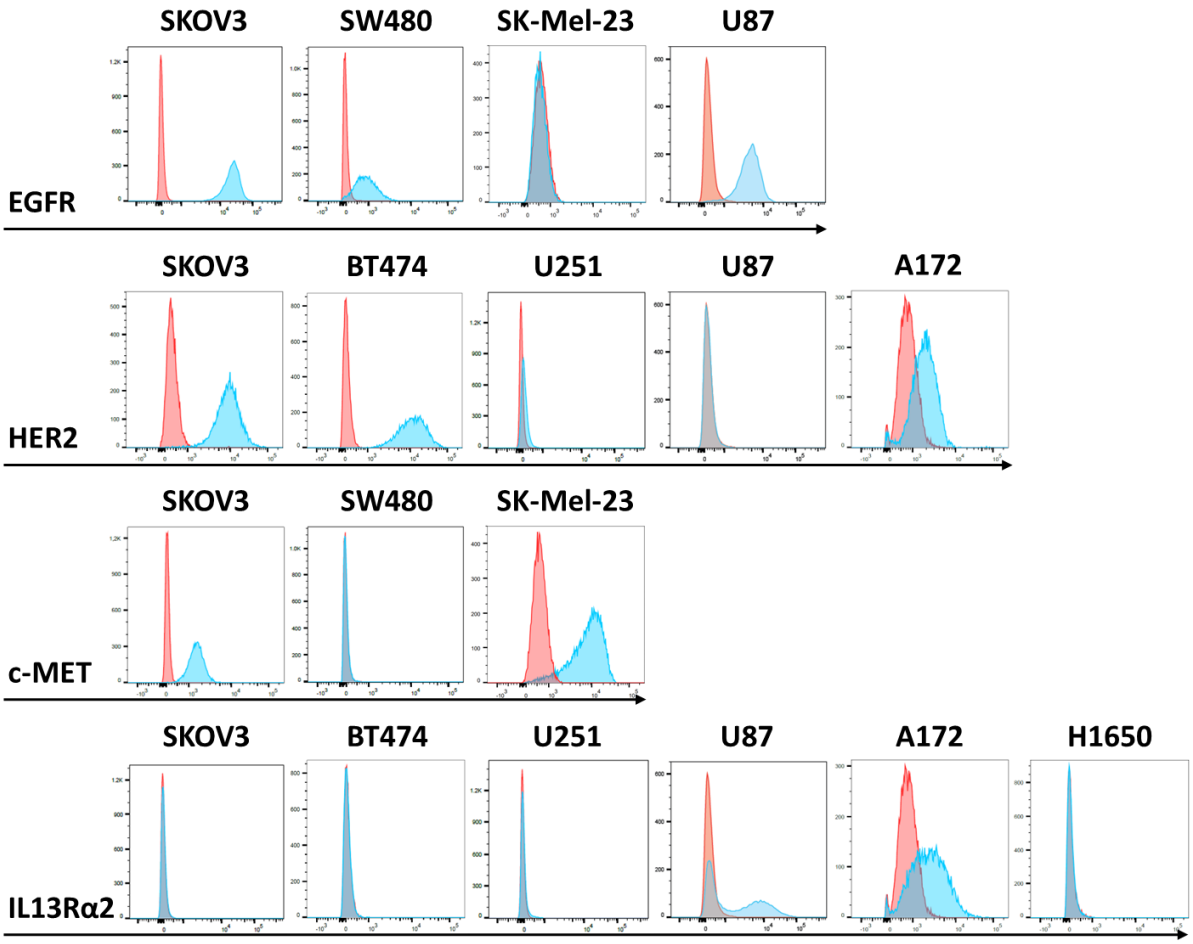

Figure 12 Flow cytometric analysis of antigen expression on target cells. Target cells were incubated with 0.4 nM of IgGs specific for either EGFR, HER2, c-MET or IL13Rα2. Binding was detected via flow cytometry using APC-anti-IgG Fc mAb (blue). An isotype control in the same concentration (red) was used as a reference. Data shown as histogram of fluorescence intensity (x-axis) and cell count (y-axis).

I performed a binding analysis on target and non-target cancer cells and $CD3^+$ Jurkat T-cells. I incubated target cells with serial dilutions of TCEs and measured fluorescence intensity via flow cytometry using a secondary detection antibody, as described in detail in chapter 2.6.2. Binding curves are shown in Figure 13. Analysis revealed binding of all TCE constructs to their respective target cells. I calculated half maximal effective concentration (EC_{50}) values for binding curves using the GraphPad Prism software and found slightly lower EC_{50} values for all scDbs compared to BiTEs, albeit with an n=1, as listed in Table 14. No unspecific binding was detected. Binding to Jurkat T-cells was very similar between scDbs and BiTEs.

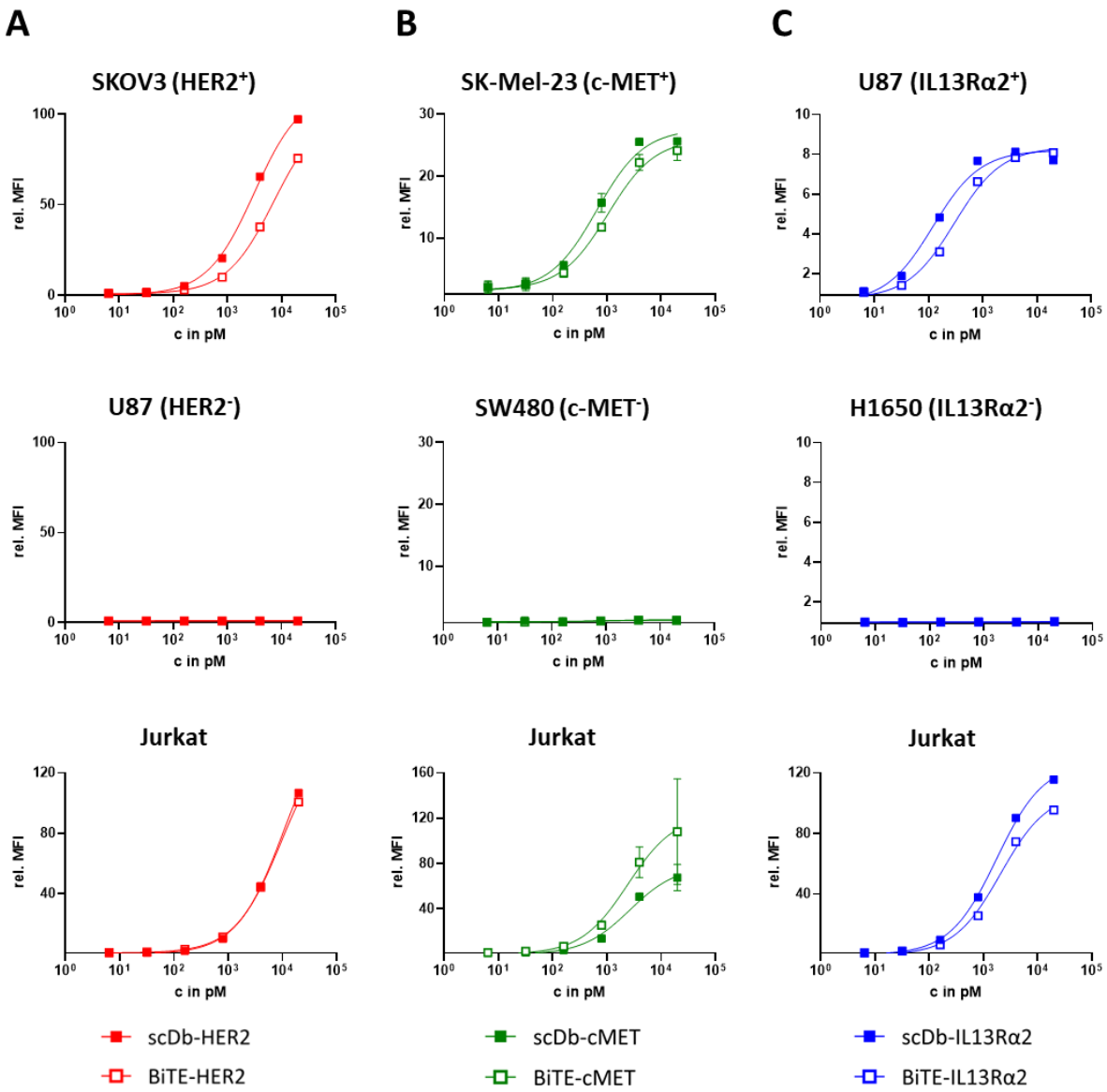

Figure 13 Binding analysis of bispecific TCEs. Comparison of binding strength and specificity of bispecific scDb and BiTE formats for A) scDb-HER2 & BiTE-HER2, B) scDb-cMET & BiTE-cMET, C) scDb-IL13Rα2 & BiTE-IL13Rα2 on target cells, non-target cancer cells and Jurkat T-cells. Binding properties were analyzed via flow cytometry, bound protein was detected using PE-anti-His mAb. Relative MFI (rel. MFI) shown (n=1) for A and C, rel. MFI shown as mean ±SD (n=2) for B. Ranges of y-axes were adjusted to fit the data.

Table 14 EC_{50} values of binding analysis of bispecific TCEs. EC_{50} values were calculated using GraphPad Prism software by a dose-response nonlinear regression with a variable slope. Values listed in nM.

	HER2	c-MET	IL13Rα2
scDb on target-cell	3.13	6.55	0.12
BiTE on target-cell	7.13	10.43	0.3
scDb on Jurkat	10.71	2.65	1.77
BiTE on Jurkat	9.79	2.45	2.1

The next step in the characterization of bispecific antibodies was to analyze induction of T-cell mediated cytotoxicity. I titrated the TCEs in cocultures of tumor cells and PBMCs and determined tumor cell viability. The viability curves are shown in Figure 14, with corresponding EC_{50} values in Table 15. scDb-HER2 and BiTE-HER2 both showed potent induction of cytotoxicity on $HER2^+$ SKOV3 cells, with both constructs inducing the same maximum cytotoxicity. The EC_{50} value of BiTE-HER2 was significantly lower than that of scDb-HER2. None of the HER2-constructs induced visible cytotoxicity on $HER2^-$ U87 cells (Figure 14A). The c-MET constructs performed almost identically on c-MET^+ SKOV3 cells, with no significant difference between EC_{50} values. On c-MET^- SW480 cells, both scDb-cMET and BiTE-cMET showed some induction of cytotoxicity, slightly lower in case of scDb-cMET (Figure 14B). In the case of scDb-IL13Rα2, it showed significantly lower induction of cytotoxicity on $IL13R\alpha2^+$ U87 cells compared to the BiTE-IL13Rα2. Additionally, the minimum viability of tumor cells in cocultures with scDb-IL13Rα2 was visibly higher than that of cocultures with BiTE-IL13Rα2 (42.87% vs 23.84%, respectively), as shown in Figure 14C. In higher concentrations, both constructs induced cytotoxicity on $IL13R\alpha2^-$ H1650 cells.

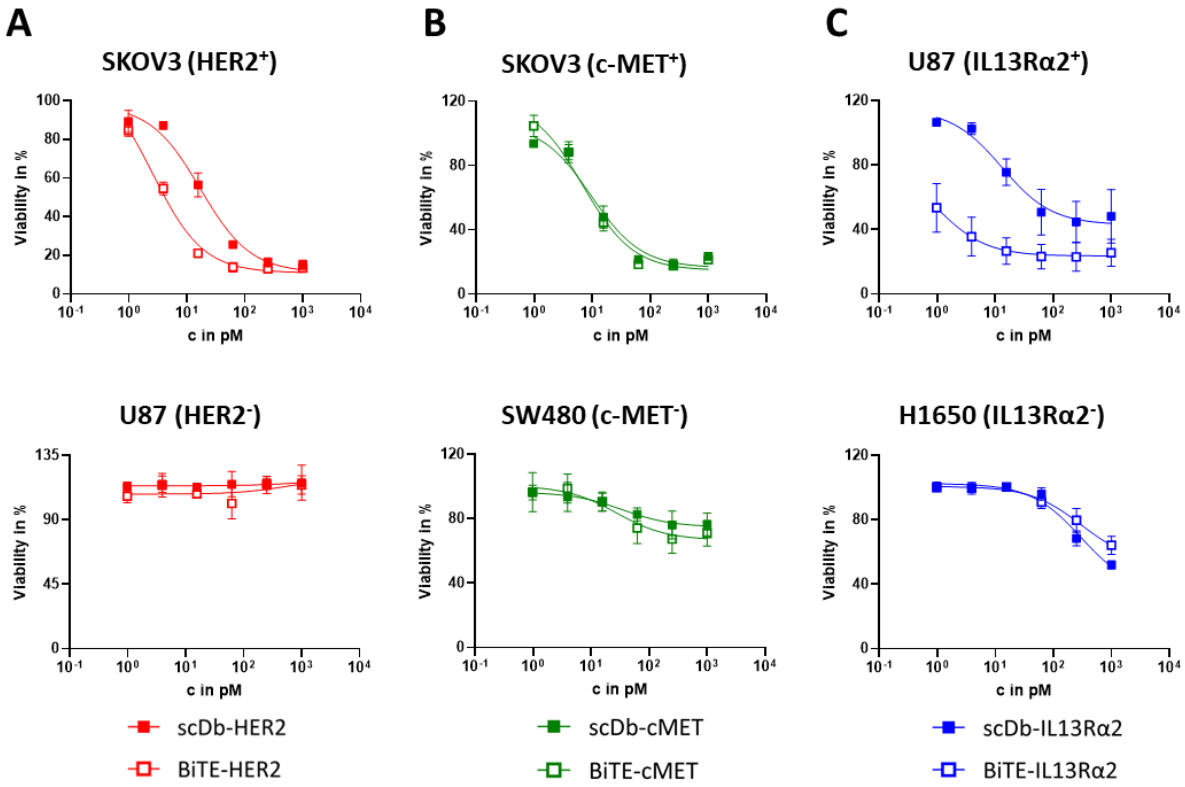

Figure 14 Induction of T-cell mediated cytotoxicity by bispecific TCEs. Cells were incubated with serial dilutions of A) scDb-HER2 & BiTE-HER2, B) scDb-cMET & BiTE-cMET, C) scDb-IL13Rα2 & BiTE-IL13Rα2. PBMCs were added in an effector:target cell ratio of 10:1. Cell viability was measured 3 days after PBMC addition using crystal violet staining and subsequent quantification. Data shown as mean ± SD, (n=3 donors, each determined in three independent experiments). Ranges of y-axes were adjusted to fit the data.

Table 15 EC_{50} values of bispecifics on target cells in cocultures. EC_{50} values were calculated using GraphPad Prism software by a dose-response nonlinear regression with a variable slope. Mean of 3 donors in pM, **P < 0.01, unpaired t test.

	HER2	c-MET	IL13Rα2
scDb on target-cell	17.05]**	9.52	12.99]**
BiTE on target-cell	2.58	6.86	0.93

In summary, I was able to produce scDbs and BiTEs targeted against HER2, c-MET and IL13Rα2, respectively. All TCEs bound their respective targets selectively with only slight differences between scDbs and BiTEs. Cytotoxicity analysis revealed a clear deficit of the scDb-IL13Rα2 compared to the BiTE-IL13Rα2, with lower maximum cytotoxicity. The BiTE-HER2 also outperformed its corresponding scDb, but the maximum cytotoxicity was equal. cMET-binding TCEs performed equally well.

3.2 Cloning, Production & Characterization of Trispecific T-cell Engagers

In order to generate trispecific TCEs that can be used for targeting of two different TAAs with a single molecule, I decided to utilize the scDb-based scDb-scFv format that has only been described as a bispecific, trivalent TCE to date[48], but can readily be designed as a trispecific, trivalent TCE. Based on the results of the cytotoxicity data of the bispecific antibodies, I decided to clone three different scDb-scFvs. Since the scDb-EGFR was already excluded by the Kontermann lab, only the scDbs -HER2, -cMET and -IL13Rα2 were possible candidates for scDb bases of the scDb-scFv constructs. The scDb-IL13Rα2 was significantly inferior to the BiTE-IL13Rα2 and was therefore also disregarded as a base for a possible scDb-scFv construct. Even though the scDb-HER2 also presented a significantly higher EC_{50} value on $HER2^+$ SKOV3 cells compared to the BiTE-HER2, it reached the same maximum cytotoxicity at higher concentrations and was therefore chosen as a base for scDb-scFvs. I selected scDb-HER2-scFv-EGFR, scDb-cMET-scFv-EGFR and scDb-HER2-scFv-IL13Rα2 for cloning and production. The molecular structure of the scDb-scFv format is depicted in Figure 15.

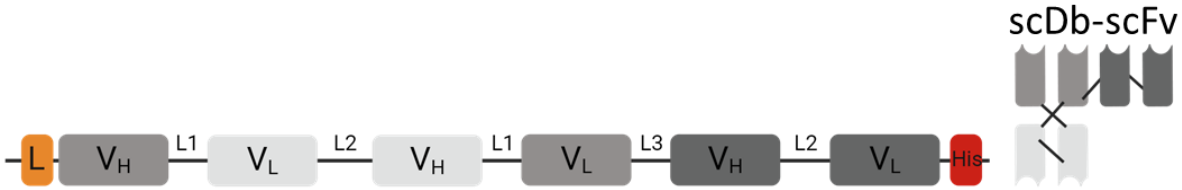

Figure 15 Composition and schematic assembly of the scDb-scFv format. L - Igκ leader; VH - heavy chain; VL - light chain; L1 – GGGGS; L2 - $(GGGGS)_3$; L3 – AAAGGSGGGGS; His - 6x Histidine-Tag.

I cloned the expression plasmids of scDb-scFvs using the same V_H and V_L sequences used for the cloning of scDbs and BiTEs. I verified plasmid sequences via restriction digest, followed by sequencing of seemingly correct clones. After transfection and suspension cell culture of Freestyle-293F by the Antibody Core Facility, I purified scDb-HER2-scFv-EGFR, scDb-HER2-scFv-IL13Rα2 and scDb-cMET-scFv-EGFR, the scDb-scFv panel is schematically shown in Figure 16.

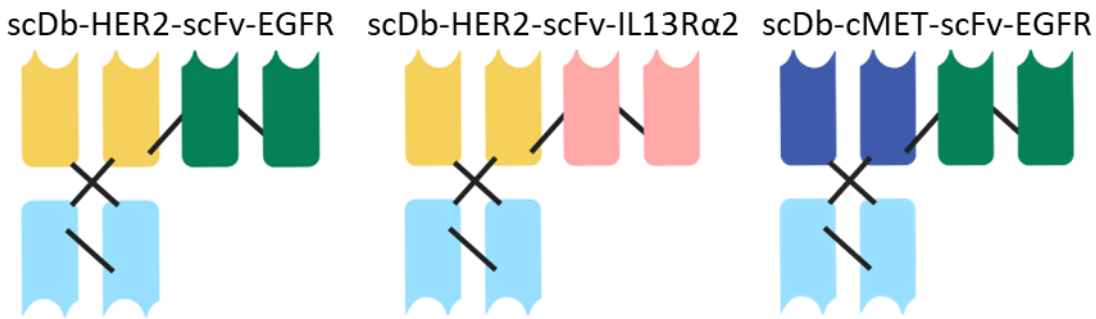

Figure 16 Panel of trispecific TCEs. Schematic depictions of scDb-HER2-scFv-EGFR, scDb-HER2-scFv-IL13Rα2 and scDb-cMET-scFv-EGFR. Light blue – CD3-binding domain; yellow – HER2-binding domain; green – EGFR-binding domain; salmon – IL13Rα2-binding domain; dark blue – c-MET-binding domain.

The yield of scDb-scFvs was generally lower than for the bispecific TCEs, I therefore concentrated all scDb-scFvs using Vivaspin protein concentrator columns. Concentrations and purities after concentration are listed in Table 16.

Table 16 Purity and concentrations of purified and concentrated scDb-scFvs.

	scDb-HER2-scFv-EGFR	scDb-cMET-scFv-EGFR	scDb-HER2-scFv-IL13Rα2
260/280	0,58	0,54	0,55
mg/ml	0,41	0,66	0,37

I analyzed purity and integrity of each scDb-scFv via SDS-PAGE. I used scDbs and BiTEs as controls, the scDbs (scDbs -HER2 and -cMET) corresponding to the scDb bases of the trispecific TCEs and the BiTEs (BiTEs -EGFR and -IL13Rα2) corresponding to the CD3 x scFv parts of the trispecifics. The results of the SDS-PAGE analysis are shown in Figure 17A. In addition to the SDS-PAGE, an analytic size-exclusion HPLC was performed for all constructs by the Kontermann lab. The results are shown in Figure 17B. For all bispecific TCEs, single, distinctive peaks were seen for all constructs. For the scDb-scFvs, a single, clean peak was seen for scDb-cMET-scFv-EGFR. scDb-HER2-scFv-EGFR and scDb-HER2-scFv-IL13Rα2 both exhibited a peak with a lower molecular weight shoulder, indicating possible fragmentation.

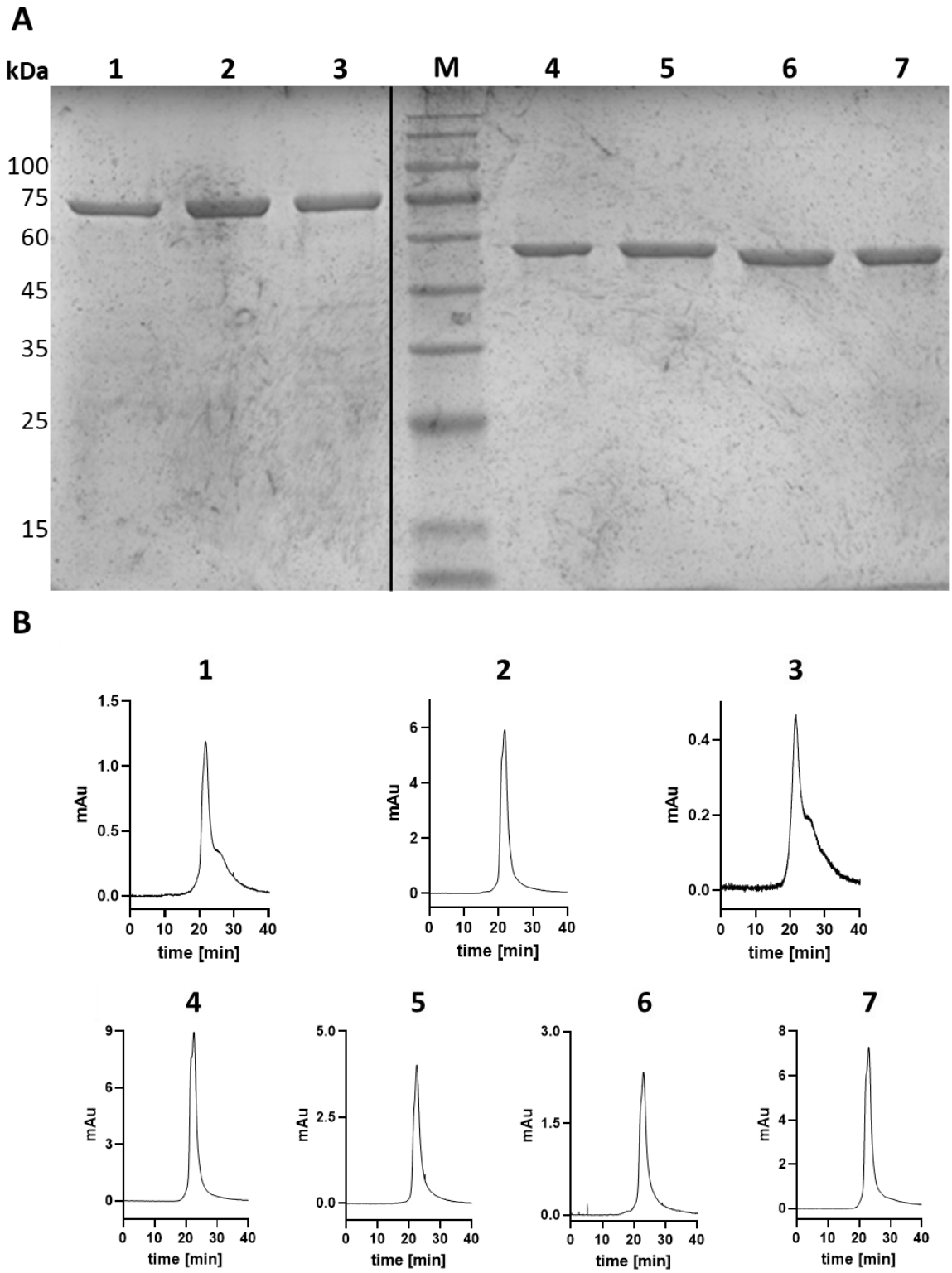

Figure 17 Biochemical characterization of trispecific scDb-scFvs and corresponding controls. A) 12 % polyacrylamide gel, 1 µg/lane, Coomassie blue staining under reducing conditions. B) Size-exclusion HPLC under native conditions (kindly provided by Oliver Seifert and Roland Kontermann, Stuttgart University). Elution times of proteins corresponding to molecular masses are indicated. 1 - scDb-HER2-scFv-EGFR; 2 - scDb-cMET-scFv-EGFR; 3 - scDb-HER2-scFv-IL13Rα2; 4 - BiTE-EGFR; 5 - BiTE-IL13Rα2; 6 - scDb-HER2; 7 - scDb-cMET; M - Marker.

Next, I analyzed the binding properties of the trispecific constructs via flow cytometry (as described for bispecific TCEs), directly comparing them to their corresponding bispecific controls. For each scDb-scFv, binding of each of the three antigen-binding domains was

analyzed and additionally, bivalent binding of TAA-binding domains was measured. The results are displayed in Figure 18 and Table 17.

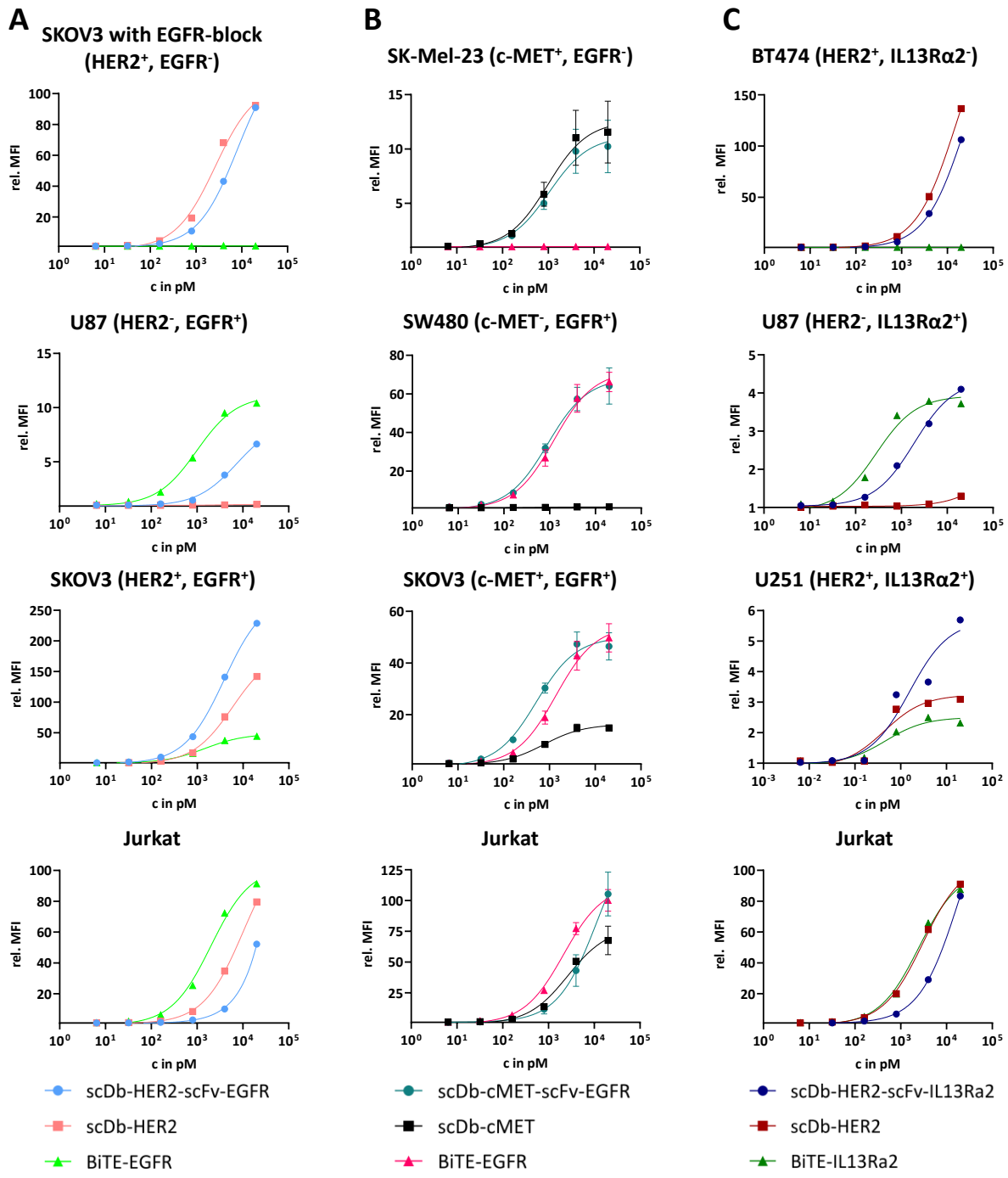

Figure 18 Binding analysis of trispecific scDb-scFvs and corresponding bispecific scDb and BiTE controls. Comparison of scDb-scFv binding to binding of bispecific controls to single and double target-positive cell lines in addition to Jurkat cells. A) scDb-HER2-scFv-EGFR vs scDb-HER2 & BiTE-EGFR on SKOV3 preincubated with Cetuximab to block EGFR binding sites, U87, SKOV3 and Jurkat cells. B) scDb-cMET-scFv-EGFR vs scDb-cMET & BiTE-EGFR on SK-Mel-23, SW480, SKOV3 and Jurkat cells. C) scDb-HER2-scFv-IL13Rα2 vs scDb-HER2 & BiTE-IL13Rα2 on BT474, U87, U251 & Jurkat cells. Binding properties were analyzed via flow cytometry, bound protein was detected using PE-anti-His mAb. Relative MFI (rel. MFI) shown (n=1) for A and C, rel. MFI shown as mean ±SD (n=2) for B.

Table 17 EC_{50} values of binding analysis of scDb-scFvs and controls on target and Jurkat cells in nM. EC_{50} values were calculated using GraphPad Prism software by a dose-response nonlinear regression with a variable slope.

		scDb-scFv	scDb	BiTE
scDb-HER2-scFv-EGFR scDb-HER2 BiTE-EGFR	SKOV3 with EGFR-block	8.06	2.65	-
	U87	7.4	-	0.99
	SKOV3	3.87	5.9	1.47
	Jurkat	15.39	10.09	2.01
scDb-cMET-scFv-EGFR scDb-cMET BiTE-EGFR	SK-Mel-23	1.04	0.97	-
	SW480	0.91	-	1.25
	SKOV3	0.52	0.76	1.39
	Jurkat	11.7	2.65	2.14
scDb-HER2-scFv-IL13Rα2 scDb-HER2 BiTE-IL13Rα2	BT474	23.88	15.04	-
	U87	1.91	-	0.28
	U251	1.55	0.44	0.47
	Jurkat	18.73	3.04	2.48

My binding analysis showed that all antigen binding domains of the three scDb-scFvs bound to their respective targets. Due to a lack of a suitable $EGFR^-/HER2^+$ cell line, $EGFR^+/HER2^+$ SKOV3 cells were preincubated with Cetuximab to block EGFR binding sites. Compared to both bispecific controls, the trispecific scDb-HER2-scFv-EGFR exhibited weaker binding to both $EGFR^-/HER2^+$ and $EGFR^+/HER2^-$ cells, as well as to Jurkat cells, reflected by higher EC_{50} values. Solely to double positive SKOV3 cells did the scDb-HER2-scFv-EGFR show stronger binding than both corresponding bispecific TCEs. Similarly, binding of scDb-HER2-scFv-IL13Rα2 was weaker to both single positive cell lines and Jurkat cells compared to the corresponding bispecific controls. On $HER2^+/IL13Rα2^+$ U251 cells, binding of the scDb-scFv was stronger in higher concentrations than for the bispecific TCEs, with a slightly higher EC_{50} value. In case of scDb-cMET-scFv-EGFR, binding to single positive cells was almost identical compared to the corresponding bispecific TCEs, but weaker on Jurkat cells. On the double positive SKOV3 cells, binding was stronger than for both bispecific controls.

In order to investigate the potencies of the trispecific TCEs of inducing T-cell mediated cytotoxicity, I set up cocultures of single and double target-positive cancer cell lines with PBMCs and serial dilutions of TCEs. Viability curves for all conducted cocultures are depicted in Figure 19 with corresponding EC_{50} values in Table 18.

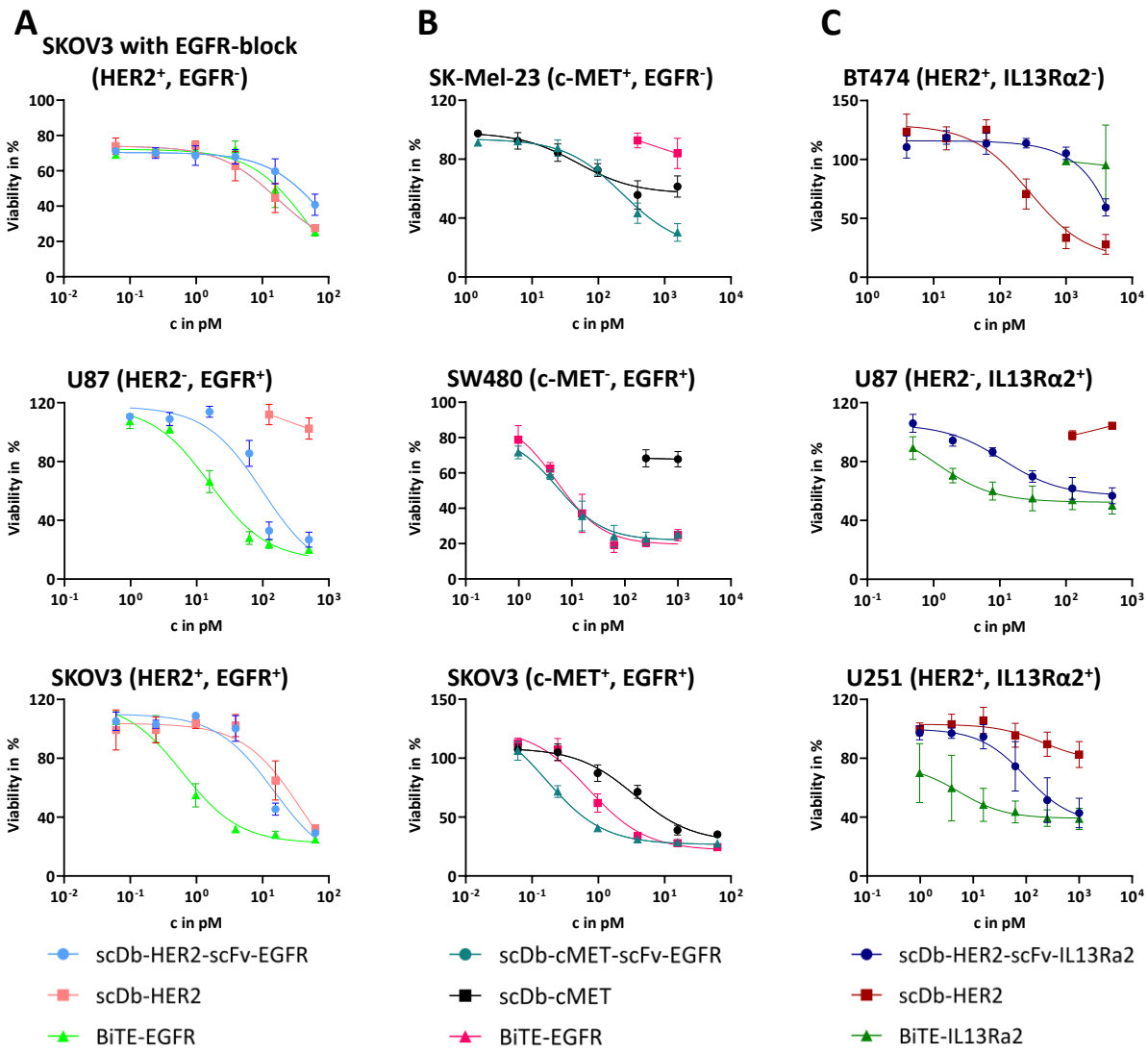

Figure 19 Induction of T-cell mediated cytotoxicity by scDb-scFvs on single-target positive and double-target positive cancer cells. Cells were incubated with a serial dilution of A) scDb-HER2-scFv-EGFR, scDb-HER2 or BiTE-EGFR, B) scDb-cMET-scFv-EGFR, scDb-cMET or BiTE-EGFR or C) scDb-HER2-scFv-IL13Rα2, scDb-HER2 or BiTE-IL13Rα2. PBMCs were added in an effector:target cell ratio of 10:1. Cell viability was measured 3 days after PBMC addition using crystal violet staining and subsequent quantification. Data shown as mean ± SD, (n=3 donors, each determined in three independent experiments).

Table 18 T-cell mediated killing of tumor cells by scDb-scFvs and corresponding scDb and BiTE controls. EC_{50} values were calculated using GraphPad Prism software by a dose-response nonlinear regression with a variable slope. EC_{50} values in pM as mean of 3 donors, each determined in three independent experiments, *P<0.05, **P < 0.01, ***P<0.001, unpaired t test.

		scDb-scFv	scDb	BiTE
scDb-HER2-scFv-EGFR scDb-HER2 BiTE-EGFR	SKOV3 with EGFR-block	94.15	16.51	50.48
	U87	100.1	n.a.	15.78
	SKOV3	14.74	38.12	0.62
scDb-cMET-scFv-EGFR scDb-cMET BiTE-EGFR	SK-Mel-23	182.7	48.9	n.a.
	SW480	5.35	n.a.	5.19
	SKOV3	0.16	3.54	0.72
scDb-HER2-scFv-IL13Rα2 scDb-HER2 BiTE-IL13Rα2	BT474	2700	282.9	n.a.
	U87	11.14	n.a.	1.08
	U251	96.72	209.9	5.42

scDb-HER2-scFv-EGFR exhibited weaker induction of cytotoxicity than the corresponding bispecific controls (Figure 19A). In cocultures with $EGFR^+/HER2^+$ SKOV3 cells that were preincubated with Cetuximab (thereafter $EGFR^{(-)}/HER2^+$), the EC_{50} value for scDb-HER2-scFv-EGFR was significantly higher than that of scDb-HER2, even though the EGFR-block did not completely abrogate induction of cytotoxicity by the BiTE-EGFR, indicating that the scDb-scFv also likely bound to EGFR in higher concentrations. Induction of cytotoxicity of the scDb-HER2-scFv-EGFR was also significantly weaker on $EGFR^+/HER2^-$ U87 and untreated SKOV3 cells compared to the BiTE-EGFR. Taken together, the corresponding bispecific antibodies scDb-HER2 and BiTE-EGFR were more effective in inducing T-cell mediated cytotoxicity on the respective single positive cell lines compared to the trispecific scDb-HER2-scFv-EGFR, fitting to the weaker binding to those cell lines (Figure 18, Table 17). Even though binding to $EGFR^+/HER2^+$ SKOV3 cells was stronger for the scDb-scFv compared to the corresponding bispecific controls, this did not translate to higher cytotoxicity on these cells.

Similarly, induction of cytotoxicity of the scDb-HER2-scFv-IL13Rα2 was significantly lower on $HER2^-/IL13Rα2^+$ U87 cells compared to the BiTE-IL13Rα2 and on $HER2^+/IL13Rα2^-$ BT474 cells compared to the scDb-HER2. On double positive U251 cells, the scDb-scFv was also outperformed by the BiTE-IL13Rα2. As the scDb-HER2-scFv-EGFR, the scDb-HER2-scFv-IL13Rα2 also exhibited weaker binding and lower induction of cytotoxicity on single-

target positive cells compared to the corresponding bispecific TCEs, in addition to lower induction of cytotoxicity on double positive U251 cells compared to the BiTE-IL13Rα2 (Figure 19C, Table 18).

In contrast, the scDb-cMET-scFv-EGFR performed equally well on c-MET$^-$/EGFR$^+$ SW480 cells compared to the BiTE-EGFR and although the EC_{50} value on c-MET$^+$/EGFR$^-$ SK-Mel-23 cells was significantly higher than for the scDb-cMET, the induction of cytotoxicity was equal for lower concentrations and visibly higher for higher concentrations. On double-target positive SKOV3 cells, induction of cytotoxicity of the scDb-scFv was significantly higher than for either corresponding bispecific antibody (Figure 19B, Table 18).

In summary, the scDb-HER2-scFv-EGFR and scDb-HER2-scFv-IL13Rα2 were both outperformed by their corresponding bispecific TCEs on single-target positive cells in regard to both binding and induction of T-cell mediated cytotoxicity. In contrast, the scDb-cMET-scFv-EGFR proved to be equally efficacious on single-target positive cell lines as the corresponding bispecific controls, making it a promising candidate for use as a dual-targeting agent. On double positive cells, both target binding and T-cell retargeting properties were superior to both corresponding bispecific controls.

3.2.1 Modification of scDb-HER2-scFv-EGFR and scDb-HER2-scFv-IL13Rα2

The weaker binding and induction of cytotoxicity observed for the trispecific scDb-HER2-scFv-EGFR and scDb-HER2-scFv-IL13Rα2 compared to the corresponding bispecific constructs indicated that the additional scFv possibly caused steric problems of the scDb-scFv format for the aforementioned constructs. Therefore, I explored switching the position of the scFv as a possible solution to the problem. I took the scFv from the C-terminal end of the scDb and fused it to the N-terminus with unchanged linkers. I named the modified construct scFv-scDb and it is schematically shown in Figure 20.

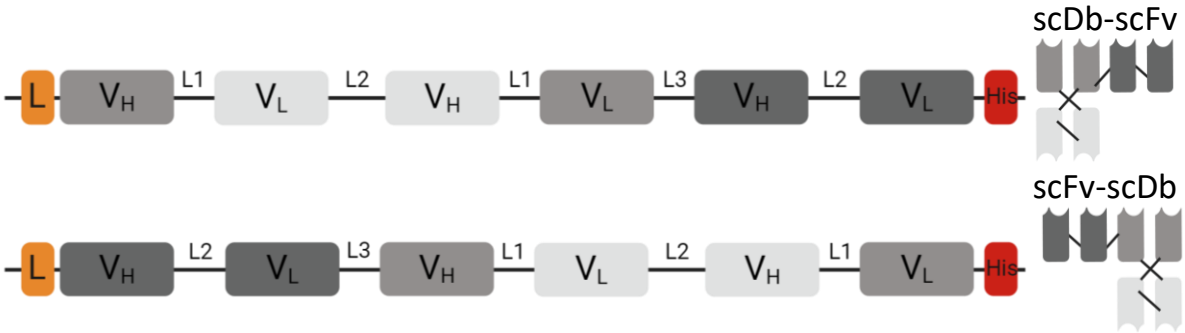

Figure 20 Composition and assembly of scDb-scFv and scFv-scDb formats in comparison. L - Igκ leader; VH - heavy chain; VL - light chain; L1 – GGGGS; L2 - $(GGGGS)_3$; L3 – AAAGGSGGGGS; His - 6x Histidine-Tag.

In order to clone these constructs, I used the expression plasmid of the scDb-HER2 and added Golden Gate cloning sites for insertion of the scFvs with the correct linkers. Production was performed by the Antibody Core Facility, as for the other constructs. I purified the scFv-scDbs as described for the scDb-scFvs. To investigate the binding properties of the scFv-scDbs, I titrated them on single and double target-positive cells together with the corresponding scDb-scFvs. The results of the flow cytometric analysis and associated EC_{50} values are shown in Figure 21 and in Table 19, respectively. The EC_{50} values for scFv-EGFR-scDb-HER2 were lower on $HER2^-/EGFR^+$ U87 and double positive SKOV3 cells, but slightly higher on $HER2^+/EGFR^-$ SKOV3 cells pretreated with Cetuximab, compared to the scDb-HER2-scFv-EGFR. Even though the EC_{50} values appeared promising, the binding strength was consistently lower for scFv-scDbs (Figure 21A). Similarly, the EC_{50} values of scFv-IL13Rα2-scDb-HER2 were lower on both single-target positive cell lines and the double positive cell line compared to the scDb-HER2-scFv-IL13Rα2, with the binding strength being lower for all cell lines as well (Figure 21B).

In conclusion, the recloning of the scDb-scFv constructs moving the scFv from C- to N-terminus did not lead to stronger binding to target cells compared to the original scDb-scFvs. In light of these results, I did not perform additional cocultures of tumor cells with PBMCs.

Based on the properties of the scDb-cMET-scFv-EGFR, it was my antibody of choice for insertion into oAds for dual antigen targeting.

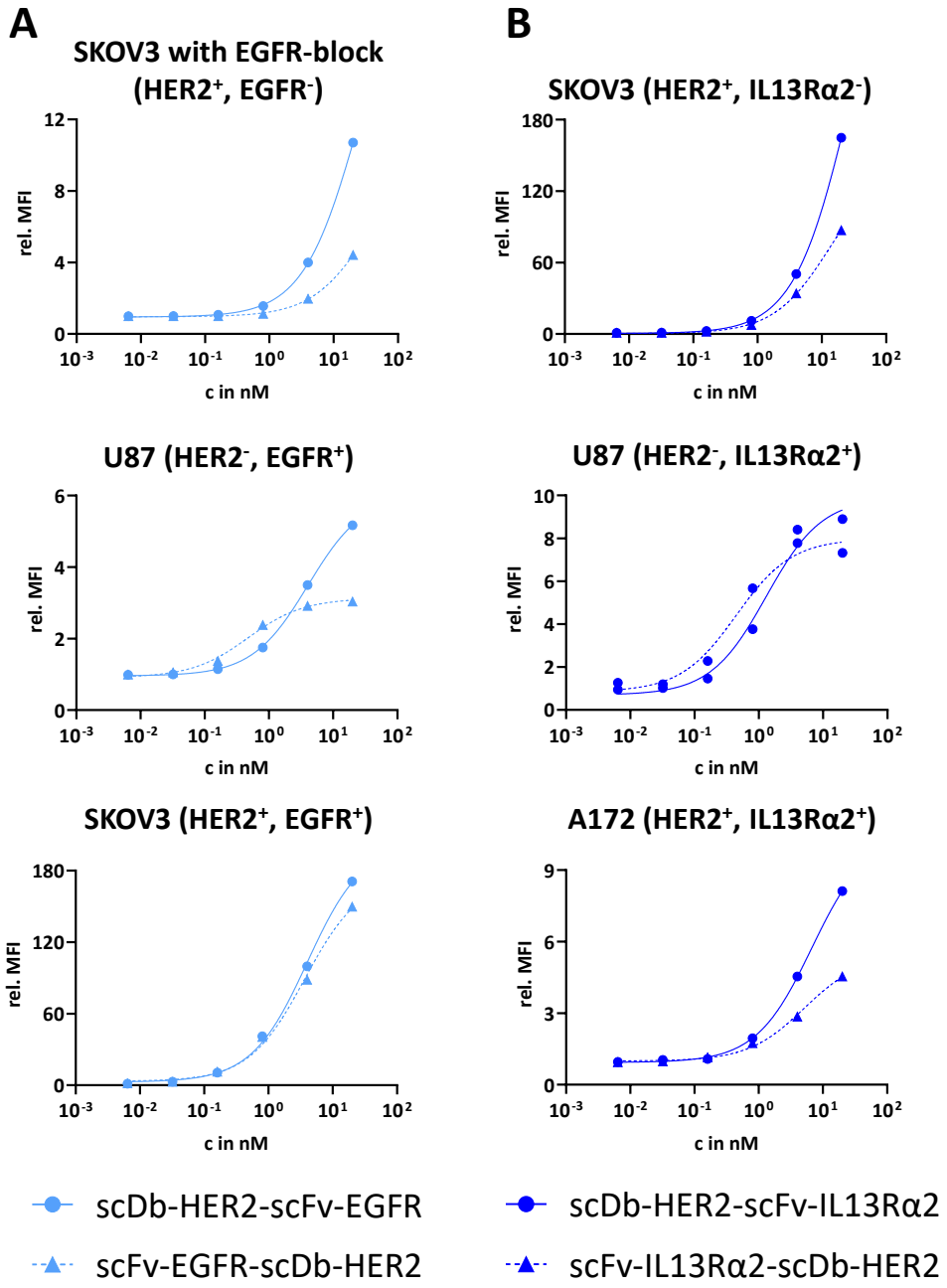

Figure 21 Binding properties of scFv-scDbs compared to scDb-scFvs. A) scFv-EGFR-scDb-HER2 vs scDb-HER2-scFv-EGFR on SKOV3 cells pretreated with Cetuximab, U87 and SKOV3 cells. B) scFv-IL13Rα2-scDb-HER2 vs scDb-HER2-scFv-IL13Rα2 on SKOV3, U87 and A172 cells. Binding properties were analyzed via flow cytometry, bound protein was detected using PE-anti-His mAb. Relative MFI (rel. MFI) shown (n=1).

Table 19 EC_{50} values of binding analysis of scFv-scDbs and scDb-scFvs on target cells in nM. EC_{50} values were calculated using GraphPad Prism software by a dose-response nonlinear regression with a variable slope.

		scDb-scFv	scFv-scDb
scDb-HER2-scFv-EGFR scFv-EGFR-scDb-HER2	SKOV3 with EGFR-block	24.90	33.14
	U87	4.07	0.47
	SKOV3	4.00	3.65
scDb-HER2-scFv-IL13Rα2 scFv-IL13Rα2-scDb-HER2	SKOV3	27.23	13.34
	U87	1.30	0.45
	A172	6.68	5.09

3.3 Cloning, Production and Characterization of Armed Oncolytic Adenoviruses

Taking together the data of the bi- and trispecific TCE characterization, I decided to clone, produce and characterize a virus panel for dual-targeting of TAAs c-MET and EGFR. For dual-targeting, I pursued three different approaches, depicted in Figure 22. The first approach was to use an oAd armed with the scDb-cMET-scFv-EGFR (Figure 22A), the second strategy was to co-express the scDb-cMET and the BiTE-EGFR using a single oAd (Figure 22B) and the third approach was to co-infect tumor cells with two different oAds, one encoding the scDb-cMET and the other driving expression of the BiTE-EGFR (Figure 22C). I investigated all three strategies, as they all offered potential advantages. Expression of the scDb-cMET-scFv-EGFR requires less genomic space than simultaneous expression of the scDb-cMET and the BiTE-EGFR. In addition, two bispecific TCEs possess more repetitive sequences than the scDb-scFv, increasing the risk for homologous recombination, which could also occur in the co-infection setting with two viruses infecting the same cell. The smaller bispecific TCEs could potentially result in slightly better tissue penetration due to their smaller size, in addition to being more stable due to their simpler structure. As the co-infection strategy employs oAds expressing a single TCE, the viruses are likely to be less attenuated compared to oAds encoding larger transgenes, but differences in viral replication might lead to one oAd outcompeting the other and eliminating it from the tumor.

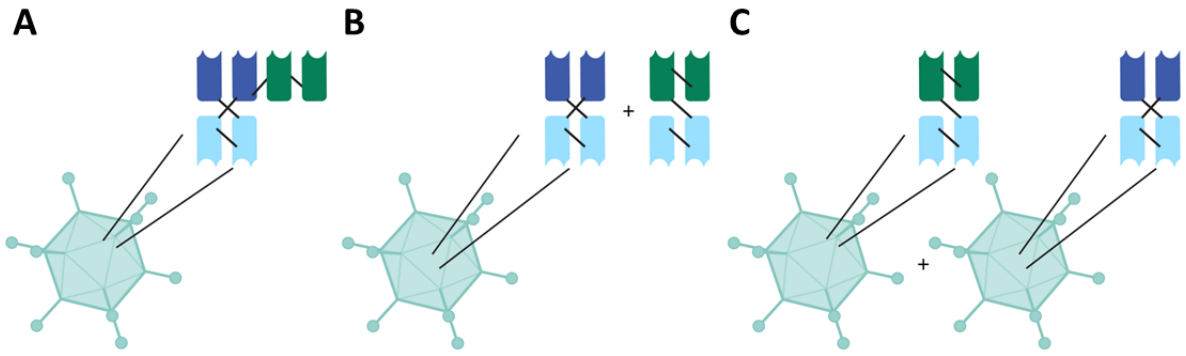

Figure 22 Dual-targeting strategies with oAds. A) One oAd encoding an scDb-scFv. B) One oAd co-expressing two bispecific TCEs. C) Co-infection of two oAds encoding a different bispecific TCE each.

3.3.1 Cloning of Dual Expression Cassettes

3.3.1.1 Bidirectional Promoter Cassettes

In order to drive expression of two different TCEs via a single oAd, I explored dual expression strategies. First, I investigated an approach with bidirectional promoter constructs, allowing transcription of two genes by a single promoter cassette, with the genes on opposing DNA strands. Because of the similarity of TCE sequences, I hypothesized that encoding the two TCE genes in opposing directions would greatly reduce the risk of recombination between identical sequence segments. In addition, a bidirectional promoter cassette would require less genomic space than two separate promoters and have fewer repetitive sequences. The promoters consisted of two different promoters that were fused tail-to-tail with a common enhancer element. These promoters were chosen due to their relatively short length, as even with an E3 deletion, the transgene capacity of Ad5 is only around 4.5 kb considering the limit of 105 % of wt genome length.[84] A bispecific TCE with Poly A tail has a DNA length of 1.8-1.9 kb, leaving approximately 600-700 bp for the bispecific promoters. I generated and tested four different promoter compositions, extracted from published sequences[172, 173]. Each cassette containing a minimal CMV (mCMV) promoter fused to either the CMV or the human phosphoglycerate kinase promoter (hPGK) in left-to-right (forward) or right-to-left (reverse) orientations. I named the promoters mCMV-CMV, CMV-mCMV (612 bp), mCMV-hPGK1 and hPGK1-mCMV (573 bp). The general principle is schematically depicted in Figure 23B. To test gene expression by the bidirectional promoter cassettes, I modified the psiCheck 2 dual luciferase vector to enable bidirectional expression of Renilla and firefly luciferase, respectively, by the different promoter cassettes. After cloning of the plasmids, I transfected them into HeLa cells and measured luciferase expression, subtracting values of untransfected cells. As a reference, I also transfected the psiCheck 2 vector. Of note, the psiCheck 2 vector uses two different promoters, the expression of the Renilla luciferase is driven by the SV40

promoter, whereas expression of the firefly luciferase is driven by the HSV-TK promoter. The SV40 promoter has a stronger activity compared to the HSV-TK promoter.[174] The results are shown in Figure 23A. I measured 5.35 x 10^5 light units (LU) for the firefly luciferase and 2.00 x 10^6 for the Renilla luciferase using the psiCheck 2 control vector. I detected expression of both luciferases for all bidirectional promoter constructs, but it was very low for mCMV-CMV and mCMV-hPGK1 promoters. For the mCMV-CMV promoter, expression of firefly vs Renilla luciferase was 2.07 x 10^4 vs 3.61 x 10^4 LU and for the mCMV-hPGK1 promoter 4.45 x 10^4 LU were measured for both luciferases. The CMV-mCMV promoter achieved luciferase expression of 1.76 x 10^5 vs 6.33 x 10^5 LU, whereas the hPGK1-mCMV promoter reached 6.09 x 10^4 vs 6.12x10^5 LU. While expression was relatively low for all bidirectional promoter cassettes compared to the psiCheck 2 control, I measured the highest expression for the CMV-mCMV construct and therefore chose it for cloning the plasmids for co-expression of TCEs.

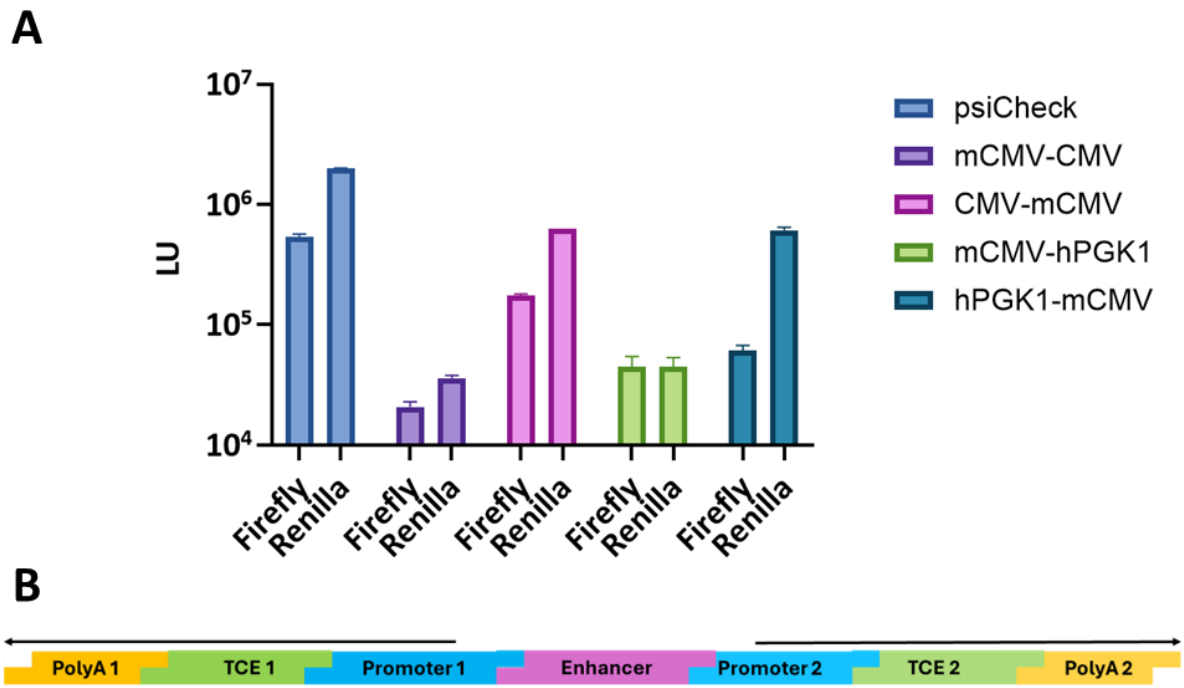

Figure 23 Expression of luciferases from bidirectional promoter cassettes. A) HeLa cells were transfected with plasmids containing bidirectional promoter cassettes for dual expression of firefly and Renilla luciferase. psiCheck 2 vector was used as control. Cells were lysed 24 h after transfection and luciferase expression was measured via luminometer using the Promega Dual-Glo® Luciferase Assay System. Light units (LU) shown as mean ±SD (n=3). B) Schematic depiction of bidirectional promoter expression cassette for two TCEs.

3.3.1.2 Dual TCE Expression via T2A Peptide

As a second dual expression strategy, I also investigated the use of a T2A peptide, which mediates polycistronic expression via ribosomal skipping.[175] The 2A sequences impair formation of a peptide bond, leading to translation of two separate proteins from a single mRNA transcript.[176] To save time, I cloned the expression cassettes directly with genes for scDb-

cMET and BiTE-EGFR and inserted them into shuttle plasmids for oAd homologous recombination (see chapter 2.2.12). The scDb-cMET had a Myc-His double-tag and the BiTE-EGFR had an HA-His double-tag to enable separate detection of both TCEs from a single sample. The composition of the different expression cassettes is depicted in Figure 24B. Expression of TCEs was driven by the CMV promoter, with the compositions CMV-scDb-cMET-T2A-BiTE-EGFR, (CMV-scDb-cMET-T2A-BiTE-EGFR)r, CMV-BiTE-EGFR-T2A-scDb-cMET and (CMV-BiTE-EGFR-T2A-scDb-cMET)r being tested, i.e. two different compositions in either forward or reverse orientation. I transfected the shuttle plasmids with the different expression cassettes into HeLa cells and used the supernatants for incubation with EGFR+/c-MET+ SKOV3 cells. After a second incubation with fluorophore-coupled anti-Myc and anti-HA secondary antibodies, I measured fluorescence intensity via flow cytometry. I calculated the concentrations based on standard curves generated using purified antibodies with known concentrations. The (CMV-scDb-cMET-T2A-BiTE-EGFR)r and CMV-BiTE-EGFR-T2A-scDb-cMET expression cassettes performed very poorly, with no scDb-cMET detected in the supernatants of transfected cells and only very low concentrations of BiTE-EGFR detected, 0.07 nM for both constructs (Figure 24A). For the other two expression cassettes, higher concentrations of both TCEs were measured. In the supernatant of cells transfected with plasmids encoding CMV-scDb-cMET-T2A-BiTE-EGFR, 2.4 nM of scDb-cMET and 4.6 nM of BiTE-EGFR could be detected. For the (CMV-BiTE-EGFR-T2A-scDb-cMET)r expression cassette, the detected concentrations were 3.8 nM and 1.1 nM, respectively.

For virus cloning, I therefore chose the CMV-scDb-cMET-T2A-BiTE-EGFR expression cassette, due to the more equal and slightly higher expression of both TCEs.

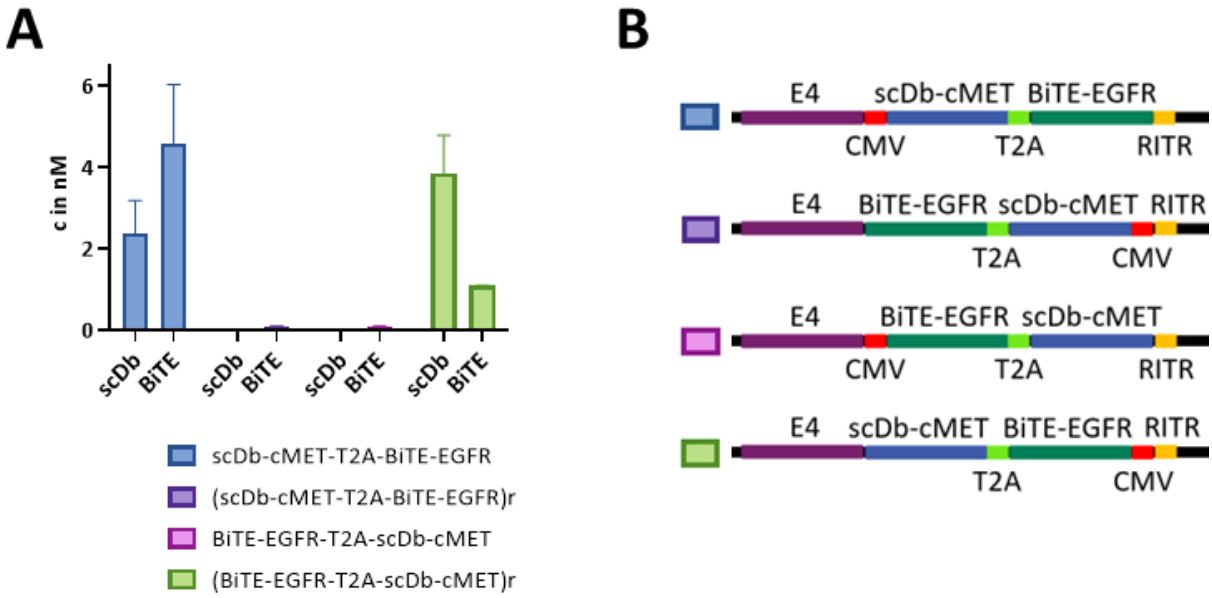

Figure 24 Expression of scDb-cMET and BiTE-EGFR with T2A peptide from transfected shuttle plasmids. A) Concentrations of scDb-cMET and BiTE-EGFR in supernatants of transfected HeLa cells in nM. Supernatants were taken 2 days post transfection and concentrations were measured via flow cytometry using standard curves calculated with purified antibodies. Data shown as mean ± SD (n=2). B) Composition of T2A expression cassettes. E4 – early transcriptional region 4; RITR – right inverted terminal repeat.

3.3.2 Design and Production of oAd Panel

Taking together the TCE characterization data and the results of the co-expression analysis, I decided to clone an oAd panel for dual-targeting of c-MET and EGFR in order to find the most effective TCE expression and dual-targeting strategy. I tested two different insertion sites. The first site, between the stop codon of L5 and E4 (after-fiber site) and the second site, between the end of the RITR and cap site of E4 mRNA (after-E4 site), have both been described.[177] Expression was driven either by the exogenous CMV promoter or the Ad40 splice acceptor (Ad40SA). A schematic depiction of insertion sites and expression strategies is shown in Figure 25.

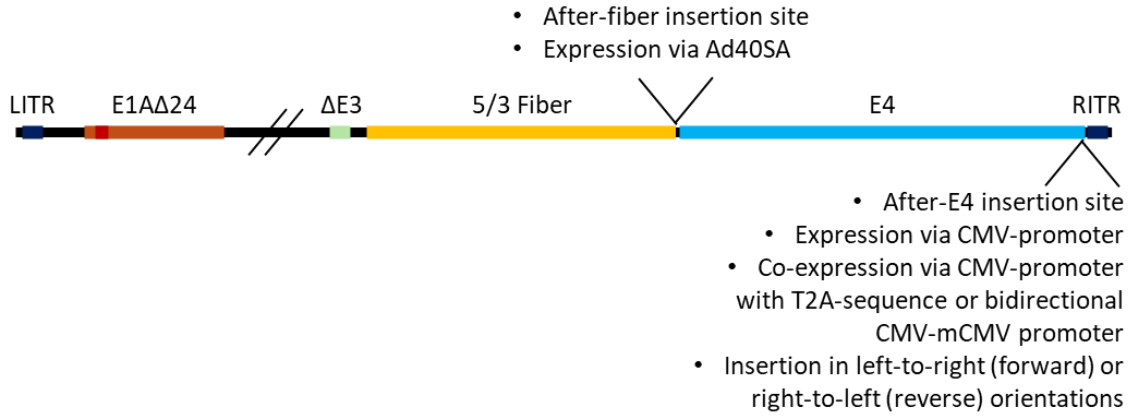

Figure 25 TCE-expression strategies. LITR – left inverted terminal repeat; E1AΔ24 – early transcription region 1A with 24 base pair deletion; ΔE3 – early transcription region 3; 5/3 fiber – chimeric serotype 5 fiber with serotype 3 knob; Ad40SA – splice-acceptor of Ad40 long fiber; E4 – early transcription region 4; RITR – right inverted terminal repeat.

I cloned plasmids containing the oAd genomes via homologous recombination of shuttle plasmids with viral backbone plasmids, as described in chapters 2.2.11 and 2.2.12. After transfection of A549 cells with oAd-genome plasmids and subsequent amplification of replicating viruses, I purified viral particles via ultracentrifugation and measured infectious virus titers via $TCID_{50}$ assay, described in chapters 2.7.1 – 2.7.3. A schematic depiction of the genomes of the virus panel is depicted in Figure 26A. Virus particle (VP) and $TCID_{50}$ titers are shown in Figure 26B, together with the $VP/TCID_{50}$ ratios. For all viruses with inserts behind the E4 region, similar ratios between 4 and 14 were measured, with exception of the bidirectional promoter viruses. Their $VP/TCID_{50}$ ratios were higher with 74.3 for the virus with insertion in the forward orientation and 22.5 for the virus with the insert in reverse orientation. The oAd with the BiTE-EGFR insert behind the fiber gene with the Ad40SA was produced at visibly lower titers than the E4-viruses, with a clearly higher $VP/TCID_{50}$ ratio (242). Compared to Ad5/3-CMV-BiTE-EGFR and Ad5/3-(CMV-BiTE-EGFR)r, the ratio was 60- and 22.5- fold higher, respectively.

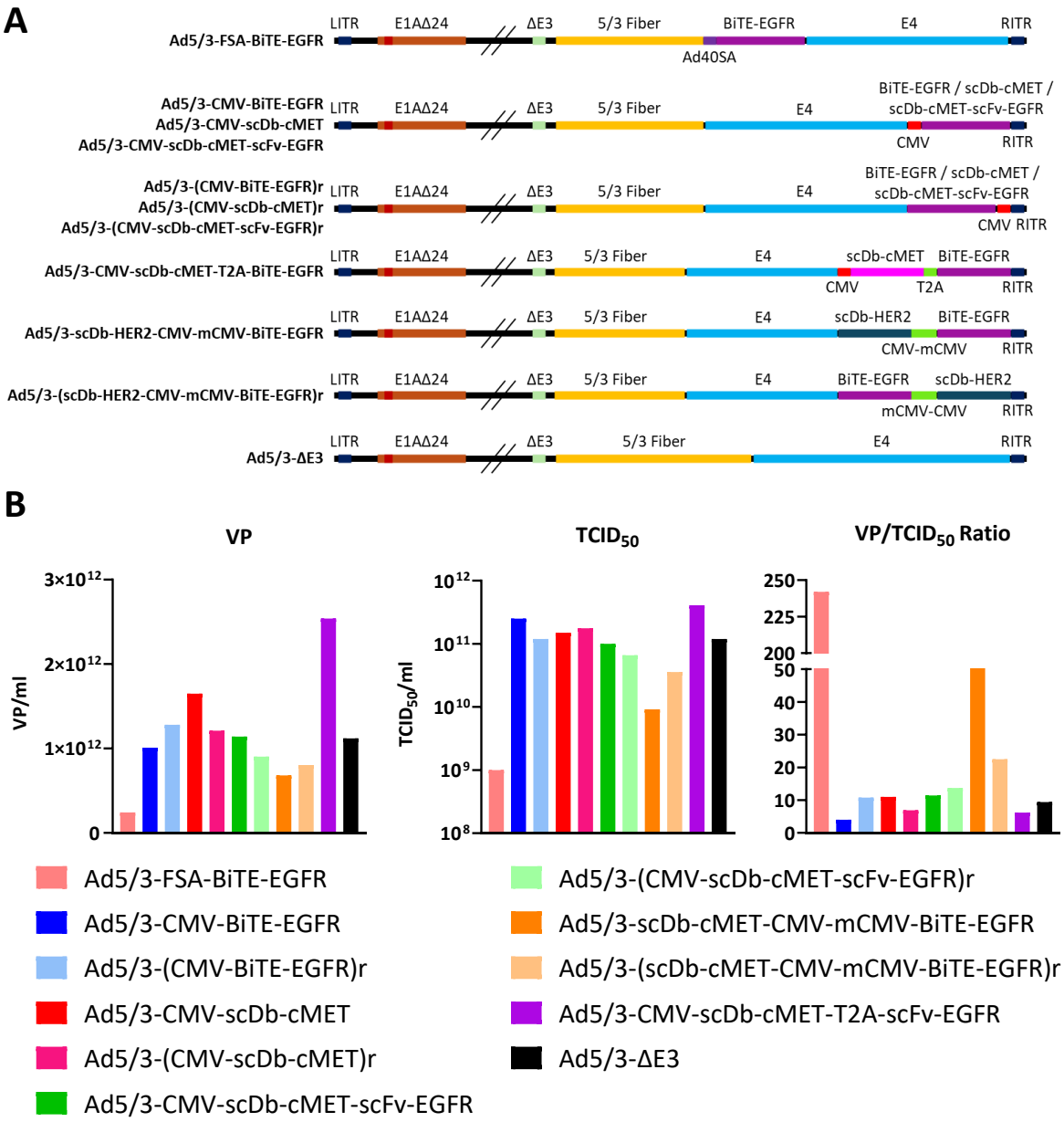

Figure 26 Panel of TCE-armed oAds. A) Schematic depiction of viral genomes. LITR - left inverted terminal repeat; E1A - E3; E4 - early viral genes; Δ24 - 24 bp deletion; ΔE3 - deleted E3-region; 5/3 Fiber - chimeric fiber with Ad5 shaft and Ad3 knob; Ad40SA - splice-acceptor of Ad40 long fiber; FSA - Fiber splice-acceptor; CMV - cytomegalovirus promoter; mCMV - minimal CMV; RITR - right inverted terminal repeat. B) Virus particle (VP) titer, tissue culture infectious dose 50 ($TCID_{50}$) titer and VP/$TCID_{50}$ ratio of virus panel.

3.3.3 Antibody Production and Oncolytic Activity

3.3.3.1 Antibody Expression via Bidirectional Promoters

To analyze the potency of bidirectional promoters for driving co-expression of two TCEs, I infected different tumor cell lines with oAds encoding bidirectional promoter cassettes and analyzed the supernatants via flow cytometry, as described in 2.6.2 and 3.3.1.2. The oAds encoding the bidirectional CMV-mCMV promoter made an exception by encoding the TCEs scDb-HER2 and BiTE-EGFR. This was due to these viruses being cloned prior to the finalization of the characterization of all TCEs. Unfortunately, the production of antibodies in

cells infected with oAds armed with bidirectional promoter cassettes was very low for BiTE-EGFR and I could not detect the scDb-HER2 at all, as seen in Figure 27A. PCRs were performed with both the plasmids containing the whole oAd genomes and purified viral genomes to check for integrity of the inserted bidirectional promoter expression cassettes. Gel electrophoresis of PCR amplicons revealed clear differences between oAd plasmids and purified viral DNA, presented in Figure 27B. While PCR of plasmids showed strong bands at expected insert size (~5300 bp) with additional smaller bands, the PCRs with purified viral DNA revealed multiple deletions in the inserts. I therefore decided to exclude the bidirectional promoter viruses from further experiments.

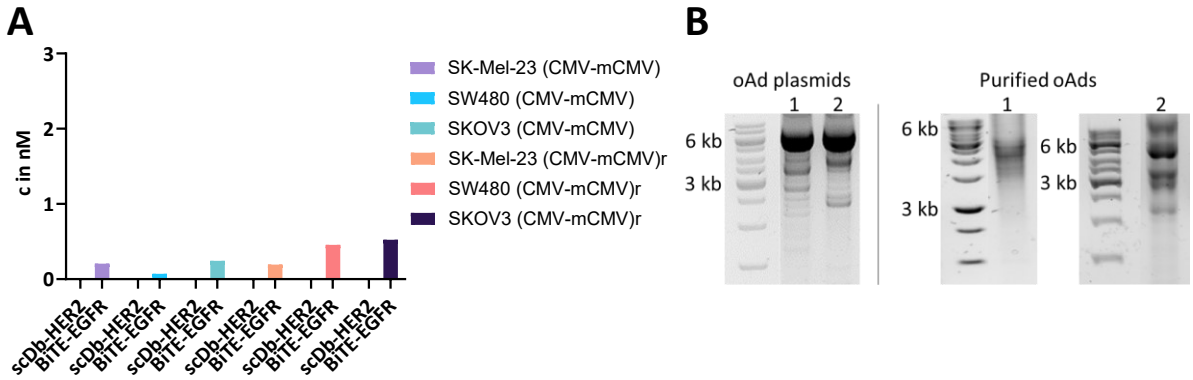

Figure 27 Characterization of bidirectional promoter viruses. A) Antibody concentrations in nM in supernatants of infected target cells. Cells were infected with MOI 5, supernatants were taken 7 dpi and analyzed via flow cytometry on SKOV3 cells. Antibodies were detected using AF647-anti-Myc or PE-anti-HA antibodies. Relative MFIs were used to calculate concentrations based on standard curves created by titration of purified antibodies. B) Gel electrophoresis of PCR amplicons of bidirectional promoter expression cassettes in 1% agarose gel. On the left, amplicons of PCR performed with oAd plasmids, on the right, amplicons of PCRs of purified virus DNA. 1 - Ad5/3-scDb-HER2-CMV-mCMV-BiTE-EGFR; 2 - Ad5/3-(scDb-HER2-CMV-mCMV-BiTE-EGFR)r.

3.3.3.2 Antibody Expression of TCE-armed oAds via Splice Acceptor or CMV Promoter

Next, I measured antibody expression following infection of tumor cell lines SK-Mel-23, SW480 and SKOV3 with oAds driving TCE-expression via the Ad40SA in the after-fiber site or via CMV promoter in the after-E4 site. I chose the cell lines due to their EGFR and c-MET expression profiles (Figure 12). The $EGFR^-/c\text{-}MET^+$ SK-Mel-23 cells, the $EGFR^+/c\text{-}MET^-$ SW480 cells and the $EGFR^+/c\text{-}MET^+$ SKOV3 cells would be used in follow-up experiments testing dual-targeting strategies in cocultures of oAd-infected tumor cells and PBMCs. I infected tumor cells with different MOIs, calculated with the $TCID_{50}$ titers. I infected SK-Mel-23 cells with an MOI of 25 and SW480 and SKOV3 cells with an MOI of 5. I removed the supernatants seven days post infection (dpi) and quantified TCEs via flow cytometry, using standard curves generated with purified antibodies. The results of the antibody quantification are shown in Figure 28.

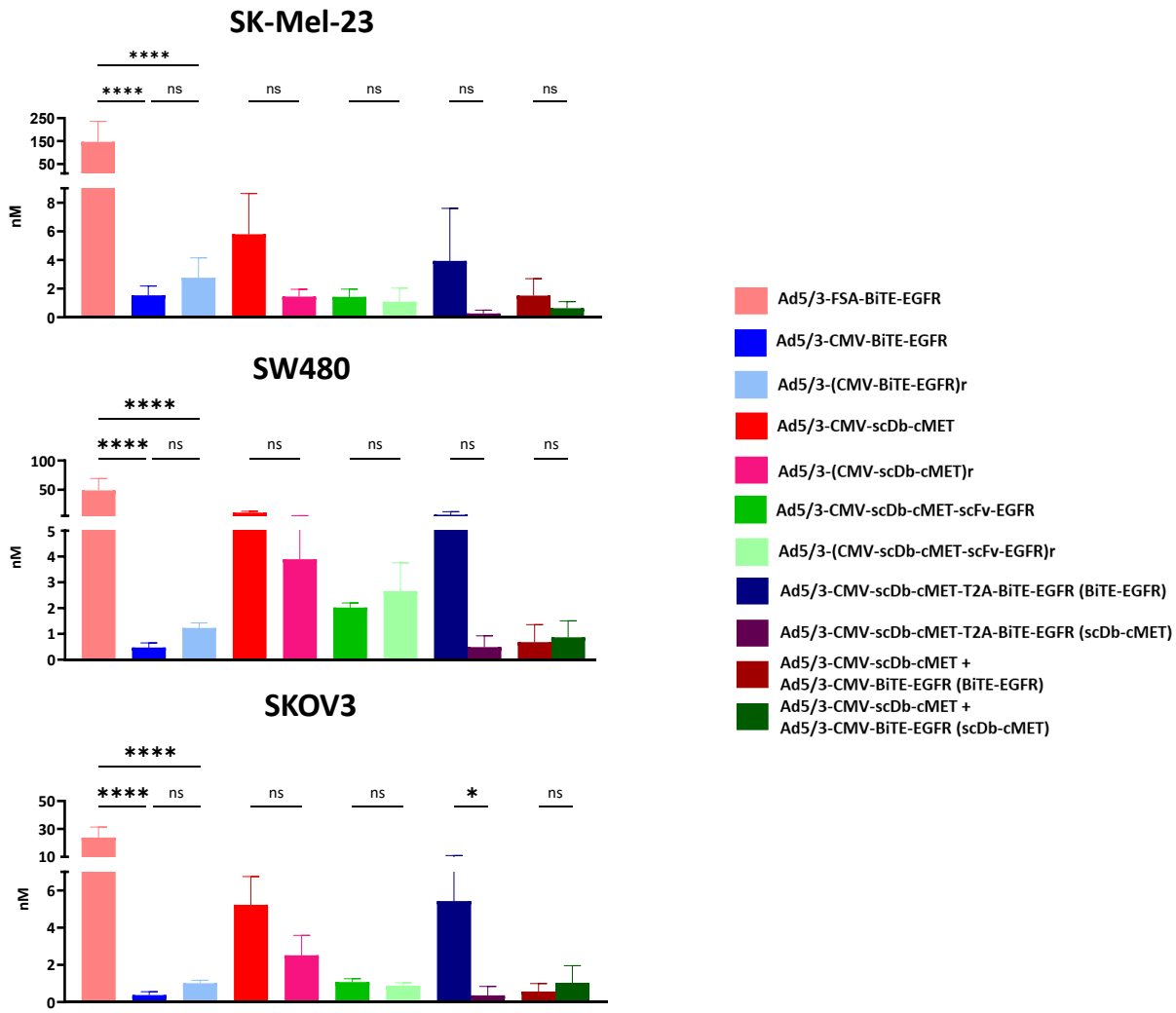

Figure 28 Antibody Production of TCE-armed oAds. Antibody concentrations were measured in supernatants of infected target cells. Cells were infected with MOI 25 (SK-Mel-23) or MOI 5 (SW480, SKOV3), supernatants were taken 7 dpi and analyzed via flow cytometry with SKOV3 cells. Antibodies were detected using a PE-anti-His antibody or in case of dual expression, AF647-anti-Myc or PE-anti-HA antibodies. Relative MFIs were used to calculate concentrations based on standard curves created by titration of purified antibodies. Values shown as mean ± SD, (n=3), *P < 0.05, **P < 0.01, ***P < 0.001, ****P < 0.0001, ns: not significant, one-way ANOVA.

The Ad5/3-FSA-BiTE-EGFR showed significantly higher production of the BiTE-EGFR compared to the BiTE-EGFR encoding viruses with inserts behind the E4 region, with p-values below 0.0001 and very high antibody concentrations between 23 and 147 nM. As described in chapter 3.2, EC_{50} values of T-cell mediated cytotoxicity for the BiTE-EGFR were between 0.62 pM on SKOV3 cells and 15.78 pM on U87 (Table 18). For the oAds encoding the BiTE-EGFR in the after-E4 site, TCE production was slightly higher in the reverse orientation. In contrast, production of the scDb-cMET was higher in oAds with insertions in the forward orientation. For the scDb-cMET-scFv-EGFR, insert orientation seemed to have no effect on the level of TCE production. The antibody titers for the E4-viruses with single TCE expression ranged between 0.35 and 10 nM. Highest titers were measured for oAds with scDb-cMET insertion,

whereas titers for BiTE-EGFR and scDb-cMET-scFv-EGFR were slightly lower and very similar.

Unequal production of TCEs was observed after infection with the Ad5/3-CMV-scDb-cMET-T2A-BiTE-EGFR. In all tested cell lines, production of the BiTE-EGFR was visibly higher than that of the scDb-cMET, in SKOV3 cells the difference was significant ($p = 0.045$). Additionally, I measured production of antibodies after co-infection with Ad5/3-CMV-BiTE-EGFR and Ad5/3-CMV-scDb-cMET. In contrast to infection with the T2A-peptide encoding virus, production of both TCEs was very similar in all tested cell lines.

The imbalance in antibody production for the Ad5/3-CMV-scDb-cMET-T2A-BiTE-EGFR raised the question of potential recombination taking place within the virus genomes. Therefore, I infected A549 cells at a low MOI and used the supernatant to infect freshly plated cells. I used purified viral genomes as templates for PCR after each passage to amplify the insert region in the oAd genome. Gel electrophoresis of PCR amplicons revealed deletions within the insert in purified viruses, as well as increasing frequency of deletions within the insert with increased passaging, shown in Figure 29. Sequencing of the smallest additional band in passage 4 revealed deletion of the sequence from the end of the CMV promoter to the beginning of the V_L of the scFv-EGFR (Figure S1). PCR of the insert region in the oAd-encoding plasmid did not reveal additional bands that would indicate possible deletions.

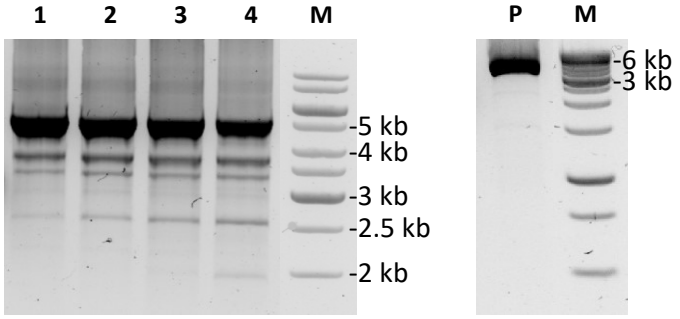

Figure 29 PCR of CMV-scDb-cMET-T2A-BiTE-EGFR inserts in passaged Ad5/3-CMV-scDb-cMET-T2A-BiTE-EGFR infected A549 cells. Gel electrophoresis of PCR amplicons in 1 % agarose gel. 1 - purified virus; 2 - passage one, 4 dpi; 3 - passage two, 9 dpi (cumulative); 4 - passage 3, 14 dpi (cumulative); M - DNA Ladder; P – oAd-encoding plasmid.

3.3.3.3 Oncolytic Activity of TCE-armed oAds

In order to analyze the oAd panel for possible attenuation, I tested the viruses for cytotoxicity, comparing oncolytic activity to a control virus without insert (Ad5/3-ΔE3). I tested oncolytic activity by titrating oAds on target cells with MOIs calculated based on $TCID_{50}$ titers. I incubated cells until CPE could be observed in the lowest MOI for one virus. I then stained the remaining cells with crystal violet and imaged the plates. Representative experiments are shown

in Figure 30 (repeats shown in Figure S2). The Ad5/3-FSA-BiTE-EGFR virus showed clear attenuation compared to the Ad5/3-ΔE3 control virus on SW480 and SKOV3 cells and slight attenuation on SK-Mel-23 cells. As described in chapter 3.3.2, I calculated a significantly higher VP/$TCID_{50}$ ratio for the Ad5/3-FSA-BiTE-EGFR compared to the other oAds, meaning that a substantially higher amount of virus particles was used for the cytotoxicity assays. Of note, amplification of the Ad5/3-FSA-BiTE-EGFR during production also required more days of incubation than any other virus of the panel, further supporting the observation that the oncolytic activity was considerably attenuated.

The oAds with inserts in the after-E4 site exhibited attenuated oncolytic activity compared to the control virus depending on the orientation of the insert. For all inserts with single TCE-expression (CMV-BiTE-EGFR, CMV-scDb-cMET and CMV-scDb-cMET-scFv-EGFR), oAds were visibly attenuated when the insert was present in the reverse orientation. In the forward orientation the oAds were not or only slightly attenuated. Due to the higher oncolytic activity of viruses with inserts in the forward orientation, I did not produce the oAd with the T2A expression cassette in a reverse orientation.

In conclusion, analysis of oncolytic activity revealed strong attenuation of the Ad5/3-FSA-BiTE-EGFR and visible attenuation of oAds carrying transgenes in the after-E4 site in the reverse orientation, but not in the forward orientation.

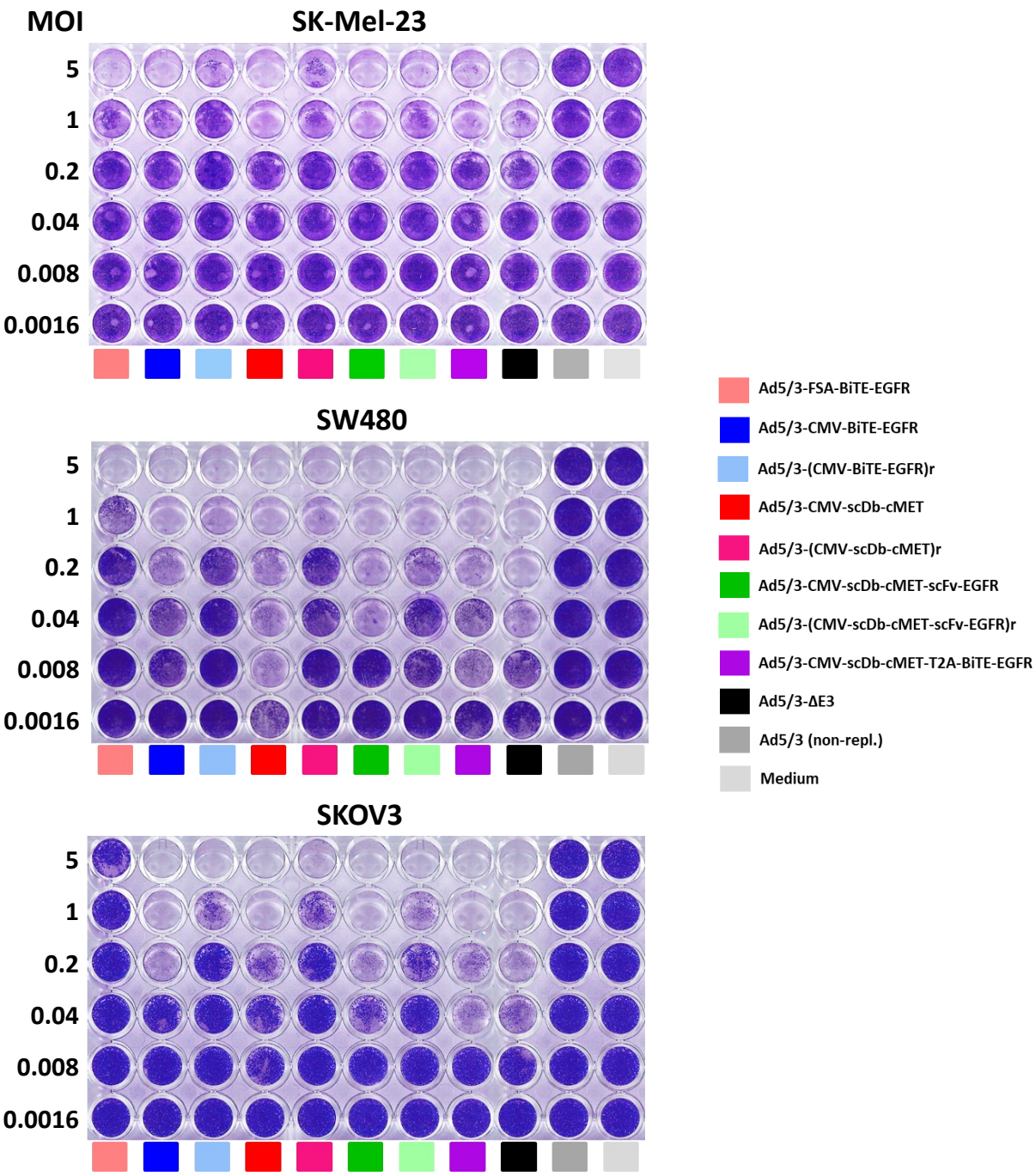

Figure 30 Oncolytic activity of oAd panel. Cytotoxicity assays of oAds on SK-Mel-23, SW480 & SKOV3. Target cells were infected with serial 5-fold dilutions of oAds (MOI = $TCID_{50}$ titer / cell). Cells were stained with crystal violet at time points of best visibility of differences between oAds. Representative experiments are shown.

3.3.4 Characterization of the Quality of Virally Produced Trispecific scDb-scFv

After having confirmed that the TCE-encoding oAds efficiently drove expression of TCEs in infected tumor cells, I addressed the question whether the virally produced TCEs performed on par with purified TCEs. I compared binding properties and induction of cytotoxicity of virally encoded scDb-cMET-scFv-EGFR to the conventionally purified antibody. I infected A549 cells with Ad5/3-(CMV-scDb-cMET-scFv-EGFR)r, as this oAd showed lower cytotoxicity

compared to its counterpart with the insert in the forward orientation, thus extending time where antibodies could be produced by live, infected cells. Antibodies were then purified following the same protocol as for antibodies purified from transfected FreeStyle-293F suspension cultures, as described in chapter 2.4.1. Size-exclusion HPLC analysis was kindly performed by the lab of Roland Kontermann (Stuttgart University) and it revealed high molecular weight species (HMWS) for the virally produced scDb-cMET-scFv-EGFR [scDb-cMET-scFv-EGFR (v)]. An overlay of the SEC of virally and non-virally produced antibody is depicted in Figure 31C. In terms of binding and cytotoxicity, the virally produced antibody showed almost equal binding with EC_{50} values of 0.81 nM for the scDb-cMET-scFv-EGFR and 1.79 nM for the scDb-cMET-scFv-EGFR (v). The binding curves are shown in Figure 31A. Induction of T-cell mediated cytotoxicity on SKOV3 cells showed a slightly higher potency of the conventionally purified antibody, with EC_{50} values of 0.36 pM and 1.26 pM for non-virally and virally produced scDb-scFvs, respectively (Figure 31B). The difference was statistically insignificant ($p = 0.2$).

In conclusion, the characterization of the virally produced scDb-scFv showed comparable properties to the purified scDb-scFv regarding antigen-binding and induction of T-cell mediated cytotoxicity.

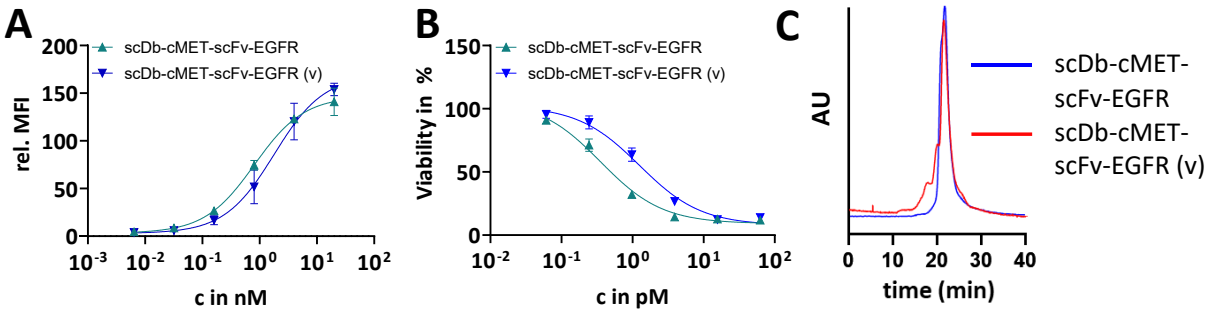

Figure 31 Characterization of virally produced scDb-cMET-scFv-EGFR (v). A) Binding properties of scDb-cMET-scFv-EGFR purified from supernatant of transfected FreeStyle-293F cells compared to scDb-cMET-scFv-EGFR purified from supernatant of oAd-infected A549 cells (v). Binding was analyzed by titration of scDb-scFvs on SKOV3 cells. Bound protein was detected using PE-anti-His mAb via flow cytometry. Relative MFI shown as mean ±SD, (n=2). B) Induction of T-cell cytotoxicity of virally (v) and non-virally produced scDb-cMET-scFv-EGFR on SKOV3 cells. Cells were incubated with a serial dilution of scDb-scFvs. PBMCs were added in an effector:target cell ratio of 10:1. Cell viability was measured 3 days after PBMC addition using crystal violet staining and subsequent quantification. Three independent experiments with different donors were conducted, data shown as mean ± SD, (n=3). C) Overlay of size-exclusion by HPLC using Superdex™ column of scDb-cMET-scFv-EGFR (blue) and scDb-cMET-scFv-EGFR (v) (red) under native conditions, kindly provided by the Kontermann lab (Stuttgart University). Elution times of proteins corresponding to molecular masses are indicated.

3.3.5 T-cell Activation Induced by TCE-armed oAds in Cocultures of Infected Tumor Cells and PBMCs

Next, I wanted to verify the potency of TCE-armed oAds as agents for dual-targeting of EGFR and c-MET. In order to assess the efficacy of TCE-armed oAds regarding their ability to mediate potent T-cell activation, I set up cocultures of oAd-infected tumor cells and PBMCs. Taking

into consideration the TCE production and oncolytic activity data, I decided to exclude the Ad5/3-FSA-BiTE-EGFR due to its poor replication and the oAds with insertions in the reverse orientation, as they induced similar levels of TCE-production with reduced oncolytic activity. I hypothesized that the Ad5/3-CMV-scDb-cMET-scFv-EGFR would be suitable for targeting both single and double target-positive cells, performing at least on par with oAds encoding a single TCE on the respective target cells and with strategies for dual expression of both BiTE-EGFR and scDb-cMET by either co-expression or co-infection.

I titrated oAds on single target-positive cell lines SK-Mel-23 ($EGFR^-$/$c\text{-}MET^+$) and SW480 ($EGFR^+$/$c\text{-}MET^-$), as well as on the double target-positive cell line SKOV3 ($EGFR^+$/$c\text{-}MET^+$). 1 dpi, I added PBMCs to the infected cells. I took supernatants of cocultures 24 h and 48 h after addition of PBMCs for quantification of cytokines IL-2 and IFNγ, respectively. Both cytokines are produced by T-cells following activation.[178, 179] In addition, I measured expression of CD69, an early T-cell activation marker[178], on CD4+ and CD8+ T-cells 24 h post addition of PBMCs. The results of the T-cell activation analysis are shown in Figure 32, with significant results indicated only for the Ad5/3-CMV-scDb-cMET-scFv-EGFR (all significant results indicated in Figure S3).

On single target-positive $EGFR^-$/$c\text{-}MET^+$ SK-Mel-23 cells, all activation markers were significantly higher for Ad5/3-CMV-scDb-cMET compared to Ad5/3-CMV-BiTE-EGFR and Ad5/3-ΔE3 infection. CD69 expression and cytokine secretion were significantly higher for all dual-targeting strategies compared to both Ad5/3-CMV-BiTE-EGFR and Ad5/3-ΔE3 infection in these cells. There were no significant differences between dual-targeting strategies and Ad5/3-CMV-scDb-cMET for any of the activation markers. Compared to the other tested cell lines, cytokine secretion and CD69 upregulation on $CD8^+$ T-cells were lower for the dual-targeting strategies, with exception of IFNγ secretion for Ad5/3-CMV-scDb-cMET-T2A-BiTE-EGFR infection and co-infection of Ad5/3-CMV-BiTE-EGFR and Ad5/3-CMV-scDb-cMET. In summary, I observed upregulation of T-cell activation markers when SK-Mel-23 cells were infected with oAds driving expression of at least one TCE targeting c-MET. These markers were not upregulated when no c-MET targeting TCE was produced.

On single target-positive $EGFR^+$/$cMET^-$ SW480 cells, all activation markers were significantly higher after infection with Ad5/3-CMV-BiTE-EGFR compared to Ad5/3-CMV-scDb-cMET or Ad5/3-ΔE3, except for IL-2 secretion. Despite the $cMET^-$ status of SW480 cells, CD69 expression was significantly higher for both $CD4^+$ and $CD8^+$ cells after infection with Ad5/3-CMV-scDb-cMET compared to the control virus. Ad5/3-CMV-scDb-cMET-scFv-EGFR

infection elevated all activation markers significantly higher than control virus infection or infection with Ad5/3-CMV-scDb-cMET. IFNγ secretion was significantly higher after Ad5/3-CMV-scDb-cMET-scFv-EGFR infection compared to all other viruses. In addition, Ad5/3-CMV-scDb-cMET-scFv-EGFR infection led to a significantly higher CD69 expression on $CD8^+$ T-cells than co-infection with Ad5/3-CMV-BiTE-EGFR and Ad5/3-CMV-scDb-cMET. Infection with the Ad5/3-CMV-scDb-cMET-T2A-BiTE-EGFR virus also led to significantly higher IFNγ secretion and CD69 expression on $CD4^+$ and $CD8^+$ T-cells than both the Ad5/3-CMV-scDb-cMET and Ad5/3-ΔE3. In addition, it led to a significant increase in IFNγ secretion compared to co-infection with Ad5/3-CMV-BiTE-EGFR and Ad5/3-CMV-scDb-cMET. In summary, Ad5/3-CMV-scDb-cMET-scFv-EGFR performed on par or better than Ad5/3-CMV-BiTE-EGFR infection and dual-targeting strategies regarding T-cell activation markers.

On double target-positive $EGFR^+/cMET^+$ SKOV3 cells, infection with all viruses led to a significant increase of CD69 expression of both $CD4^+$ and $CD8^+$ T-cells compared to the control virus. In both cases, infection with Ad5/3-CMV-scDb-cMET-scFv-EGFR reached the highest level of significance. Secretion of cytokines IL-2 and IFNγ was also significantly elevated after infection with all viruses compared to the control virus, except for Ad5/3-CMV-scDb-cMET. The Ad5/3-CMV-scDb-cMET performed poorest regarding IL-2 secretion, with all other armed oAds eliciting a significantly higher response. While IFNγ secretion was also lowest for this virus, only Ad5/3-CMV-scDb-cMET-scFv-EGFR and Ad5/3-CMV-scDb-cMET-T2A-BiTE-EGFR infection reached significantly higher secretion. There were no significant differences between dual-targeting strategies for any of the markers, except for significantly higher IL-2 secretion after Ad5/3-CMV-scDb-cMET-T2A-BiTE-EGFR infection compared to co-infection with Ad5/3-CMV-BiTE-EGFR and Ad5/3-CMV-scDb-cMET. In summary, T-cell activation markers were upregulated in all tested cocultures where TCEs were expressed, albeit with an overall lower T-cell activation for the Ad5/3-CMV-scDb-cMET.

In conclusion, the T-cell activation data showed that on single target-positive tumor cells, infection with Ad5/3-CMV-scDb-cMET-scFv-EGFR consistently performed at least on par with the single TCE encoding viruses on single target- and double target-positive cell lines and similarly to the other dual-targeting strategies, indicating efficacy of dual-targeting approaches using TCE-armed oAds. Infection with oAds encoding the non-targeting TCEs led to little to no T-cell activation. The oAd encoding the trispecific antibody performed very similarly to the Ad5/3-CMV-scDb-cMET-T2A-BiTE-EGFR across all tested T-cell activation markers, except for significantly higher IFNγ expression on SW480 cells.

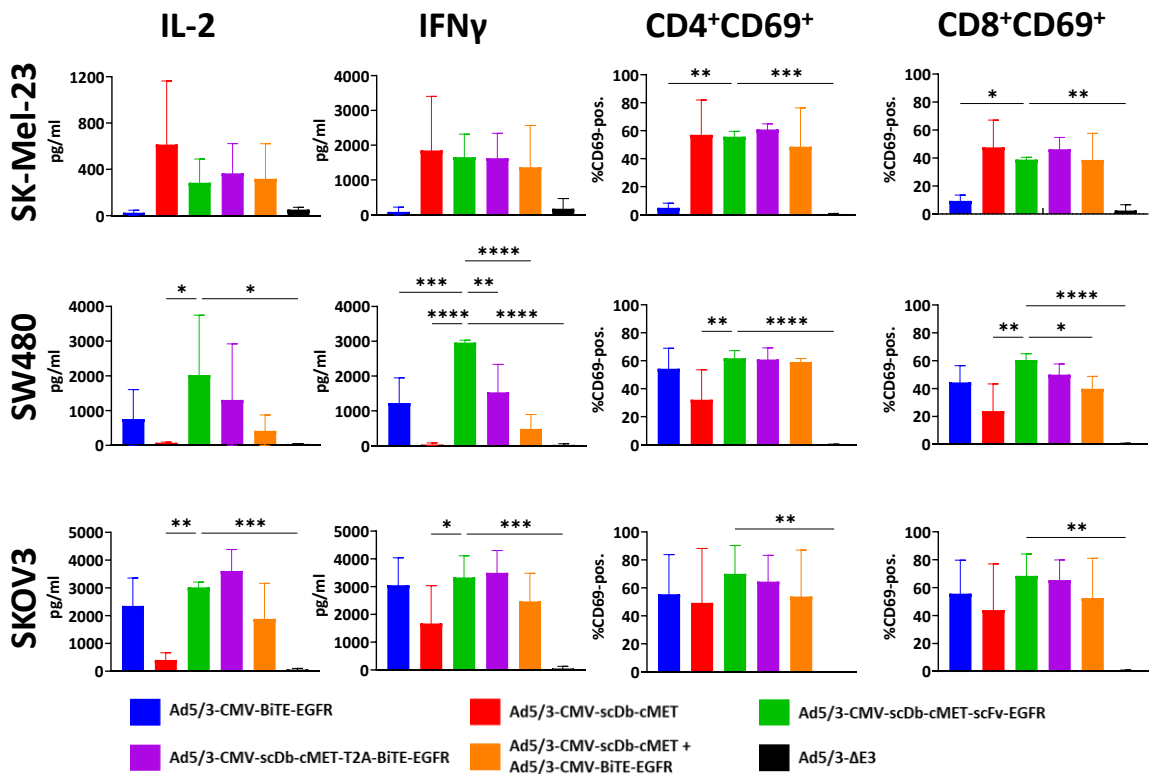

Figure 32 T-cell activation markers of PBMCs cocultured with oAd-infected target cells. Cells were infected with MOI 5 (SK-Mel-23) or MOI 1 (SW480, SKOV3). PBMCs were added 1 dpi in a 3:1 effector:target cell ratio for SW480 and SKOV3 and 6:1 for SK-Mel-23. IL-2 concentrations in the supernatant and CD69 surface expression were measured 24h post addition of PBMCs. IFNγ concentrations in supernatants were measured 48h post addition of PBMCs. Cytokine levels were measured via ELISA, CD69-expression via flow cytometry. Data gathered from 3 independent experiments with different donors, values shown as mean ± SD (n=3), *P < 0.05, **P < 0.01, ***P < 0.001, ****P < 0.0001, one-way ANOVA. Only significant differences between values for Ad5/3-CMV-scDb-cMET-scFv-EGFR and other viruses shown.

3.3.6 Cytotoxicity of TCE-armed oAds in Cocultures of Infected Tumor Cells and PBMCs

Lastly, I intended to build on the T-cell activation data by analyzing the combined effect of oncolysis and T-cell mediated cytotoxicity in cocultures of tumor cells infected with TCE-armed oAds and PBMCs. As I had already confirmed functionality of TCEs encoded by oAds in chapter 3.3.4, I did not analyze TCE-mediated killing via T-cells independently of viral oncolysis in these assays. I tested the cytotoxicity of the viruses on SK-Mel-23, SW480 or SKOV3 cells in the presence or absence of PBMCs. For SKOV3, I analyzed the cytotoxicity in the same experiments that I conducted for analysis of T-cell activation. For SK-Mel-23 and SW480, I set up additional experiments with different donors and used the donors with the highest induction of T-cell mediated cytotoxicity for the final analysis. Results of the cytotoxicity analysis are shown in Figure 33 for the MOIs with the largest difference in cytotoxicity in the conditions with or without PBMCs. Viability curves showing all MOIs are shown in Figure S4.

On EGFR$^-$/c-MET$^+$ SK-Mel-23 cells, only infection with Ad5/3-CMV-scDb-cMET-scFv-EGFR (MOI 1) led to a significantly increased cytotoxicity in presence of PBMCs, decreasing mean viability from 70% to 38%. With a p-value of 0.0571, infection with Ad5/3-CMV-scDb-cMET also led to an increase in cytotoxicity that was close to statistical significance.

On EGFR$^+$/c-MET$^-$ SW480 cells, I observed a significant increase in cytotoxicity after infection with the Ad5/3-ΔE3 at MOI 0.2 (84% mean viability without PBMCs to 48% with PBMCs). This was not the case for the other tested cell lines. Infection with the viruses Ad5/3-CMV-BiTE-EGFR, Ad5/3-CMV-scDb-cMET, Ad5/3-CMV-scDb-cMET-scFv-EGFR and co-infection with the single TCE encoding viruses also led to a significant increase in cytotoxicity in presence of PBMCs. The highest level of significance was reached by Ad5/3-CMV-scDb-cMET-scFv-EGFR with a p-value of 0.0052 (decrease in mean viability from 72% to 22% in presence of PBMCs). Cytotoxicity increase with Ad5/3-CMV-scDb-cMET-T2A-BiTE-EGFR was at the border of statistical significance with a p-value of 0.0506, close to Ad5/3-CMV-scDb-cMET with a p-value of 0.0478.

On EGFR$^+$/c-MET$^+$ SKOV3 cells, increase in cytotoxicity was highly significant for all armed oAds with p-values below 0.001 at MOI 0.2. I observed no decrease in viability for the control virus. Highest level of significance was again reached by the Ad5/3-CMV-scDb-cMET-scFv-EGFR ($p < 0.0001$, mean viability decrease from 103% to 17% in presence of PBMCs).

In summary, cytotoxicity data demonstrated that oAds armed with genes for TCEs were able to induce T-cell mediated cytotoxicity, significantly increasing killing of tumor cells in cocultures with PBMCs. The effect was relatively low on SK-Mel-23 cells with significance only for Ad5/3-CMV-scDb-cMET-scFv-EGFR, intermediate on SW480 cells with T-cell mediated cytotoxicity also observed for the unarmed oAd and very high on SKOV3 cells. Ad5/3-CMV-scDb-cMET-scFv-EGFR exhibited the strongest effect across all tested cell lines.

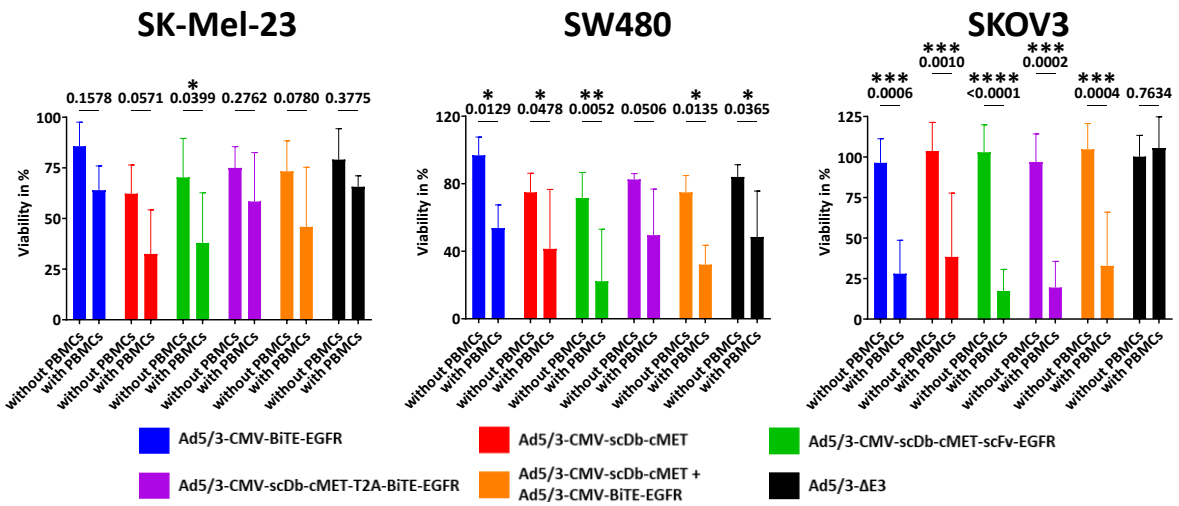

Figure 33 Cytotoxicity in cocultures of oAd-infected target cells with PBMCs. Tumor cells were infected MOI 1 for SK-Mel-23 and MOI 0.2 for SW480 and SKOV3. PBMCs were added 1 dpi and cell viability was measured via crystal violet staining 5 days after addition of PBMCs. Data shown as viability with or without PBMCs. PBMCs were added in an effector:target cell ratio of 3:1 for SKOV3 and SW480 and 6:1 for SK-Mel-23. Data gathered from 3 independent experiments with different donors. P-values for each comparison of cocultures with or without PBMCs shown, *P < 0.05, **P < 0.01, ***P < 0.001, ****P < 0.0001 two-way ANOVA.

4. Discussion

Tumor heterogeneity, resistance to conventional therapy, toxicity and insufficient selectivity of conventional therapeutic agents render many standard cancer therapy approaches ineffective. OVs have emerged as promising therapeutic alternatives, but often lacked clinical efficacy. In solid tumors, physical barriers and the innate antiviral response impair the spread of OVs.[180] In addition, the immunosuppressive TME imposes critical hurdles for OV therapy. Secretion of immunosuppressive cytokines, such as IL-10 and transforming growth factor β (TGF-β), as well as recruitment of inhibitory cells, including regulatory T-cells (T_{reg}s) and tumor-associated macrophages and fibroblasts all contribute to dysfunctional antitumor immune responses.[181, 182] TCE therapy has shown promising potency in blood malignancies but could not develop its full potential in solid tumors, due to a lack of tumor infiltration by T-cells and the TME, as well as on-target, off-tumor activity leading to varying degrees of off-tumor toxicity.[46] Here, I armed oAds with genes encoding bispecific scDbs and BiTEs or the novel trispecific scDb-scFv for dual-antigen-targeting of tumors with locally produced TCEs to overcome limitations of conventional TCE therapy and virotherapy, as well as address the problem of tumor heterogeneity with a viro-antibody-therapy approach.

For this thesis, I designed, cloned, produced and characterized bispecific TCEs targeting EGFR, HER2, c-MET and IL13Rα2, associated with various different tumor entities[135, 140-145, 151], in two different formats, i.e. scDbs and BiTEs. I conducted a first of its kind comparison of the two formats and found that all BiTEs were efficacious as TCEs, but only two scDbs were efficacious in direct comparison (scDb-HER2 and scDb-cMET). I successfully used the two efficacious scDbs as bases for the novel scDb-scFv format that had previously been described as a bispecific, trivalent TCE.[48] I designed, cloned, produced and characterized three trispecific, trivalent scDb-scFvs, namely scDb-HER2-scFv-EGFR, scDb-HER2-scFv-IL13Rα2 and scDb-cMET-scFv-EGFR. The scDb-cMET-scFv-EGFR exhibited potent dual-targeting properties, performing on par with the corresponding scDb-cMET and BiTE-EGFR on single target-positive cells and outperforming the controls on double target-positive cells. I subsequently devised an oAd panel for a viro-antibody-therapy approach, targeting EGFR and c-MET. I was able to identify a TCE expression strategy that did not attenuate oAds and drove expression of TCEs in efficacious amounts. I tested dual-targeting strategies via expression of the trispecific scDb-scFv, co-expression of scDb-cMET and BiTE-EGFR via T2A peptide and co-infection of oAds driving expression of scDb-cMET and BiTE-EGFR, respectively. I was able to show potent T-cell activation and induction of T-cell-mediated cytotoxicity in cocultures

of TCE-armed oAd-infected tumor cells and PBMCs. Of the dual-targeting approaches, the oAd encoding the scDb-cMET-scFv-EGFR showed the overall highest efficacy, importantly showing potent cytotoxicity on both $EGFR^-/c\text{-}MET^+$ and $EGFR^+/c\text{-}MET^-$ cell lines, underlining its potential as an agent for targeting heterogeneous tumors.

4.1 Characterization of Bispecific Antibodies

In order to find suitable TCEs for dual-targeting of the selected TAAs EGFR, HER2, c-MET and IL13Rα2, I cloned a panel of scDbs and BiTEs to perform a comparison of the two TCE formats. The scDb-EGFR was communicated to be ineffective in inducing T-cell mediated cytotoxicity by the Kontermann lab, therefore scDbs and BiTEs were both produced for all the targets, with the exception of the scDb-EGFR.

BiTEs are tandem-scFvs[35] and have been extensively studied, with Blinatumomab, a CD3xCD19 BiTE, being the first BiTE approved for treatment of ALL and many more used in clinical trials.[183] So far, BiTEs in clinical trials have focused on targets associated with hematological malignancies.[184] scDbs are a novel type of recombinant BsAb that have been used as TCEs and as such are structurally similar to BiTEs. In the only direct comparison performed to date by Korn et al., binding properties of scDbs and tandem-scFvs were shown to be identical, the only difference being higher stability of the scDbs under physiological conditions.[47] The analysis regarding antigen binding was in line with my findings for the comparison of scDbs and BiTEs targeting HER2, c-MET and IL13Rα2. As shown in Figure 13 and Table 14, binding analysis on target, non-target and $CD3^+$ Jurkat cells resulted in very similar binding curves and EC_{50} values, with slight advantages of scDbs for target binding. Cytotoxicity analysis in cocultures of target tumor cells with PBMCs revealed clear differences between scDbs and BiTEs targeting HER2 and IL13Rα2 (Figure 14, Table 15). In both cases, EC_{50} values of T-cell mediated cytotoxicity were significantly higher for the scDb format (6.6-fold for scDb-HER2 and 14.0-fold for scDb-IL13Rα2). In contrast to the scDb-IL13Rα2, the scDb-HER2 still reached the same maximum cytotoxicity as the corresponding BiTE, the generated dose-response curves for scDb and BiTE therefore presenting a clean shift, both within the low picomolar range. The scDb-IL13Rα2 did not reach the same level of T-cell mediated cytotoxicity as the BiTE on target cells, suggesting a structural deficit of the scDb format. Induction of cytotoxicity has not yet been directly compared for scDb and BiTE formats. The differences in structure result in lower flexibility of the scDb format that would not influence binding to either the TAAs or CD3, but could lead to steric hindrance when both antigen binding sites of the scDb are to be engaged at the same time. Work by Asano et al.

comparing different domain orders for diabodies has shown that binding affinities were not notably influenced by V_H/V_L domain rearrangement, but significant differences in cross-linking efficacies were observed. This was not the case for tandem-scFv molecules, where antigen binding sites can rotate freely.[185] Furthermore, the design of linkers plays a crucial role for the function of BsAbs. Amino acid composition and lengths of the linkers could be modified for optimal scFv configurations.[186] Steric hindrance could also be explained by inaccessibility of the epitope when scDbs are bound to TCRs or vice versa. Choosing a more accessible epitope might lead to more effective cross-linking. These various points of modification highlight the importance of structural optimization of scDbs. The scDb-cMET characterized here performed on par with the BiTE-cMET, exhibiting equal binding properties and level of T-cell mediated killing, suggesting an effective configuration of this molecule.

Because of their potential of inducing T-cell mediated cytotoxicity, I chose scDbs -HER2 and -cMET as suitable bases for production of novel trispecific scDb-scFvs.

4.2 Characterization of Trispecific Antibodies

The trispecific scDb-scFvs are a novel type of dual-targeting agents only described as trivalent, bispecific molecules to date, with a CD3 binding domain and two TAA binding domains directed at HER3.[48] The scDb-scFv exhibited increased binding to $HER3^+$ cancer cells compared to the corresponding scDb, resulting in increased T-cell activation, proliferation and induction of T-cell mediated killing. Here, I targeted two different TAAs with a single trispecific molecule. Encouraging results of other trispecific TCEs have been described. A nanobody-based trispecific TCE consisting of three fused together nanobodies targeting CD3, FAP and PD1, has demonstrated antigen-specific killing and potent T-cell activation *in vitro* and additionally suppressed tumor growth and enhanced T-cell infiltration of solid tumors in a mouse model.[187] In a different approach, two nanobodies, or heavy-chain-only antibodies (V_{HH}), targeting EpCAM and EGFR, respectively, were fused to a CD3-binding scFv. This TCE also showed potent target cell specific cytotoxicity *in vitro* and prolonged survival of tumor bearing mice *in vivo*.[188] Recently, a trispecific antibody named DTriTE, constructed via fusion of three scFvs specific for CD3, IL13Rα2 and EGFRvIII, was described.[189] Compared to bispecific antibodies, this trispecific TCE demonstrated superior outcomes in both *in vitro* and *in vivo* models and importantly, enhanced control of heterogeneous tumors in long-term survival experiments. Fusion of three scFvs used to construct this antibody resulted in a structure similar to the scDb-scFv. The more flexible V_H/V_L arrangement of this format is likely to make it less prone to steric hindrance during binding and cross-linking, but might come at

the cost of stability under physiological conditions compared to the scDb-scFv, which, due to its more rigid structure, is potentially better protected from proteolytic degradation.[47]

Based on my results for the scDb and BiTE characterization, I cloned and produced three trispecific scDb-scFvs, namely scDb-HER2-scFv-EGFR, scDb-HER2-scFv-IL13Rα2 and scDb-cMET-scFv-EGFR. Dual-targeting for these antigen combinations has been previously described.[161-165, 167] I confirmed purity of all three scDb-scFvs via SDS-PAGE and subsequent size-exclusion HPLC (Figure 17). All constructs eluted as one major peak, a low molecular weight shoulder was observed for scDb-HER2-scFv-EGFR and scDb-HER2-scFv-IL13Rα2, likely due to the very low yield following elution and subsequent strong concentration on concentrator columns, leading to concentration of fragments and impurities. The SEC analysis is similar to the results presented for the bispecific scDb-scFv.[48] Binding analysis confirmed antigen-binding of all binding domains for all three scDb-scFvs (Figure 18, Table 17). For scDb-HER2-scFv-EGFR and scDb-HER2-scFv-IL13Rα2, I detected slightly weaker binding to Jurkat cells compared to the corresponding scDbs (and BiTEs), which was in line with the scDb-scFv characterization of the Kontermann lab.[48] The markedly weaker binding to TAAs targeted by the scFv domain of the trispecific scDb-scFv compared to the corresponding BiTEs could point to steric hindrance for binding of these domains. The scDb-cMET-scFv-EGFR showed equal binding properties compared to its corresponding bispecific TCEs, suggesting that there was no interference between antigen binding domains for this construct. Considering that all TCEs were produced in the same configuration, this might suggest that the optimal configuration is different for each construct, depending on the incorporated V_Hs and V_Ls. Differences in configuration of the same V_H and V_L domains in a trispecific DTriTE have been shown to influence binding properties and T-cell activation, where the most potent configuration for the analyzed construct was observed with a central positioning of the anti-CD3 scFv.[189] The deficiencies of scDb-HER2-scFv-EGFR and scDb-HER2-scFv-IL13Rα2 seen in the binding analysis also translated into weaker induction of T-cell mediated cytotoxicity in cocultures of target cells and PBMCs compared to the corresponding bispecific TCEs (Figure 19, Table 18). Interestingly, this was also the case for cocultures with double target-positive cell lines, although binding was stronger for the scDb-scFvs in these cell lines than for corresponding scDbs and BiTEs. This might be due to the weaker CD3 binding of these scDb-scFvs and/or steric hindrance during cross-linking.

In an attempt to overcome the limitations of the scDb-scFv format, I reconfigured the TCEs scDb-HER2-scFv-EGFR and scDb-HER2-scFv-IL13Rα2, moving the scFv from the C-

terminus to the N-terminus. For the TriTE, a trispecific antibody consisting of an scFv with variable domains of heavy-chain only antibodies (V_{HH}s) fused to both N- and C-terminus of the scFv, significantly weaker binding and cross-linking abilities of the C-terminal V_{HH} were described.[188] In a similar trispecific format (TriTAC) consisting of an scFv with fused V_{HH}s, significantly weaker binding of the N-terminally V_{HH} was shown for one of the described constructs.[190] These results show that positioning of domains in a trispecific antibody is complex and depends on both the format and sequence of domains. I compared the new scFv-EGFR-scDb-HER2 and scFv-IL13Rα2-scDb-HER2 to their corresponding scDb-scFvs regarding target cell binding. Unfortunately, I could not show improved scFv-scDb binding compared to the corresponding scDb-scFvs, suggesting that the positioning of the scFvs was not causal for the observed binding properties (Figure 21). Another possible modification would be an adjustment of linker lengths, which is known to affect antigen binding properties.[191] Other scFv-based trispecific antibody formats consisting of the same basic elements as the scDb-scFv are the aforementioned DTriTE and the Triplebody. The Triplebody also links three scFvs together as a single-chain molecule. It has shown promising efficacy *in vitro*, with specific antigen binding and cell lysis, both as TCE and NCKE.[192-195] Rearrangement of V_Hs and V_Ls of scDb-scFvs to create DTriTEs / Triplebodies could be easily performed as another alternative.

My results showed that in contrast to the scFv-EGFR-scDb-HER2 and scFv-IL13Rα2-scDb-HER2, the scDb-cMET-scFv-EGFR exhibited convincing potency in cocultures, performing on par with corresponding bispecific TCEs on single target-positive cells and with significantly higher induction of T-cell killing in double positive cells. These properties of the scDb-cMET-scFv-EGFR made it a very promising TCE for dual-targeting of c-MET and EGFR via intratumoral delivery by oAds. Compared to a combination of two bispecific TCEs, the scDb-scFv requires less genomic space in an oAd, reducing the risk of genomic instability and attenuation. Furthermore, two bispecific TCEs possess two identical anti-CD3 scFvs, dramatically increasing the risk of homologous recombination. Lastly, the trispecific scDb-scFv is less likely to become subject to the high-dose hook effect[196] compared to two bispecific TCEs. In high antibody concentrations that could be reached during phases of TCE-armed oAd replication within the tumor, binding sites on both target cells and T-cells could become saturated, reducing the formation of immune synapses. This effect would be observed in lower concentrations of two bispecific TCEs compared to one trispecific TCE, due to the additional CD3-binding domain.

4.3 Characterization of Armed oAds

The final part of this thesis aimed to produce and characterize oAds armed with genes for TCEs for dual-targeting of EGFR and c-MET, testing different expression strategies and insertion sites. c-MET is expressed on healthy epithelial cells of numerous organs throughout life[197] and overexpression of c-MET and its constitutive activation has been described for a great variety of tumors.[198] Similarly, EGFR is also expressed on cells of many healthy organs and dysregulation of the EGFR pathway, accompanied by its overexpression on cell surfaces, is a characteristic of numerous human cancers.[199] The presence of these two receptors on healthy cells of most human organs poses challenges for systemic administration of c-MET and EGFR targeting agents.[200, 201] In order to effectively target c-MET and EGFR while minimizing systemic side effects, intratumoral delivery of therapeutics such as TCEs via oAds can be a promising alternative.

The combination of virotherapy and antibody therapy has been extensively studied since over 15 years, with numerous antibody formats, including whole immunoglobulins, antibody fragments and bi- and trispecific antibodies, having been described.[110, 202] To date, an OV driving expression of an antibody targeting two distinct tumor antigens has not been described. Antibodies can be administered either separately as proteins or as transgenes encoded in the OVs. If delivered via transgenes, antibodies are produced locally in the tumor, mitigating systemic toxicity of encoded antibodies and allowing for higher concentrations of therapeutic antibodies *in situ* with better tumor perfusion.[203]

4.3.1 Dual Expression Cassettes

In order to effectively compare expression of a trispecific TCE to that of two bispecific TCEs regarding anti-tumor activity, I explored two dual-expression strategies. On the one hand, I investigated expression of an scDb and a BiTE via a bidirectional promoter cassette and on the other hand dual-expression via a T2A peptide. I explored these two expression strategies due to their smaller genomic size compared to two full length promoters. An expression cassette for a bispecific TCE, including the CMV promoter, the TCE gene and the poly A tail, was approx. 2.3 kb long. This meant that dual-expression via two independent expression cassettes would have surpassed the size limit of 105 % of the wt genome, which allowed for insertion of a maximum of approx. 4.5 kb. In addition, the use of bidirectional promoters or T2A peptides would also reduce the number of repetitive sequences, reducing the risk of homologous recombination.

Both strategies have been described for transgene expression by OVs. ONCR-177, an HSV that underwent a phase I clinical trial in 2023, expresses a total of five transgenes driven by a bidirectional promoter cassette consisting of the CMV early enhancer/chicken β actin (CAG) and the synthetic MND promoter (a synthetic promoter containing the U3 region of a modified Moloney murine leukemia virus long terminal repeat). The transgenes expressed via these promoters were separated by T2A sequences.[204, 205] Here, I constructed bidirectional promoter cassettes using the minimal CMV promoter with either the full CMV promoter or the hPGK1 promoter in a tail-to-tail fusion with a common enhancer element (Figure 23B). The mCMV-hPGK1 promoter has been described as functional in driving expression of the puromycin and green fluorescent protein (GFP) gene.[206] The mCMV-CMV promoter was adapted from Alcocer and colleagues, that showed functioning expression of TCRα and TCRβ chains with the bidirectional CMV promoter.[207] The bidirectional promoter constructs I tested here were all able to drive expression of both firefly and Renilla luciferase, measured following transient transfection of HeLa cells (Figure 23A). Both bidirectional promoter constructs exhibited overall higher expression levels when the mCMV promoter was driving expression of the Renilla luciferase and the full length promoter was driving expression of the firefly luciferase (CMV-mCMV and hPGK1-mCMV), suggesting a more effective transcription for this orientation of the promoter cassettes. Bidirectional promoters similar to the mCMV-CMV and CMV-mCMV promoters I employed here, were described by Andersen et al. using a CMV enhancer flanked by minimal CMV promoters in opposing directions. They found a 2:1 preference for transcription of the gene following the CMV enhancer in its natural orientation.[208]. My results indicated this preference as well, although I could not directly compare expression strengths of the two different luciferases in the assays. I chose the CMV-mCMV promoter for further experiments, as it showed the highest overall expression.

While I could show expression of luciferases after transfection of HeLa cells, the bidirectional CMV-mCMV promoter did not retain its activity as driver of TCE expression by oAds. As shown in Figure 27, only the BiTE-EGFR (transcription driven by full length CMV) was expressed at low levels in either insert orientation and transduced cell line. Expression of the scDb-HER2 was below detection limit, PCR analysis of the insert regions showed multiple bands, suggesting recombination events with deletions within the inserts. The large size of the inserts, 4367 bp, was close to the maximum insert size of approx. 4.5 kb that would keep the oAd genomes below 105 % of the wt genome. The large insert size and presence of identical sequences could therefore have led to instability of the genomes facilitated by homologous recombination, greatly increasing the probability for loss of unessential genes or gene

segments.[84] To mitigate the problems of low expression and genomic instability, expanding the repertoire of bidirectional promoter cassettes or optimization of the described promoters could be performed, as well as using a different Ad serotype that could harbor a larger transgene without exceeding or coming too close to the 105 % genome size limit.

My second approach for expression of two TCEs was using T2A peptides, that have been shown to facilitate equimolar expression of transgenes.[209] Surprisingly, I could not measure production of TCEs for two of the tested configurations [(scDb-cMET-T2A-BiTE-EGFR)r and BiTE-EGFR-T2A-scDb-cMET] after transfection of HeLa cells (Figure 24). Furthermore, TCE expression did not appear equimolar for the working constructs [scDb-cMET-T2A-BiTE-EGFR and (BiTE-EGFR-T2A-scDb-cMET)r], with a preference for the TCE behind the T2A-peptide. This might also be explained by effects of the C-terminal residue of the T2A peptide, which has been shown to interfere with protein function, which in this case could interfere with detection antibodies binding to the C-terminal HA- or Myc-tag of the first TCE in the cassette.[210] Due to the more equimolar expression with the scDb-cMET-T2A-BiTE-EGFR, I selected it for oAd cloning. As for the bidirectional constructs, the oAds with T2A dual expression cassettes did not confer equimolar expression of TCEs (Figure 28). Preference was again on the TCE after the T2A peptide. In addition to possible detection interference by the T2A peptide, PCR of the insert region revealed multiple bands for the Ad5/3-CMV-scDb-cMET-T2A-BiTE-EGFR with increasing intensity following multiple passaging, suggesting possible deletions within the T2A expression cassette. Sequencing of the smallest band confirmed deletion of the sequence between the end of the CMV promoter and the V_L of the scFv-EGFR (Figure S1). In contrast to the bidirectional promoter cassettes, the TCEs expressed via T2A are encoded unidirectionally, increasing the probability of homologous recombination between TCE sequences. The CD3 binding domain, linker sequences and sequences of constant V_H/V_L regions are almost identical in scDb-cMET and BiTE-EGFR.

Taken together, I was able to clone dual expression cassettes with both directional promoters and T2A peptides that conferred dual expression of TCEs after transfection. The bidirectional promoter strategy failed to keep its dual-expression properties in the viral context. Although I detected expression of both TCEs following infection of target cells with the Ad5/3-CMV-scDb-cMET-T2A-BiTE-EGFR, expression was not equimolar analysis of the insert via PCR and sequencing revealed deletions within the insert. These results underline the risk for genomic instability when using large inserts and repetitive sequences, highlighting the advantage of the trispecific scDb-scFv opposed to two bispecific TCEs.

4.3.2 Oncolysis and Antibody Production

All viruses were produced at VP/$TCID_{50}$ ratios similar to the Ad5/3-ΔE3 control virus, with the exception of the Ad5/3-FSA-BiTE-EGFR and the viruses encoding the bidirectional promoter cassettes. As discussed before, the bidirectional promoter viruses carried inserts close to the maximal transgene size, which could lead to unstable genomes and impaired replication.[84] The Ad5/3-FSA-BiTE-EGFR exhibited the highest VP/$TCID_{50}$ ratio, with a markedly higher ratio than the two viruses carrying the same TCE in the insert site behind the E4 region (Figure 26) in addition to poor oncolytic activity compared to the other oAds, even when infectious titers were used (Figure 30). A previous study directly compared expression from the after-fiber site with the after-E4 site with the same expression strategy and found that the after-fiber site showed enhanced transgene expression that came at the expense of oncolytic potency.[85] This would be in line with the clear attenuation of the Ad5/3-FSA-BiTE-EGFR found here and suggests a link between the expression strategy for BiTE-EGFR and oncolytic activity of the oAds. Another study by Jin et al. did not show this attenuation for Ad5 viruses expressing GFP via SA in the after-fiber site, suggesting a dependency of the attenuation on the insert sequence.[177] I did not test expression in the after-fiber site or after-E4 site with the same promoter/splice acceptor, so a definitive conclusion regarding transgene expression could not be reached here, although the higher transgene expression in the after-fiber position compared to the after-E4 position has also been described elsewhere.[211] Although I did not include the Ad5/3-FSA-BiTE-EGFR in the final oAd panel, the expression strategy is highly preferrable for approaches where high transgene expression is desired. Furthermore, the slow replication compared to the other oAds could potentially delay clearance by the immune system, as it might evoke a weaker immune response, prolonging transgene expression.[212]

For the viruses expressing TCEs via a CMV promoter, I found a clear link between insert orientation and oncolytic activity. For all virus pairs [Ad5/3-CMV-BiTE-EGFR and Ad5/3-(CMV-BiTE-EGFR)r, Ad5/3-CMV-scDb-cMET and Ad5/3-(CMV-scDb-cMET)r, Ad5/3-CMV-scDb-cMET-scFv-EGFR and Ad5/3-(CMV-scDb-cMET-scFv-EGFR)r] I observed an attenuation of oAds when transgenes were inserted in the reverse orientation (Figure 30). Work by Suzuki et al. showed that insertion of different transgenes in the after-E4 site in forward and reverse orientation did not result in significantly differing infectious titers of oAds, suggesting that my observed attenuation of oAds with inserts in the reverse orientation may be sequence-dependent.[213] Their work also showed that the orientation of transgenes in the after-E4 insertion site was inconsequential for transgene expression, similar to my own findings for my

oAd panel. This effect was highly dependent on the transgene itself and other publications have shown higher expression of transgenes in the after-E4 site in the reverse orientation, supporting the finding that the RITR has transcription initiation properties.[177, 214] Here, I showed slightly higher expression levels in the reverse orientation only for the Ad5/3-(CMV-BiTE-EGFR)r compared to the Ad5/3-CMV-BiTE-EGFR.

Overall, the TCE concentrations that I measured for oAds with transgenes in the after-E4 site were in the range of approx. 1-5 nM, 7 dpi at MOI 25 for SK-Mel-23 and MOI 5 for SW480 and SKOV3. The EC_{50} values and concentrations where maximum toxicity was reached in cocultures of tumor cells and PBMCs were all in the subnanomolar range (Figure 19, Table 18), indicating that TCE production of oAds would be sufficient to effectively induce T-cell mediated killing in tumors. The in comparison very high concentrations reached with the Ad5/3-FSA-BiTE-EGFR (approx. 20 nM in SKOV3, 50 nM in SW480 and 150 nM in SK-Mel-23) are likely to lead to the high-dose hook effect in tumor sites proximal to oAd-replication, but could also provide higher concentration of TCEs in more distal tumor sites. If this would also lead to more systemic leakage of TCEs and increased risk of on-target, off-tumor effects would have to be investigated *in vivo*.

Another consideration for interpretation of the antibody expression data are limitations of the quantification method. I performed quantification of TCEs with the supernatant of infected cells, which themselves express the TCE targets. A fraction of the produced antibodies would be bound to the cells and would not appear in the quantification. I measured the highest production of the BiTE-EGFR after infection of the $EGFR^-$ SK-Mel-23 cell line, whereas highest scDb-cMET production was measured in supernatants of infected $c\text{-}MET^-$ SW480 cells. Additionally, BiTE-EGFR production was slightly higher compared to scDb-cMET production after co-infection with Ad5/3-CMV-BiTE-EGFR and Ad5/3-CMV-scDb-cMET of SK-Mel-23 cells and the opposite was the case after co-infection of SW480 cells, albeit with a minimal difference. Co-infection of $EGFR^+/c\text{-}MET^+$ SKOV3 cells also led to measurement of slightly higher scDb-cMET titers, which would fit the data of better binding of BiTE-EGFR to SKOV3 cells compared to scDb-cMET (Figure 18B). Importantly, my data showed that co-expression of two TCEs either via co-expression driven by one oAd or via co-infection of two single TCE-encoding oAds was feasible.

4.3.3 Validation of Bioactivity of Virally Produced TCE

After I could show TCE secretion from infected cells in amounts sufficient to induce T-cell mediated killing, I confirmed bioactivity of virally encoded scDb-cMET-scFv-EGFR compared to conventionally produced scDb-cMET-scFv-EGFR. Analysis showed only insignificant differences between scDb-cMET-scFv-EGFR and scDb-cMET-scFv-EGFR (v), with slightly higher potency of the conventionally purified TCE. Size-exclusion HPLC revealed the presence of HMWS for the virally produced TCE. HMWS have been shown to be potentially immunogenic, which could lead to immune-mediated adverse effects.[215] The presence of HMWS here could be explained by the production process that differs from the production of the other purified antibodies.[216] For production of the virally encoded scDb-scFv, cells were kept in medium containing FCS, which increases the risk of contaminants and components interfering with the purification process.[217] Optimization of the production and purification method for virally produced antibodies could allow for a more precise comparison.

4.3.4 T-cell Activation and Cytotoxicity

In order to elucidate the combined effects of oncolysis and TCE mediated cytotoxicity, I prepared and analyzed cocultures with tumor cells, viruses and PBMCs. With this method, I did not measure bystander killing mediated by virally encoded TCEs separately, but rather detected the additive effect of oncolysis and T-cell mediated cytotoxicity. By comparing cytotoxicity in cocultures with or without PBMCs, I had to ensure that the T-cell mediated effect was not lost due to strong oncolytic effects by optimizing MOIs and ratios of effector to target cells. Similar setups for characterization of BiTE-armed oAds have been previously described.[123, 124] Alternatively, separating oncolysis and bystander killing is feasible as well by using supernatants of TCE-armed oAd-infected cells for cocultures of tumor cells and PBMCs.[119-121] As I had extensively characterized the TCEs and confirmed bioactivity of virally encoded oAds, I chose the assay for analysis of the combined oncolytic and T-cell mediated cytotoxic effect. I narrowed down the virus panel in the cocultures to the viruses with transgenes in the after-E4 site, with inserts in the forward orientation. I chose these viruses due to their higher oncolytic activity and equal antibody production in comparison to the oAds with inserts in reverse orientation.

The cocultures revealed that all armed oAds were capable of activating T-cells, measured by secretion of IL-2 and IFNγ and surface expression of CD69 (Figure 32). In cocultures of single bispecific TCE-expressing oAds on single positive cells, I observed T-cell activation only when

the antigen-binding TCE was produced, showing target cell specificity of produced TCEs. When the non-binding TCE was produced, cytokine secretion was at the level of Ad5/3-ΔE3. This very clear selectivity was lost to some degree in the cytotoxicity data (Figure 33), where I observed T-cell mediated cytotoxicity also for the oAds expressing the non-binding TCE and for Ad5/3-ΔE3. In both $EGFR^-/c\text{-}MET^+$ SK-Mel-23 and $EGFR^+/c\text{-}MET^-$ SW480 cocultures, I detected enhanced killing in the presence of PBMCs after infection with non-targeting viruses (Ad5/3-CMV-BiTE-EGFR and Ad5/3-ΔE3 for SK-Mel-23 and Ad5/3-CMV-scDb-cMET and Ad5/3-ΔE3 for SW480). In SW480, the cytotoxicity was significantly enhanced in both cases. Two thresholds have been described for activation of cytotoxic T-cells, the first threshold inducing T-cell killing and the second threshold inducing release of cytokines.[218] This phenomenon described by Faroudi et al. was elucidated by analysis of spikes in the intracellular Ca^{2+} concentration of T-cells. Flow cytometric analysis of target cell lines SK-Mel-23 and SW480 showed no expression of EGFR for SK-Mel-23 and no expression of c-MET for SW480 (Figure 12), but a more sensitive analysis has revealed low expression of these TAAs for these cell lines.[219] It is therefore possible that lytic synapses were formed in the presence of elevated TCE concentrations following infection, without crossing the second threshold for cytokine secretion. An approach to test this hypothesis might be the use of different EGFR- or c-MET-negative cell lines or knock-downs of either EGFR or c-MET, insuring the absence of the TCE targets. Another mechanism that might have contributed to the observed cytotoxicity is the release of TAAs, PAMPs and DAMPs following viral oncolysis, which could induce T-cell mediated cytotoxicity through residual DCs.[220] Furthermore, the ICD signature differs between cell lines and while there is no specific data for SW480, it is possible that a stronger ICD signature of SW480 contributed to the significantly enhanced cytotoxicity in cocultures with oAds and PBMCs, reducing the TCE-mediated effect.[221]

In regard to the co-targeting approaches, co-infection with Ad5/3-CMV-BiTE-EGFR and Ad5/3-CMV-scDb-cMET showed equimolar antibody production (Figure 28), but the overall lowest level of T-cell activation compared to the other co-targeting strategies. Expression levels of the BiTE-EGFR were notably higher following infection with the Ad5/3-CMV-scDb-cMET-T2A-BiTE-EGFR compared to the co-infection strategy, fitting to the more pronounced T-cell activation in $EGFR^+/c\text{-}MET^-$ SW480 and $EGFR^+/c\text{-}MET^-$ SKOV3 cells, but only slight differences in $EGFR^-/c\text{-}MET^+$ SK-Mel-23 cells. Concerning cytotoxicity, the co-infection approach outperformed the co-expression approach in SK-Mel-23 and SW480, but not in SKOV3. A risk of the co-infection strategy are differences in replication that would lead to more efficient spread of one virus *in vivo* and consequent loss of the other virus, and therefore one

TCE, in the tumor. A study analyzing co-infection of tumor cells with a panel of armed HSV-1 has shown that the co-infection approach is feasible and effective at delivering multiple transgenes while retaining viral replication *in vitro*, although imbalances in replication of the different viruses could not be excluded.[222] In addition, co-infection of cells with two different oAds might lead to recombination events between the viral genomes, leading to loss or modification of transgenes.[106] Lastly, regulatory challenges have to be considered when using two distinct therapeutic agents instead of one.

The Ad5/3-CMV-scDb-cMET-scFv-EGFR was able to elicit T-cell activation and cytotoxicity across all tested target cell lines at least equally well as the other viruses of the oAd panel (Figures 32 and 33). With the exception of IFNγ secretion in cocultures with SW480 cells, I measured no significant differences of T-cell activation markers between Ad5/3-CMV-scDb-cMET-scFv-EGFR and Ad5/3-CMV-scDb-cMET-T2A-BiTE-EGFR. I observed the same significant difference for the co-infection strategy, in addition to significantly lower CD69-positive $CD8^+$ T-cells in SW480 cocultures. Concerning cytotoxicity, both co-expression and co-infection strategies were inferior to the Ad5/3-CMV-scDb-cMET-scFv-EGFR. Lower efficacy of the Ad5/3-CMV-scDb-cMET-T2A-BiTE-EGFR can be explained by the non-equimolar production of scDb-cMET and BiTE-EGFR. The additional problem of homologous recombination for this virus was discussed in chapter 4.3.1. In addition to the aforementioned problems of the co-infection approach, I measured slightly higher concentrations of the scDb-scFv in supernatants of infected cells compared to the co-infection strategy, possibly contributing to the higher cytotoxicity of the Ad5/3-CMV-scDb-cMET-scFv-EGFR in cocultures.

Activation of T-cells in cocultures of Ad5/3-CMV-scDb-cMET-scFv-EGFR and PBMCs on both single- and double-positive target cells proves cross-linking abilities of the secreted scDb-cMET-scFv-EGFR for both EGFR and c-MET and supports its potential for the treatment of heterogeneous tumors. The effect of T-cell mediated cytotoxicity was greater in cocultures with Ad5/3-CMV-scDb-cMET-scFv-EGFR than for any other virus across all cell lines, fitting to the T-cell activation data. Interestingly, cocultures with Ad5/3-CMV-scDb-cMET-scFv-EGFR showed overall higher potency than the other co-targeting strategies with Ad5/3-CMV-scDb-cMET-T2A-BiTE-EGFR and co-infection of Ad5/3-CMV-BiTE-EGFR and Ad5/3-CMV-scDb-cMET.

In conclusion, the T-cell activation and cytotoxicity data showed that a dual-antigen-targeting approach using TCE-armed oAds was feasible. All tested co-targeting strategies successfully

activated T-cells and induced T-cell killing in addition to viral oncolysis on single target- and double target-positive cell lines. Importantly, the Ad5/3-CMV-scDb-cMET-scFv-EGFR offered multiple advantages compared to either co-infection or co-expression approaches, i.e. stable equimolar targeting of both antigens, genomic stability and more potent T-cell activation and induction of T-cell mediated cytotoxicity across all single-target and double-target positive cell lines.

4.4 Dual-Antigen-Targeting

My work proposes a novel dual-antigen-targeting strategy to address the problem of tumor heterogeneity via a viro-antibody-therapy approach. Alternative dual-antigen-targeting approaches have been described for small molecules, antibody and CAR-T cell therapy, in many cases with the goal of increasing tumor selectivity. In case of BsAbs, dual-targeting approaches make up only a small percentage of constructs under clinical evaluation and are almost exclusively bispecific IgG antibodies, but many more formats are in development.[159, 223] While dual-targeting via BsAbs offers advantages such as increased tumor selectivity, enhanced payload delivery for ADCs and modulation of two cellular pathways simultaneously, BsAbs still face the challenge of short half-lives in circulation and on-target off tumor toxicities that can be mitigated by *in situ* production using OVs, eliminating the need for continuous infusion and combatting the immunosuppressive TME.[224]

TCEs and NKCEs have also been explored for dual-targeting approaches, where at least trivalent molecules or the simultaneous administration of two antibodies are required. An NKCE co-targeting B-cell maturation antigen (BCMA) and CD200 has shown highly increased selectivity of NK-cell mediated killing for double-positive target cells *in vitro*, proposed to reduce off-tumor toxicities.[225] Similarly, a trispecific NKCE co-targeting EGFR and PD-L1 on tumor cells has also been described as a more tumor-selective agent compared to bispecific constructs.[226] Apart from increased tumor selectivity, it induced immune checkpoint inhibition and exhibited potent NK-cell mediated cytotoxicity *in vitro*. Numerous trispecific TCEs are also under investigation, described in detail in chapter 4.2. An innovative co-targeting approach was proposed by Banaszek et al., introducing the hemibody format that consists of a TAA-binding scFv fused to either the V_H or V_L of an scFv-CD3.[227] Complementary hemibodies targeting EGFR and HER2 showed selective induction of T-cell mediated cytotoxicity on a double target-positive breast cancer cell line *in vivo*. Although dual-targeting TCEs and NKCEs show promising results, they face similar challenges as BsAbs, i.e. the need for continuous administration for effective concentrations in the TME and systemic toxicities.

CAR-T cells are also increasingly explored as dual-antigen-targeting agents. Infusion of two different single-antigen-targeting CAR-T cells, infusion of T-cells with two CARs or administration of T-cells with bispecific CARs have been described.[158] In a murine MM model, co-targeting of BCMA and G protein-coupled receptor calls C group-5 member-D (GPRC5D) prevented BCMA-escape-mediated relapse.[228] In this model, all aforementioned strategies for dual-targeting via CAR-T cells were compared and the bicistronic CAR construct, expressing two different CARs in one T-cell, was found to be the most efficacious approach. An encouraging phase 1 clinical trial demonstrated preliminary safety and bioactivity of bicistronic CAR-T cells co-targeting EGFR and IL13Rα2 to address the problem of tumor heterogeneity in GBM.[15] Reduced antigen escape was also observed by Hegde et al. using CAR-T cells with extracellular CAR domains consisting of a HER2-binding scFv and a mutated IL-13 molecule for co-targeting of HER2 and IL13Rα2.[167] The use of CAR-T cells presents a promising strategy for dual-antigen-targeting, but also faces important challenges in solid tumors, mainly the immunosuppressive TME and poor trafficking to and persistence in the tumor.[181] The combination of CAR-T cells with OVs is increasingly investigated, as OVs can help overcome challenges faced by OVs, importantly by reverting tumor immunosuppression and the possibility of introducing transgenes stimulating CAR-T cell function.[181, 229]

In conclusion, effective dual-antigen-targeting approaches have been described for different antibody formats and CAR-T cells, pursuing both higher tumor selectivity and reducing antigen escape. Both antibody- and CAR-T cell-strategies face important challenges that could be combatted by combination with OV therapy.

4.4.1 Dual-Targeting of EGFR and c-MET

My results show that dual-targeting of EGFR and c-MET is effectively feasible with TCE-armed oAds, targeting both single and double target-positive cells. To date, dual-targeting of EGFR and c-MET has been described for small molecule and antibody approaches. Importantly, it has been shown that an interplay between EGFR and c-MET expression is seen in cancer, where monotherapy targeting one receptor leads to compensatory mechanisms and upregulation of the other receptor, underlining the rationale for co-targeting EGFR and c-MET.[230, 231] TC-N19, a novel dual-inhibitor of EGFR and c-MET overcame resistance of EGFR TKI therapy in an *in vivo* model of NSCLC, suppressing xenograft tumor growth.[161] Doxazosin, a drug used for treatment of benign prostate hyperplasia and hypertension, showed suppression of tumor growth, angiogenesis and metastases in an orthotopic allograft model of TNBC by

simultaneous disruption of EGFR and c-MET signaling pathways.[162] In an *in vivo* model of HNSCC, administration of an anti-EGFR and anti-c-MET TKI simultaneously led to increased tumor control compared to monotherapy.[163] While these small molecules show encouraging results for dual-inhibition of EGFR and c-MET, small molecules face important limitations, including a wide range of side effects that affect various organ systems.[232] The property of OVs enabling local delivery of biotherapeutics can circumvent systemic toxicities, supporting the principle of co-targeting EGFR and c-MET via OVs.

The second strategy currently followed for dual-targeting of EGFR and c-MET is the use of BsAbs. Amivantamab, an FDA-approved bispecific antibody for the treatment of NSCLC, inhibits ligand binding to both EGFR and c-MET and additionally facilitates ADCC.[233] It has been used in multiple clinical trials as both mono- and combination therapy with encouraging results, but is associated with notable limitations regarding its safety profile stemming from the need of continuous systemic administration.[148] Another bispecific antibody targeting EGFR and c-MET, EMB-01, is currently recruiting for a phase I/II clinical trial (NCT03797391) and has shown similar efficacy to Amivantamab in an *in vivo* patient-derived xenograft model of NSCLC.[234]

In conclusion, dual-targeting strategies of EGFR and c-MET with small molecules and BsAbs have shown promising results, but face important challenges, especially regarding their safety profile. My work showing functional co-targeting of EGFR and c-MET via oAd-mediated local production of a trispecific TCE could mitigate systemic toxicities.

4.5 Conclusions and Outlook

In summary, my study revealed limitations of the scDb format concerning its cross-linking abilities as a TCE in comparison to BiTEs. However, scDb-HER2 and scDb-cMET were identified as suitable bases for the novel, trispecific scDb-scFv format. Characterization of scDb-cMET-scFv-EGFR revealed promising dual-targeting efficacy, setting the groundwork for production of an oAd panel for dual-targeting of EGFR and c-MET. I was able to show that co-targeting was feasible via co-expression of two TCEs via one oAd, co-infection of two oAds encoding one TCE each and infection with an oAd encoding the trispecific scDb-cMET-scFv-EGFR. The trispecific TCE-armed Ad5/3-CMV-scDb-cMET-scFv-EGFR activated T-cells and induced T-cell mediated killing in both single target- and double target-positive cell lines. Taking the data of all tested cell lines together, it outperformed the other viruses of the virus panel, including single TCE-armed oAds and strategies for delivery of two bispecific TCEs.

Future experiments should be performed to optimize the agents that I generated in this thesis. My work has clearly showed limitations of both the scDb and the scDb-scFv format. If future constructs in the scDb or scDb-scFv format are explored, possibly for targeting of different antigens, they will have to be thoroughly characterized in regard to antigen binding and induction of T-cell mediated cytotoxicity. As only one out of the three scDb-scFvs described here were efficacious for co-targeting and rearrangement of the scDb and scFv moieties did not resolve the lack of efficacy for the inferior constructs, exploring other trispecific antibody formats described in 4.2, especially the DTriTE / Triplebody format, as V_Hs and V_Ls of scDb-scFvs can be readily reorganized into DTriTEs / Triplebodies, might be a promising alternative. Nevertheless, the antibody formats described here can be used for targeting any single antigen or combination of antigens in future experiments, as engagers for T-cells or other immune cells, such as NK-cells or macrophages. Furthermore, the expression strategies I employed here can be optimized. While I was able to identify an insertion site and expression strategy that did not or only slightly attenuate oAds, the co-expression strategies using bidirectional promoters and T2A peptides showed clear limitations. Future experiments could be conducted to optimize the bidirectional expression cassettes described here or explore other promoters for bidirectional expression. Using the Ad5 platform with an E3 deletion allows for a transgene size of approximately 4.5 kb, restricting the choice of promoters regarding their lengths. Using an alternative adenovirus serotype or another OV platform with a higher genomic cargo capacity might offer more flexibility regarding the choice of promoters.

Using the Ad5/3-CMV-scDb-cMET-scFv-EGFR, next steps for characterization would include experiments to test efficacy in heterogeneous tumor models. For *in vivo* characterization of a DTriTE targeting EGFRvIII and IL13Rα2, Park et al. generated a heterogeneous tumor model by coculturing EGFRvIII$^+$/IL13Rα2$^-$ U87vIII cells and EGFRvIII$^-$/IL13Rα2$^+$ U251 cells in a 1:1 ratio to grow heterogeneous tumors in an intracranial GBM model.[189] In another approach, Hegde et al. observed antigen escape of the U373 GBM cell line after monotargeting of either HER2 or IL13Rα2. They showed that dual-targeting of HER2 and IL13Rα2 with CAR-T cells mitigated antigen escape *in vitro* and *in vivo*.[167] These preclinical models could readily be transferred to characterization of TCE-armed oAds. It would be important to monitor systemic TCE concentrations in the mouse models in order to elucidate the risk of on-target off-tumor effects of locally delivered TCEs.

In conclusion, the Ad5/3-CMV-scDb-cMET-scFv-EGFR, armed with a novel trispecific TCE, represents a promising therapeutic agent for treatment of EGFR- and/or c-MET-positive tumors.

Further studies, especially *in vivo* assays, are needed to further characterize the Ad5/3-CMV-scDb-cMET-scFv-EGFR, investigating its clinical potential and safety in a 3D setting. The Ad5/3-CMV-scDb-cMET-scFv-EGFR is not restricted to any tumor entity and could therefore be employed for treatment of a variety of tumors.

References

1. Sung, H., et al., *Global Cancer Statistics 2020: GLOBOCAN Estimates of Incidence and Mortality Worldwide for 36 Cancers in 185 Countries.* CA: A Cancer Journal for Clinicians, 2021. **71**(3): p. 209-249.
2. Liu, B., et al., *Exploring treatment options in cancer: tumor treatment strategies.* Signal Transduction and Targeted Therapy, 2024. **9**(1): p. 175.
3. Lamers, C., *Overcoming the Shortcomings of Peptide-Based Therapeutics.* Future Drug Discovery, 2022. **4**(2): p. FDD75.
4. Chandra, R.A., et al., *Contemporary radiotherapy: present and future.* The Lancet, 2021. **398**(10295): p. 171-184.
5. De Angelis, C., *Side effects related to systemic cancer treatment: are we changing the Promethean experience with molecularly targeted therapies?* Curr Oncol, 2008. **15**(4): p. 198-9.
6. Baskar, R., et al., *Cancer and radiation therapy: current advances and future directions.* Int J Med Sci, 2012. **9**(3): p. 193-9.
7. Guha, P., et al., *Assessing the Future of Solid Tumor Immunotherapy.* Biomedicines, 2022. **10**(3): p. 655.
8. Lynes, J., et al., *Current Options and Future Directions in Immune Therapy for Glioblastoma.* Front Oncol, 2018. **8**: p. 578.
9. Wachsmann, T.L.A., et al., *Comparing CAR and TCR engineered T cell performance as a function of tumor cell exposure.* Oncoimmunology, 2022. **11**(1): p. 2033528.
10. Galon, J. and D. Bruni, *Approaches to treat immune hot, altered and cold tumours with combination immunotherapies.* Nat Rev Drug Discov, 2019. **18**(3): p. 197-218.
11. Hiltensperger, M. and A.M. Krackhardt, *Current and future concepts for the generation and application of genetically engineered CAR-T and TCR-T cells.* Front Immunol, 2023. **14**: p. 1121030.
12. Labanieh, L., R.G. Majzner, and C.L. Mackall, *Programming CAR-T cells to kill cancer.* Nat Biomed Eng, 2018. **2**(6): p. 377-391.
13. Peng, L., et al., *CAR-T and CAR-NK as cellular cancer immunotherapy for solid tumors.* Cellular & Molecular Immunology, 2024. **21**(10): p. 1089-1108.
14. Barros, L.R.C., et al., *Systematic Review of Available CAR-T Cell Trials around the World.* Cancers (Basel), 2022. **14**(11).

15. Bagley, S.J., et al., *Intrathecal bivalent CAR T cells targeting EGFR and IL13Rα2 in recurrent glioblastoma: phase 1 trial interim results.* Nature Medicine, 2024. **30**(5): p. 1320-1329.
16. Crescioli, S., et al., *Antibodies to watch in 2024.* MAbs, 2024. **16**(1): p. 2297450.
17. Lu, R.M., et al., *Development of therapeutic antibodies for the treatment of diseases.* J Biomed Sci, 2020. **27**(1): p. 1.
18. Kothari, M., et al., *A Comprehensive Review of Monoclonal Antibodies in Modern Medicine: Tracing the Evolution of a Revolutionary Therapeutic Approach.* Cureus, 2024. **16**(6): p. e61983.
19. Wang, Z., et al., *Development of therapeutic antibodies for the treatment of diseases.* Mol Biomed, 2022. **3**(1): p. 35.
20. Köhler, G. and C. Milstein, *Continuous cultures of fused cells secreting antibody of predefined specificity.* Nature, 1975. **256**(5517): p. 495-7.
21. Richards, J.M., N.J. Vogelzang, and J.A. Bluestone, *Neurotoxicity after treatment with muromonab-CD3.* N Engl J Med, 1990. **323**(7): p. 487-8.
22. Liu, A.Y., et al., *Production of a mouse-human chimeric monoclonal antibody to CD20 with potent Fc-dependent biologic activity.* The Journal of Immunology, 1987. **139**(10): p. 3521-3526.
23. LoBuglio, A.F., et al., *Mouse/human chimeric monoclonal antibody in man: kinetics and immune response.* Proceedings of the National Academy of Sciences, 1989. **86**(11): p. 4220-4224.
24. Harding, F.A., et al., *The immunogenicity of humanized and fully human antibodies: residual immunogenicity resides in the CDR regions.* MAbs, 2010. **2**(3): p. 256-65.
25. Lonberg, N., *Fully human antibodies from transgenic mouse and phage display platforms.* Curr Opin Immunol, 2008. **20**(4): p. 450-9.
26. Hafeez, U., et al., *Antibody-Drug Conjugates for Cancer Therapy.* Molecules, 2020. **25**(20).
27. Tan, S., et al., *Immune Checkpoint Inhibitor Therapy in Oncology.* JACC: CardioOncology, 2022. **4**(5): p. 579-597.
28. Wang, C., et al., *Immune checkpoint inhibitor-associated myocarditis: a systematic analysis of case reports.* Front Immunol, 2023. **14**: p. 1275254.
29. Stanfield, R.L. and I.A. Wilson, *Antibody Structure.* Microbiol Spectr, 2014. **2**(2).
30. Hansel, T.T., et al., *The safety and side effects of monoclonal antibodies.* Nature Reviews Drug Discovery, 2010. **9**(4): p. 325-338.

31. Chen, F., et al., *Ultrasmall targeted nanoparticles with engineered antibody fragments for imaging detection of HER2-overexpressing breast cancer.* Nat Commun, 2018. **9**(1): p. 4141.
32. Sedykh, S.E., et al., *Bispecific antibodies: design, therapy, perspectives.* Drug Des Devel Ther, 2018. **12**: p. 195-208.
33. Demaria, O., et al., *Natural killer cell engagers in cancer immunotherapy: Next generation of immuno-oncology treatments.* European Journal of Immunology, 2021. **51**(8): p. 1934-1942.
34. Labrijn, A.F., et al., *Bispecific antibodies: a mechanistic review of the pipeline.* Nature Reviews Drug Discovery, 2019. **18**(8): p. 585-608.
35. Brinkmann, U. and R.E. Kontermann, *The making of bispecific antibodies.* MAbs, 2017. **9**(2): p. 182-212.
36. Rolin, C., J. Zimmer, and C. Seguin-Devaux, *Bridging the gap with multispecific immune cell engagers in cancer and infectious diseases.* Cellular & Molecular Immunology, 2024. **21**(7): p. 643-661.
37. Zhu, A., et al., *Natural killer cell engagers: From bi-specific to tri-specific and tetra-specific engagers for enhanced cancer immunotherapy.* Clin Transl Med, 2024. **14**(11): p. e70046.
38. Li, J., et al., *Membrane-Proximal Epitope Facilitates Efficient T Cell Synapse Formation by Anti-FcRH5/CD3 and Is a Requirement for Myeloma Cell Killing.* Cancer Cell, 2017. **31**(3): p. 383-395.
39. Ross, S.L., et al., *Bispecific T cell engager (BiTE®) antibody constructs can mediate bystander tumor cell killing.* PLoS One, 2017. **12**(8): p. e0183390.
40. Huehls, A.M., T.A. Coupet, and C.L. Sentman, *Bispecific T-cell engagers for cancer immunotherapy.* Immunol Cell Biol, 2015. **93**(3): p. 290-6.
41. Bluemel, C., et al., *Epitope distance to the target cell membrane and antigen size determine the potency of T cell-mediated lysis by BiTE antibodies specific for a large melanoma surface antigen.* Cancer Immunol Immunother, 2010. **59**(8): p. 1197-209.
42. Liang, X., et al., *Comparison of CAR T-cell and bispecific antibody as third-line or later-line treatments for multiple myeloma: a meta-analysis.* J Immunother Cancer, 2024. **12**(11).
43. Esfandiari, A., S. Cassidy, and R.M. Webster, *Bispecific antibodies in oncology.* Nat Rev Drug Discov, 2022. **21**(6): p. 411-412.

44. Singh, K., et al., *For whom the T cells troll? Bispecific T-cell engagers in glioblastoma.* Journal for ImmunoTherapy of Cancer, 2021. **9**(11): p. e003679.
45. Shanshal, M., et al., *T-Cell Engagers in Solid Cancers-Current Landscape and Future Directions.* Cancers (Basel), 2023. **15**(10).
46. Qin, X., et al., *Stepping forward: T-cell redirecting bispecific antibodies in cancer therapy.* Acta Pharmaceutica Sinica B, 2024. **14**(6): p. 2361-2377.
47. Korn, T., et al., *Recombinant bispecific antibodies for the targeting of adenoviruses to CEA-expressing tumour cells: a comparative analysis of bacterially expressed single-chain diabody and tandem scFv.* J Gene Med, 2004. **6**(6): p. 642-51.
48. Aschmoneit, N., et al., *A scDb-based trivalent bispecific antibody for T-cell-mediated killing of HER3-expressing cancer cells.* Sci Rep, 2021. **11**(1): p. 13880.
49. Müller, D. and R.E. Kontermann, *Diabodies, Single-Chain Diabodies, and Their Derivatives*, in *Bispecific Antibodies*, R.E. Kontermann, Editor. 2011, Springer Berlin Heidelberg: Berlin, Heidelberg. p. 83-100.
50. Engeland, C.E. and J.C. Bell, *Introduction to Oncolytic Virotherapy*, in *Oncolytic Viruses*, C.E. Engeland, Editor. 2020, Springer New York: New York, NY. p. 1-6.
51. Zhao, Y., et al., *Oncolytic Adenovirus: Prospects for Cancer Immunotherapy.* Frontiers in Microbiology, 2021. **12**.
52. Ma, R., et al., *The emerging field of oncolytic virus-based cancer immunotherapy.* Trends Cancer, 2023. **9**(2): p. 122-139.
53. Chiocca, E.A. and S.D. Rabkin, *Oncolytic viruses and their application to cancer immunotherapy.* Cancer Immunol Res, 2014. **2**(4): p. 295-300.
54. Russell, S.J., K.W. Peng, and J.C. Bell, *Oncolytic virotherapy.* Nat Biotechnol, 2012. **30**(7): p. 658-70.
55. Seymour, L.W. and K.D. Fisher, *Oncolytic viruses: finally delivering.* Br J Cancer, 2016. **114**(4): p. 357-61.
56. Guo, Z.S., Z. Liu, and D.L. Bartlett, *Oncolytic Immunotherapy: Dying the Right Way is a Key to Eliciting Potent Antitumor Immunity.* Front Oncol, 2014. **4**: p. 74.
57. van Vloten, J.P., et al., *Critical Interactions between Immunogenic Cancer Cell Death, Oncolytic Viruses, and the Immune System Define the Rational Design of Combination Immunotherapies.* J Immunol, 2018. **200**(2): p. 450-458.
58. Eissa, I.R., et al., *The Current Status and Future Prospects of Oncolytic Viruses in Clinical Trials against Melanoma, Glioma, Pancreatic, and Breast Cancers.* Cancers (Basel), 2018. **10**(10).

59. Shalhout, S.Z., et al., *Therapy with oncolytic viruses: progress and challenges.* Nature Reviews Clinical Oncology, 2023. **20**(3): p. 160-177.
60. Zheng, M., et al., *Oncolytic Viruses for Cancer Therapy: Barriers and Recent Advances.* Mol Ther Oncolytics, 2019. **15**: p. 234-247.
61. Muthukutty, P. and S.Y. Yoo, *Oncolytic Virus Engineering and Utilizations: Cancer Immunotherapy Perspective.* Viruses, 2023. **15**(8).
62. Li, K., et al., *Advances in the clinical development of oncolytic viruses.* Am J Transl Res, 2022. **14**(6): p. 4192-4206.
63. *HAdV Working Group*. March 2024 January 2025]; Available from: hadvwg.gmu.edu.
64. Baker, A.T., et al., *Designer Oncolytic Adenovirus: Coming of Age.* Cancers (Basel), 2018. **10**(6).
65. Banerjee, N.S., et al., *Analyses of melanoma-targeted oncolytic adenoviruses with tyrosinase enhancer/promoter-driven E1A, E4, or both in submerged cells and organotypic cultures.* Mol Cancer Ther, 2004. **3**(4): p. 437-49.
66. Russell, W.C., *Adenoviruses: update on structure and function.* Journal of General Virology, 2009. **90**(1): p. 1-20.
67. Davison, A.J., M. Benkő, and B. Harrach, *Genetic content and evolution of adenoviruses.* J Gen Virol, 2003. **84**(Pt 11): p. 2895-2908.
68. Kulanayake, S. and S.K. Tikoo, *Adenovirus Core Proteins: Structure and Function.* Viruses, 2021. **13**(3).
69. Vellinga, J., S. Van der Heijdt, and R.C. Hoeben, *The adenovirus capsid: major progress in minor proteins.* J Gen Virol, 2005. **86**(Pt 6): p. 1581-1588.
70. Bulcha, J.T., et al., *Viral vector platforms within the gene therapy landscape.* Signal Transduction and Targeted Therapy, 2021. **6**(1): p. 53.
71. Chroboczek, J., R.W. Ruigrok, and S. Cusack, *Adenovirus fiber.* Curr Top Microbiol Immunol, 1995. **199 (Pt 1)**: p. 163-200.
72. Bergelson, J.M., et al., *Isolation of a common receptor for Coxsackie B viruses and adenoviruses 2 and 5.* Science, 1997. **275**(5304): p. 1320-3.
73. Wickham, T.J., et al., *Integrins alpha v beta 3 and alpha v beta 5 promote adenovirus internalization but not virus attachment.* Cell, 1993. **73**(2): p. 309-19.
74. Matthews, D.A. and W.C. Russell, *Adenovirus core protein V interacts with p32--a protein which is associated with both the mitochondria and the nucleus.* J Gen Virol, 1998. **79 (Pt 7)**: p. 1677-85.

75. Russell, W.C., *Update on adenovirus and its vectors.* J Gen Virol, 2000. **81**(Pt 11): p. 2573-2604.
76. Jounaidi, Y., J.C. Doloff, and D.J. Waxman, *Conditionally replicating adenoviruses for cancer treatment.* Curr Cancer Drug Targets, 2007. **7**(3): p. 285-301.
77. Hay, R.T., et al., *Molecular interactions during adenovirus DNA replication.* Curr Top Microbiol Immunol, 1995. **199 (Pt 2)**: p. 31-48.
78. Bennett, E.M., et al., *Cutting edge: adenovirus E19 has two mechanisms for affecting class I MHC expression.* J Immunol, 1999. **162**(9): p. 5049-52.
79. Tollefson, A.E., et al., *The E3-11.6-kDa adenovirus death protein (ADP) is required for efficient cell death: characterization of cells infected with adp mutants.* Virology, 1996. **220**(1): p. 152-62.
80. Halbert, D.N., J.R. Cutt, and T. Shenk, *Adenovirus early region 4 encodes functions required for efficient DNA replication, late gene expression, and host cell shutoff.* J Virol, 1985. **56**(1): p. 250-7.
81. Evans, J.D. and P. Hearing, *Distinct roles of the Adenovirus E4 ORF3 protein in viral DNA replication and inhibition of genome concatenation.* J Virol, 2003. **77**(9): p. 5295-304.
82. Fessler, S.P. and C.S. Young, *Control of adenovirus early gene expression during the late phase of infection.* J Virol, 1998. **72**(5): p. 4049-56.
83. Hearing, P., et al., *Identification of a repeated sequence element required for efficient encapsidation of the adenovirus type 5 chromosome.* J Virol, 1987. **61**(8): p. 2555-8.
84. Bett, A.J., L. Prevec, and F.L. Graham, *Packaging capacity and stability of human adenovirus type 5 vectors.* J Virol, 1993. **67**(10): p. 5911-21.
85. Farrera-Sal, M., et al., *Arming Oncolytic Adenoviruses: Effect of Insertion Site and Splice Acceptor on Transgene Expression and Viral Fitness.* Int J Mol Sci, 2020. **21**(14).
86. Bett, A.J., et al., *An efficient and flexible system for construction of adenovirus vectors with insertions or deletions in early regions 1 and 3.* Proceedings of the National Academy of Sciences, 1994. **91**(19): p. 8802-8806.
87. Stephens, C. and E. Harlow, *Differential splicing yields novel adenovirus 5 E1A mRNAs that encode 30 kd and 35 kd proteins.* Embo j, 1987. **6**(7): p. 2027-35.
88. Fueyo, J., et al., *A mutant oncolytic adenovirus targeting the Rb pathway produces anti-glioma effect in vivo.* Oncogene, 2000. **19**(1): p. 2-12.

89. Knudsen, E.S., et al., *Pan-cancer molecular analysis of the RB tumor suppressor pathway.* Commun Biol, 2020. **3**(1): p. 158.
90. Horwitz, M.S., Fields, B. N., Knipe, D. M., Howley, P. M., *Virology*. Lippincot-Raven, Philadephia ed. Vol. 2. 1996.
91. Liu, H., L. Wu, and Z.H. Zhou, *Model of the trimeric fiber and its interactions with the pentameric penton base of human adenovirus by cryo-electron microscopy.* J Mol Biol, 2011. **406**(5): p. 764-74.
92. Wohlfahrt, M.E., et al., *A capsid-modified, conditionally replicating oncolytic adenovirus vector expressing TRAIL Leads to enhanced cancer cell killing in human glioblastoma models.* Cancer Res, 2007. **67**(18): p. 8783-90.
93. Vanderkwaak, T.J., et al., *An Advanced Generation of Adenoviral Vectors Selectively Enhances Gene Transfer for Ovarian Cancer Gene Therapy Approaches.* Gynecologic Oncology, 1999. **74**(2): p. 227-234.
94. Dmitriev, I., et al., *An adenovirus vector with genetically modified fibers demonstrates expanded tropism via utilization of a coxsackievirus and adenovirus receptor-independent cell entry mechanism.* J Virol, 1998. **72**(12): p. 9706-13.
95. Wang, H., et al., *Desmoglein 2 is a receptor for adenovirus serotypes 3, 7, 11 and 14.* Nature Medicine, 2011. **17**(1): p. 96-104.
96. Robinson, M., et al., *Comparison of the E3 and L3 regions for arming oncolytic adenoviruses to achieve a high level of tumor-specific transgene expression.* Cancer Gene Therapy, 2008. **15**(1): p. 9-17.
97. Jetzer, T., et al., *Engineered Human Adenoviruses of Species B and C Report Early, Intermediate Early, and Late Viral Gene Expression.* Human Gene Therapy, 2023. **34**(23-24): p. 1230-1247.
98. Mühlemann, O., et al., *A novel type of splicing enhancer regulating adenovirus pre-mRNA splicing.* Mol Cell Biol, 2000. **20**(7): p. 2317-25.
99. Carette, J.E., et al., *Replication-dependent transgene expression from a conditionally replicating adenovirus via alternative splicing to a heterologous splice-acceptor site.* J Gene Med, 2005. **7**(8): p. 1053-62.
100. Fuerer, C. and R. Iggo, *5-Fluorocytosine increases the toxicity of Wnt-targeting replicating adenoviruses that express cytosine deaminase as a late gene.* Gene Ther, 2004. **11**(2): p. 142-51.
101. Marino, N., et al., *Development of a versatile oncolytic virus platform for local intra-tumoural expression of therapeutic transgenes.* PLoS One, 2017. **12**(5): p. e0177810.

102. Schaack, J., et al., *Promoter Strength in Adenovirus Transducing Vectors: Down-Regulation of the Adenovirus E1A Promoter in 293 Cells Facilitates Vector Construction.* Virology, 2001. **291**(1): p. 101-109.
103. Liu, W., et al., *Oncolytic adenovirus-mediated intratumoral expression of TRAIL and CD40L enhances immunotherapy by modulating the tumor microenvironment in immunocompetent mouse models.* Cancer Letters, 2022. **535**: p. 215661.
104. Small, J.C., et al., *Construction and characterization of E1- and E3-deleted adenovirus vectors expressing two antigens from two separate expression cassettes.* Hum Gene Ther, 2014. **25**(4): p. 328-38.
105. Bauzon, M., et al., *Multigene expression from a replicating adenovirus using native viral promoters.* Molecular Therapy, 2003. **7**(4): p. 526-534.
106. Wang, Y., et al., *Phylogenetic evidence for intratypic recombinant events in a novel human adenovirus C that causes severe acute respiratory infection in children.* Scientific Reports, 2016. **6**(1): p. 23014.
107. Duigou, G.J. and C.S. Young, *Replication-competent adenovirus formation in 293 cells: the recombination-based rate is influenced by structure and location of the transgene cassette and not increased by overproduction of HsRad51, Rad51-interacting, or E2F family proteins.* J Virol, 2005. **79**(9): p. 5437-44.
108. Kleinpeter, P., et al., *Vectorization in an oncolytic vaccinia virus of an antibody, a Fab and a scFv against programmed cell death -1 (PD-1) allows their intratumoral delivery and an improved tumor-growth inhibition.* Oncoimmunology, 2016. **5**(10): p. e1220467.
109. Dias, J.D., et al., *Targeted cancer immunotherapy with oncolytic adenovirus coding for a fully human monoclonal antibody specific for CTLA-4.* Gene Ther, 2012. **19**(10): p. 988-98.
110. Kontermann, R.E., G. Ungerechts, and D.M. Nettelbeck, *Viro-antibody therapy: engineering oncolytic viruses for genetic delivery of diverse antibody-based biotherapeutics.* MAbs, 2021. **13**(1): p. 1982447.
111. Liikanen, I., et al., *Oncolytic Adenovirus Expressing Monoclonal Antibody Trastuzumab for Treatment of HER2-Positive Cancer.* Mol Cancer Ther, 2016. **15**(9): p. 2259-69.
112. Weibel, S., et al., *Treatment of malignant effusion by oncolytic virotherapy in an experimental subcutaneous xenograft model of lung cancer.* Journal of Translational Medicine, 2013. **11**(1): p. 106.

113. Gholami, S., et al., *A novel vaccinia virus with dual oncolytic and anti-angiogenic therapeutic effects against triple-negative breast cancer.* Breast Cancer Research and Treatment, 2014. **148**(3): p. 489-499.
114. Huang, T., et al., *Expression of anti-VEGF antibody together with anti-EGFR or anti-FAP enhances tumor regression as a result of vaccinia virotherapy.* Molecular Therapy - Oncolytics, 2015. **2**.
115. Frentzen, A., et al., *Anti-VEGF single-chain antibody GLAF-1 encoded by oncolytic vaccinia virus significantly enhances antitumor therapy.* Proceedings of the National Academy of Sciences, 2009. **106**(31): p. 12915-12920.
116. Heidbuechel, J.P.W. and C.E. Engeland, *Oncolytic viruses encoding bispecific T cell engagers: a blueprint for emerging immunovirotherapies.* J Hematol Oncol, 2021. **14**(1): p. 63.
117. Scott, E.M., et al., *Solid Tumor Immunotherapy with T Cell Engager-Armed Oncolytic Viruses.* Macromol Biosci, 2018. **18**(1).
118. Twumasi-Boateng, K., et al., *Oncolytic viruses as engineering platforms for combination immunotherapy.* Nature Reviews Cancer, 2018. **18**(7): p. 419-432.
119. Freedman, J.D., et al., *An Oncolytic Virus Expressing a T-cell Engager Simultaneously Targets Cancer and Immunosuppressive Stromal Cells.* Cancer Research, 2018. **78**(24): p. 6852-6865.
120. de Sostoa, J., et al., *Targeting the tumor stroma with an oncolytic adenovirus secreting a fibroblast activation protein-targeted bispecific T-cell engager.* Journal for ImmunoTherapy of Cancer, 2019. **7**(1): p. 19.
121. Freedman, J.D., et al., *Oncolytic adenovirus expressing bispecific antibody targets T-cell cytotoxicity in cancer biopsies.* EMBO Mol Med, 2017. **9**(8): p. 1067-1087.
122. Wang, Q., et al., *Oncolytic adenovirus with MUC16-BiTE shows enhanced antitumor immune response by reversing the tumor microenvironment in PDX model of ovarian cancer.* OncoImmunology, 2022. **11**(1): p. 2096362.
123. Fajardo, C.A., et al., *Oncolytic Adenoviral Delivery of an EGFR-Targeting T-cell Engager Improves Antitumor Efficacy.* Cancer Res, 2017. **77**(8): p. 2052-2063.
124. Wing, A., et al., *Improving CART-Cell Therapy of Solid Tumors with Oncolytic Virus–Driven Production of a Bispecific T-cell Engager.* Cancer Immunology Research, 2018. **6**(5): p. 605-616.

125. Havunen, R., et al., *Oncolytic Adenoviruses Armed with Tumor Necrosis Factor Alpha and Interleukin-2 Enable Successful Adoptive Cell Therapy.* Mol Ther Oncolytics, 2017. **4**: p. 77-86.
126. Sangro, B., et al., *Phase I trial of intratumoral injection of an adenovirus encoding interleukin-12 for advanced digestive tumors.* J Clin Oncol, 2004. **22**(8): p. 1389-97.
127. Armstrong, L., et al., *Generation of a novel, cyclooxygenase-2-targeted, interferon-expressing, conditionally replicative adenovirus for pancreatic cancer therapy.* Am J Surg, 2012. **204**(5): p. 741-50.
128. Koski, A., et al., *Treatment of cancer patients with a serotype 5/3 chimeric oncolytic adenovirus expressing GMCSF.* Mol Ther, 2010. **18**(10): p. 1874-84.
129. Minati, R., C. Perreault, and P. Thibault, *A Roadmap Toward the Definition of Actionable Tumor-Specific Antigens.* Front Immunol, 2020. **11**: p. 583287.
130. Carter, P., L. Smith, and M. Ryan, *Identification and validation of cell surface antigens for antibody targeting in oncology.* Endocrine-Related Cancer Endocr Relat Cancer, 2004. **11**(4): p. 659-687.
131. Leko, V. and S.A. Rosenberg, *Identifying and Targeting Human Tumor Antigens for T Cell-Based Immunotherapy of Solid Tumors.* Cancer Cell, 2020. **38**(4): p. 454-472.
132. Talukdar, S., et al., *Chapter Four - EGFR: An essential receptor tyrosine kinase-regulator of cancer stem cells*, in *Advances in Cancer Research*, R. Kumar and P.B. Fisher, Editors. 2020, Academic Press. p. 161-188.
133. Blume-Jensen, P. and T. Hunter, *Oncogenic kinase signalling.* Nature, 2001. **411**(6835): p. 355-365.
134. Butti, R., et al., *Receptor tyrosine kinases (RTKs) in breast cancer: signaling, therapeutic implications and challenges.* Mol Cancer, 2018. **17**(1): p. 34.
135. Arteaga, C.L. and J.A. Engelman, *ERBB receptors: from oncogene discovery to basic science to mechanism-based cancer therapeutics.* Cancer Cell, 2014. **25**(3): p. 282-303.
136. Ayati, A., et al., *A review on progression of epidermal growth factor receptor (EGFR) inhibitors as an efficient approach in cancer targeted therapy.* Bioorganic Chemistry, 2020. **99**: p. 103811.
137. Chhouri, H., D. Alexandre, and L. Grumolato, *Mechanisms of Acquired Resistance and Tolerance to EGFR Targeted Therapy in Non-Small Cell Lung Cancer.* Cancers (Basel), 2023. **15**(2).
138. Goldberg, R.M., *Cetuximab.* Nat Rev Drug Discov, 2005. **Suppl**: p. S10-1.

139. High, P., et al., *The Evolving Paradigm of Antibody-Drug Conjugates Targeting the ErbB/HER Family of Receptor Tyrosine Kinases.* Pharmaceutics, 2024. **16**(7).
140. Wang, Z., *ErbB Receptors and Cancer*, in *ErbB Receptor Signaling: Methods and Protocols*, Z. Wang, Editor. 2017, Springer New York: New York, NY. p. 3-35.
141. Mineo, J.-F., et al., *Low HER2-expressing glioblastomas are more often secondary to anaplastic transformation of low-grade glioma.* Journal of Neuro-Oncology, 2007. **85**(3): p. 281-287.
142. Ahmed, N., et al., *HER2-specific T cells target primary glioblastoma stem cells and induce regression of autologous experimental tumors.* Clin Cancer Res, 2010. **16**(2): p. 474-85.
143. Zhang, Y., R.K. Jain, and M. Zhu, *Recent Progress and Advances in HGF/MET-Targeted Therapeutic Agents for Cancer Treatment.* Biomedicines, 2015. **3**(1): p. 149-181.
144. Bussolino, F., et al., *Hepatocyte growth factor is a potent angiogenic factor which stimulates endothelial cell motility and growth.* J Cell Biol, 1992. **119**(3): p. 629-41.
145. Boccaccio, C. and P.M. Comoglio, *MET, a driver of invasive growth and cancer clonal evolution under therapeutic pressure.* Curr Opin Cell Biol, 2014. **31**: p. 98-105.
146. Okamoto, W., et al., *TAK-701, a humanized monoclonal antibody to hepatocyte growth factor, reverses gefitinib resistance induced by tumor-derived HGF in non-small cell lung cancer with an EGFR mutation.* Mol Cancer Ther, 2010. **9**(10): p. 2785-92.
147. Sano, Y., et al., *Combining onartuzumab with erlotinib inhibits growth of non-small cell lung cancer with activating EGFR mutations and HGF overexpression.* Mol Cancer Ther, 2015. **14**(2): p. 533-41.
148. Wang, K. and R. Hsu, *Anti-MET Antibody Therapies in Non-Small-Cell Lung Cancer: Current Progress and Future Directions.* Antibodies (Basel), 2024. **13**(4).
149. Fichtner-Feigl, S., et al., *IL-13 signaling through the IL-13alpha2 receptor is involved in induction of TGF-beta1 production and fibrosis.* Nat Med, 2006. **12**(1): p. 99-106.
150. Barderas, R., et al., *High expression of IL-13 receptor α2 in colorectal cancer is associated with invasion, liver metastasis, and poor prognosis.* Cancer Res, 2012. **72**(11): p. 2780-90.
151. Okamoto, H., et al., *Interleukin-13 receptor α2 is a novel marker and potential therapeutic target for human melanoma.* Scientific Reports, 2019. **9**(1): p. 1281.

152. Jarboe, J.S., et al., *Expression of interleukin-13 receptor alpha2 in glioblastoma multiforme: implications for targeted therapies.* Cancer Res, 2007. **67**(17): p. 7983-6.
153. Zhuo, S., et al., *Unveiling the significance of cancer-testis antigens and their implications for immunotherapy in glioma.* Discov Oncol, 2024. **15**(1): p. 602.
154. Lawson, D.A., et al., *Tumour heterogeneity and metastasis at single-cell resolution.* Nat Cell Biol, 2018. **20**(12): p. 1349-1360.
155. Chen, K., T.W.H. Shuen, and P.K.H. Chow, *The association between tumour heterogeneity and immune evasion mechanisms in hepatocellular carcinoma and its clinical implications.* British Journal of Cancer, 2024. **131**(3): p. 420-429.
156. Plaks, V., et al., *CD19 target evasion as a mechanism of relapse in large B-cell lymphoma treated with axicabtagene ciloleucel.* Blood, 2021. **138**(12): p. 1081-1085.
157. Jia, Q., et al., *Heterogeneity of the tumor immune microenvironment and its clinical relevance.* Exp Hematol Oncol, 2022. **11**(1): p. 24.
158. van der Schans, J.J., N.W.C.J. van de Donk, and T. Mutis, *Dual Targeting to Overcome Current Challenges in Multiple Myeloma CAR T-Cell Treatment.* Frontiers in Oncology, 2020. **10**.
159. Kontermann, R.E., *Dual targeting strategies with bispecific antibodies.* MAbs, 2012. **4**(2): p. 182-97.
160. Al-Hamaly, M.A., et al., *Zebrafish Cancer Avatars: A Translational Platform for Analyzing Tumor Heterogeneity and Predicting Patient Outcomes.* Int J Mol Sci, 2023. **24**(3).
161. Wu, D.W., et al., *TC-N19, a novel dual inhibitor of EGFR and cMET, efficiently overcomes EGFR-TKI resistance in non-small-cell lung cancer cells.* Cell Death & Disease, 2016. **7**(6): p. e2290-e2290.
162. Kim, S., et al., *Suppression of TNBC metastasis by doxazosin, a novel dual inhibitor of c-MET/EGFR.* Journal of Experimental & Clinical Cancer Research, 2023. **42**(1): p. 292.
163. Xu, H., et al., *Dual blockade of EGFR and c-Met abrogates redundant signaling and proliferation in head and neck carcinoma cells.* Clin Cancer Res, 2011. **17**(13): p. 4425-38.
164. Assenat, E., et al., *Dual targeting of HER1/EGFR and HER2 with cetuximab and trastuzumab in patients with metastatic pancreatic cancer after gemcitabine failure: results of the "THERAPY"phase 1-2 trial.* Oncotarget, 2015. **6**(14): p. 12796-808.

165. Larbouret, C., et al., *Combined cetuximab and trastuzumab are superior to gemcitabine in the treatment of human pancreatic carcinoma xenografts.* Ann Oncol, 2010. **21**(1): p. 98-103.
166. Yin, Y., et al., *Locally secreted BiTEs complement CAR T cells by enhancing killing of antigen heterogeneous solid tumors.* Mol Ther, 2022. **30**(7): p. 2537-2553.
167. Hegde, M., et al., *Tandem CAR T cells targeting HER2 and IL13Rα2 mitigate tumor antigen escape.* J Clin Invest, 2016. **126**(8): p. 3036-52.
168. Goldstein, N.I., et al., *Biological efficacy of a chimeric antibody to the epidermal growth factor receptor in a human tumor xenograft model.* Clin Cancer Res, 1995. **1**(11): p. 1311-8.
169. Carter, P., et al., *Humanization of an anti-p185HER2 antibody for human cancer therapy.* Proc Natl Acad Sci U S A, 1992. **89**(10): p. 4285-9.
170. Kong-Beltran, M., J. Stamos, and D. Wickramasinghe, *The Sema domain of Met is necessary for receptor dimerization and activation.* Cancer Cell, 2004. **6**(1): p. 75-84.
171. Balyasnikova, I.V., et al., *Characterization and Immunotherapeutic Implications for a Novel Antibody Targeting Interleukin (IL)-13 Receptor α2*.* Journal of Biological Chemistry, 2012. **287**(36): p. 30215-30227.
172. Carrara, S.C., et al., *Recombinant Antibody Production Using a Dual-Promoter Single Plasmid System.* Antibodies (Basel), 2021. **10**(2).
173. van Galen, P., et al., *Reduced Lymphoid Lineage Priming Promotes Human Hematopoietic Stem Cell Expansion.* Cell Stem Cell, 2014. **14**(1): p. 94-106.
174. Toktay, Y., B. Dayanc, and S. Senturk, *Engineering and validation of a dual luciferase reporter system for quantitative and systematic assessment of regulatory sequences in Chinese hamster ovary cells.* Scientific Reports, 2022. **12**(1): p. 6050.
175. Wang, X. and M.A. Marchisio, *Synthetic polycistronic sequences in eukaryotes.* Synth Syst Biotechnol, 2021. **6**(4): p. 254-261.
176. Ryan, M.D., et al., *A Model for Nonstoichiometric, Cotranslational Protein Scission in Eukaryotic Ribosomes.* Bioorganic Chemistry, 1999. **27**(1): p. 55-79.
177. Jin, F., P.J. Kretschmer, and T.W. Hermiston, *Identification of novel insertion sites in the Ad5 genome That utilize the Ad splicing machinery for therapeutic gene expression.* Molecular Therapy, 2005. **12**(6): p. 1052-1063.
178. Smith-Garvin, J.E., G.A. Koretzky, and M.S. Jordan, *T cell activation.* Annu Rev Immunol, 2009. **27**: p. 591-619.

179. Castro, F., et al., *Interferon-Gamma at the Crossroads of Tumor Immune Surveillance or Evasion.* Front Immunol, 2018. **9**: p. 847.
180. Jain, R.K. and T. Stylianopoulos, *Delivering nanomedicine to solid tumors.* Nat Rev Clin Oncol, 2010. **7**(11): p. 653-64.
181. Guedan, S. and R. Alemany, *CAR-T Cells and Oncolytic Viruses: Joining Forces to Overcome the Solid Tumor Challenge.* Front Immunol, 2018. **9**: p. 2460.
182. Sharp, D.W. and E.C. Lattime, *Recombinant Poxvirus and the Tumor Microenvironment: Oncolysis, Immune Regulation and Immunization.* Biomedicines, 2016. **4**(3).
183. Goebeler, M.-E., G. Stuhler, and R. Bargou, *Bispecific and multispecific antibodies in oncology: opportunities and challenges.* Nature Reviews Clinical Oncology, 2024. **21**(7): p. 539-560.
184. Tian, Z., et al., *Bispecific T cell engagers: an emerging therapy for management of hematologic malignancies.* Journal of Hematology & Oncology, 2021. **14**(1): p. 75.
185. Asano, R., et al., *Domain order of a bispecific diabody dramatically enhances its antitumor activity beyond structural format conversion: the case of the hEx3 diabody.* Protein Eng Des Sel, 2013. **26**(5): p. 359-67.
186. Wang, Q., et al., *Design and Production of Bispecific Antibodies.* Antibodies (Basel), 2019. **8**(3).
187. Ding, Z., et al., *Nanobody-based trispecific T cell engager (Nb-TriTE) enhances therapeutic efficacy by overcoming tumor-mediated immunosuppression.* Journal of Hematology & Oncology, 2023. **16**(1): p. 115.
188. Tapia-Galisteo, A., et al., *Trispecific T-cell engagers for dual tumor-targeting of colorectal cancer.* Oncoimmunology, 2022. **11**(1): p. 2034355.
189. Park, D.H., et al., *Novel tri-specific T-cell engager targeting IL-13Rα2 and EGFRvIII provides long-term survival in heterogeneous GBM challenge and promotes antitumor cytotoxicity with patient immune cells.* J Immunother Cancer, 2024. **12**(12).
190. Austin, R.J., et al., *TriTACs, a Novel Class of T-Cell–Engaging Protein Constructs Designed for the Treatment of Solid Tumors.* Molecular Cancer Therapeutics, 2021. **20**(1): p. 109-120.
191. Wu, X. and S.J. Demarest, *Building blocks for bispecific and trispecific antibodies.* Methods, 2019. **154**: p. 3-9.

192. Schubert, I., et al., *A recombinant triplebody with specificity for CD19 and HLA-DR mediates preferential binding to antigen double-positive cells by dual-targeting.* MAbs, 2012. **4**(1): p. 45-56.
193. Roskopf, C.C., et al., *Dual-targeting triplebody 33-3-19 mediates selective lysis of biphenotypic CD19+ CD33+ leukemia cells.* Oncotarget, 2016. **7**(16): p. 22579-89.
194. Kügler, M., et al., *A recombinant trispecific single-chain Fv derivative directed against CD123 and CD33 mediates effective elimination of acute myeloid leukaemia cells by dual targeting.* British Journal of Haematology, 2010. **150**(5): p. 574-586.
195. Schiller, C.B., et al., *CD19-specific triplebody SPM-1 engages NK and γδ T cells for rapid and efficient lysis of malignant B-lymphoid cells.* Oncotarget, 2016. **7**(50): p. 83392-83408.
196. Roy, R.D., C. Rosenmund, and M.I. Stefan, *Cooperative binding mitigates the high-dose hook effect.* BMC Syst Biol, 2017. **11**(1): p. 74.
197. Comoglio, P.M., S. Giordano, and L. Trusolino, *Drug development of MET inhibitors: targeting oncogene addiction and expedience.* Nat Rev Drug Discov, 2008. **7**(6): p. 504-16.
198. Organ, S.L. and M.S. Tsao, *An overview of the c-MET signaling pathway.* Ther Adv Med Oncol, 2011. **3**(1 Suppl): p. S7-s19.
199. Chen, J., et al., *Expression and Function of the Epidermal Growth Factor Receptor in Physiology and Disease.* Physiological Reviews, 2016. **96**(3): p. 1025-1069.
200. Li, W. and W. Wang, *Toxicity burden patterns of MET-selective tyrosine kinase inhibitors: evidence from real-world pharmacovigilance.* Investigational New Drugs, 2024. **42**(3): p. 335-339.
201. Hirsh, V., *Managing treatment-related adverse events associated with egfr tyrosine kinase inhibitors in advanced non-small-cell lung cancer.* Curr Oncol, 2011. **18**(3): p. 126-38.
202. Scott, E.M., et al., *Bi- and tri-valent T cell engagers deplete tumour-associated macrophages in cancer patient samples.* J Immunother Cancer, 2019. **7**(1): p. 320.
203. Wan, P.K., R.A. Fernandes, and L.W. Seymour, *Oncolytic viruses and antibodies: are they more successful when delivered separately or when engineered as a single agent?* J Immunother Cancer, 2023. **11**(8).
204. Fava Gaspar, C., et al., *658P First-in-human phase I trial of oncolytic herpes simplex virus ONCR-177 alone or in combination with pembrolizumab in advanced solid tumors.* Annals of Oncology, 2024. **35**: p. S519.

205. Haines, B.B., et al., *ONCR-177, an Oncolytic HSV-1 Designed to Potently Activate Systemic Antitumor Immunity.* Cancer Immunol Res, 2021. **9**(3): p. 291-308.
206. Golding, M.C. and M.R.W. Mann, *A bidirectional promoter architecture enhances lentiviral transgenesis in embryonic and extraembryonic stem cells.* Gene Therapy, 2011. **18**(8): p. 817-826.
207. Wang, R., et al., *Towards a surrogate system to express human lipid binding TCRs.* Biotechnology Letters, 2019. **41**(10): p. 1095-1104.
208. Andersen, C.R., et al., *Efficient Expression from One CMV Enhancer Controlling Two Core Promoters.* Molecular Biotechnology, 2011. **48**(2): p. 128-137.
209. Thomas, S., H.J. Stauss, and E.C. Morris, *Molecular immunology lessons from therapeutic T-cell receptor gene transfer.* Immunology, 2010. **129**(2): p. 170-177.
210. Mukherjee, M. and Z.Q. Wang, *A well-characterized polycistronic-like gene expression system in yeast.* Biotechnology and Bioengineering, 2023. **120**(1): p. 260-271.
211. Fernández-Ulibarri, I., et al., *Genetic delivery of an immunoRNase by an oncolytic adenovirus enhances anticancer activity.* International Journal of Cancer, 2015. **136**(9): p. 2228-2240.
212. Bocharov, G., et al., *Underwhelming the immune response: effect of slow virus growth on CD8+-T-lymphocyte responses.* J Virol, 2004. **78**(5): p. 2247-54.
213. Suzuki, M., et al., *Preferable sites and orientations of transgene inserted in the adenovirus vector genome: The E3 site may be unfavorable for transgene position.* Gene Ther, 2015. **22**(5): p. 421-9.
214. Pei, Z., et al., *Adenovirus vectors lacking virus-associated RNA expression enhance shRNA activity to suppress hepatitis C virus replication.* Sci Rep, 2013. **3**: p. 3575.
215. Lundahl, M.L.E., et al., *Aggregation of protein therapeutics enhances their immunogenicity: causes and mitigation strategies.* RSC Chem Biol, 2021. **2**(4): p. 1004-1020.
216. Hu, M., et al., *Host cell protein identification in monoclonal antibody high molecular weight species.* Journal of Chromatography B, 2022. **1210**: p. 123448.
217. Ghasemi, N., M. Bandehpour, and J. Ranjbari, *Optimization of Key Factors in Serum Free Medium for Production of Human Recombinant GM-CSF Using Response Surface Methodology.* Iran J Pharm Res, 2019. **18**(Suppl1): p. 146-156.

218. Faroudi, M., et al., *Lytic versus stimulatory synapse in cytotoxic T lymphocyte/target cell interaction: manifestation of a dual activation threshold.* Proc Natl Acad Sci U S A, 2003. **100**(24): p. 14145-50.
219. Jin, H., et al., *Systematic transcriptional analysis of human cell lines for gene expression landscape and tumor representation.* Nat Commun, 2023. **14**(1): p. 5417.
220. Chuang, C.M., et al., *Combination of viral oncolysis and tumor-specific immunity to control established tumors.* Clin Cancer Res, 2009. **15**(14): p. 4581-8.
221. Aaes, T.L. and P. Vandenabeele, *The intrinsic immunogenic properties of cancer cell lines, immunogenic cell death, and how these influence host antitumor immune responses.* Cell Death Differ, 2021. **28**(3): p. 843-860.
222. Vitiello, A., et al., *Simultaneous Expression of Different Therapeutic Genes by Infection with Multiple Oncolytic HSV-1 Vectors.* Biomedicines, 2024. **12**(7).
223. Huang, S., et al., *Bispecific antibodies targeting dual tumor-associated antigens in cancer therapy.* J Cancer Res Clin Oncol, 2020. **146**(12): p. 3111-3122.
224. Li, H., P. Er Saw, and E. Song, *Challenges and strategies for next-generation bispecific antibody-based antitumor therapeutics.* Cell Mol Immunol, 2020. **17**(5): p. 451-461.
225. Gantke, T., et al., *Trispecific antibodies for CD16A-directed NK cell engagement and dual-targeting of tumor cells.* Protein Engineering, Design and Selection, 2017. **30**(9): p. 673-684.
226. Harwardt, J., et al., *Generation of a symmetrical trispecific NK cell engager based on a two-in-one antibody.* Front Immunol, 2023. **14**: p. 1170042.
227. Banaszek, A., et al., *On-target restoration of a split T cell-engaging antibody for precision immunotherapy.* Nat Commun, 2019. **10**(1): p. 5387.
228. Fernández de Larrea, C., et al., *Defining an Optimal Dual-Targeted CAR T-cell Therapy Approach Simultaneously Targeting BCMA and GPRC5D to Prevent BCMA Escape-Driven Relapse in Multiple Myeloma.* Blood Cancer Discov, 2020. **1**(2): p. 146-154.
229. McGrath, K. and G. Dotti, *Combining Oncolytic Viruses with Chimeric Antigen Receptor T Cell Therapy.* Hum Gene Ther, 2021. **32**(3-4): p. 150-157.
230. Engelman, J.A., et al., *MET amplification leads to gefitinib resistance in lung cancer by activating ERBB3 signaling.* Science, 2007. **316**(5827): p. 1039-43.
231. Sohn, J., et al., *cMET Activation and EGFR-Directed Therapy Resistance in Triple-Negative Breast Cancer.* J Cancer, 2014. **5**(9): p. 745-53.

232. Shyam Sunder, S., U.C. Sharma, and S. Pokharel, *Adverse effects of tyrosine kinase inhibitors in cancer therapy: pathophysiology, mechanisms and clinical management.* Signal Transduction and Targeted Therapy, 2023. **8**(1): p. 262.
233. Grugan, K.D., et al., *Fc-mediated activity of EGFR x c-Met bispecific antibody JNJ-61186372 enhanced killing of lung cancer cells.* MAbs, 2017. **9**(1): p. 114-126.
234. Xu, Y., et al., *Integrative genomic analysis of drug resistance in MET exon 14 skipping lung cancer using patient-derived xenograft models.* Front Oncol, 2022. **12**: p. 1024818.

Supplements

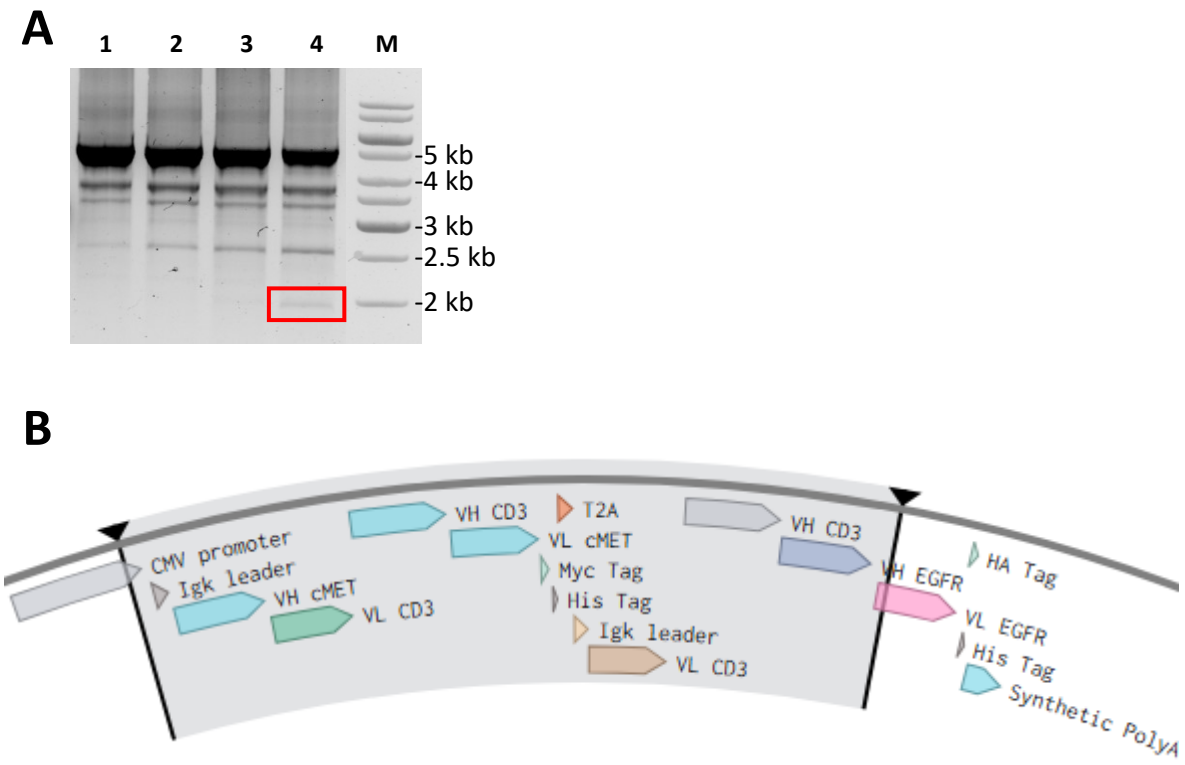

Figure S1 Deletion of sequence in Ad5/3-CMV-scDb-cMET-T2A-BiTE-EGFR. A) Gel electrophoresis of PCR amplicons in 1 % agarose gel. 1 - purified virus; 2 - passage one, 4 dpi; 3 - passage two, 9 dpi (cumulative); 4 - passage 3, 14 dpi (cumulative). Red rectangle marks sequenced band. B) Annotated insert area of oAd genome. Highlighted area marks deleted sequence as confirmed via Sanger sequencing.

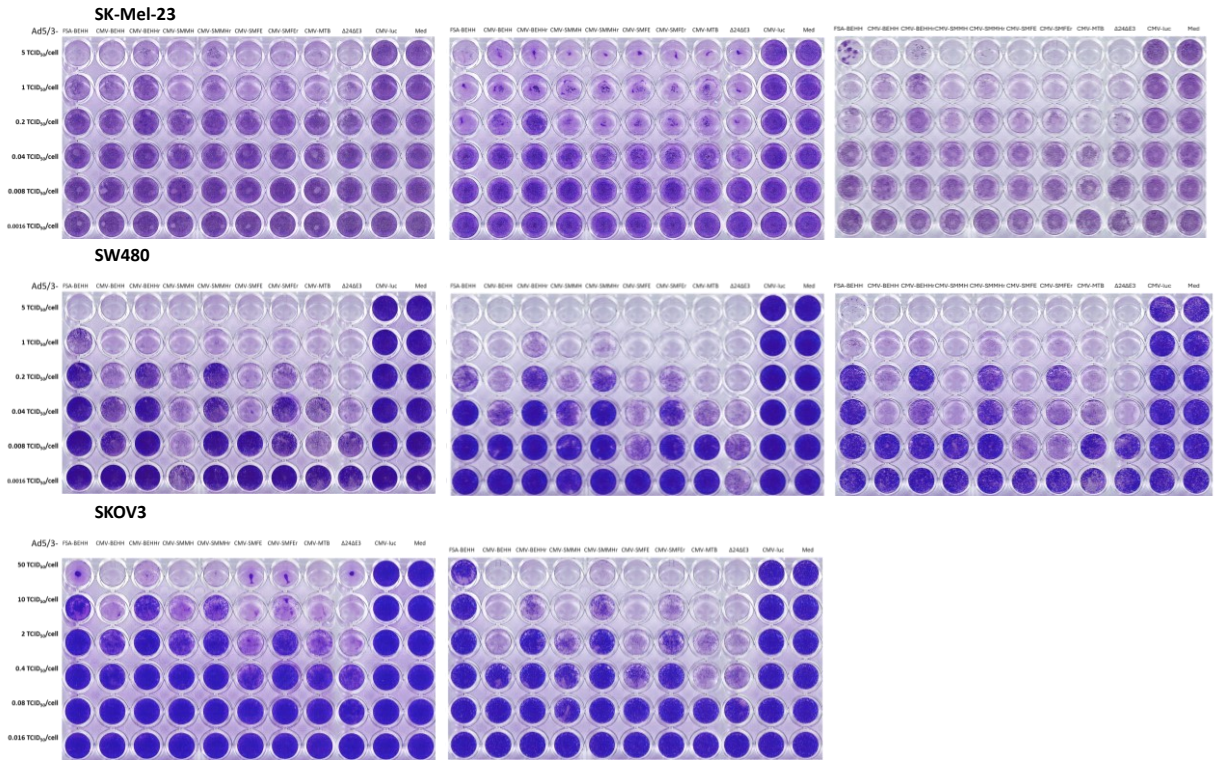

Figure S2 Oncolytic activity of oAds. Cytotoxicity assays of oAds on SK-Mel-23, SW480 & SKOV3. Target cells were infected with serial 5-fold dilutions of oAds (MOI = $TCID_{50}$ titer / cell). Cells were stained with crystal violet at time points of best visibility of differences between oAds. FSA-BEHH – Ad5/3-FSA-BiTE-EGFR; CMV-BEHH - Ad5/3-CMV-BiTE-EGFR; CMV-BEHHr - Ad5/3-(CMV-BiTE-EGFR)r; CMV-SMMH - Ad5/3-CMV-scDb-cMET; CMV-SMMHr - Ad5/3-(CMV-scDb-cMET)r; CMV-SMFE - Ad5/3-CMV-scDb-cMET-scFv-EGFR; CMV-SMFEr - Ad5/3-(CMV-scDb-cMET-scFv-EGFR)r; CMV-MTB - Ad5/3-CMV-scDb-cMET-T2A-BiTE-EGFR; Δ24ΔE3 - Ad5/3-ΔE3; CMV-luc – Ad5/3 (non repl.); Med - medium

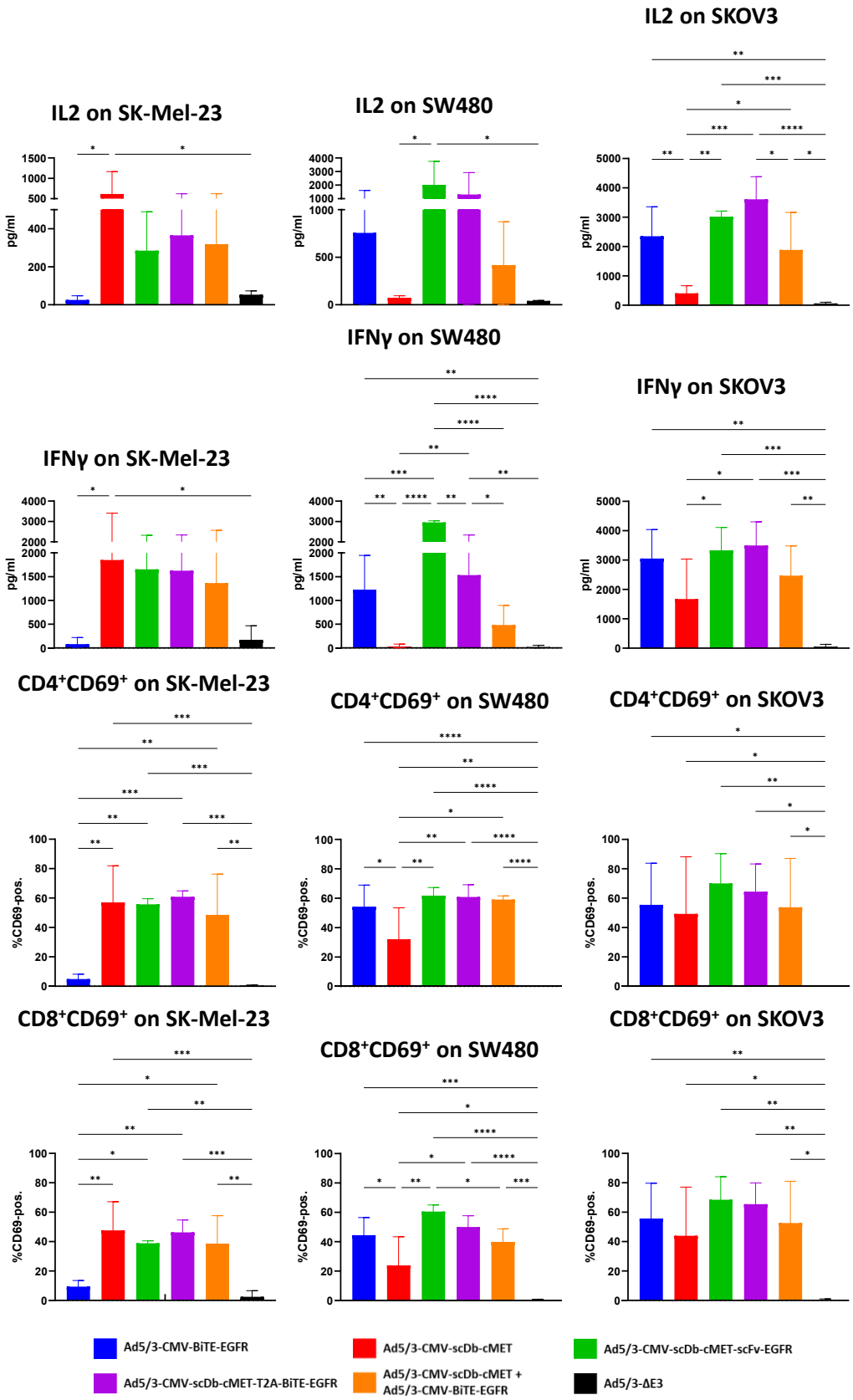

Figure S3 T-cell activation data with all significant differences indicated. Cells were infected with MOI 5 (SK-Mel-23) or MOI 1 (SW480, SKOV3). PBMCs were added 1 dpi, IL-2 concentrations in the supernatant and CD69 surface expression were measured 24h post addition of PBMCs. IFNγ concentrations in supernatants were measured 48h post addition of PBMCs. Cytokine levels were measured via ELISA, CD69-expression via flow cytometry. Data gathered from 3 independent experiments with different donors, values shown as mean ± SD (n=3), *P < 0.05, **P < 0.01, ***P < 0.001, ****P < 0.0001, one-way ANOVA.

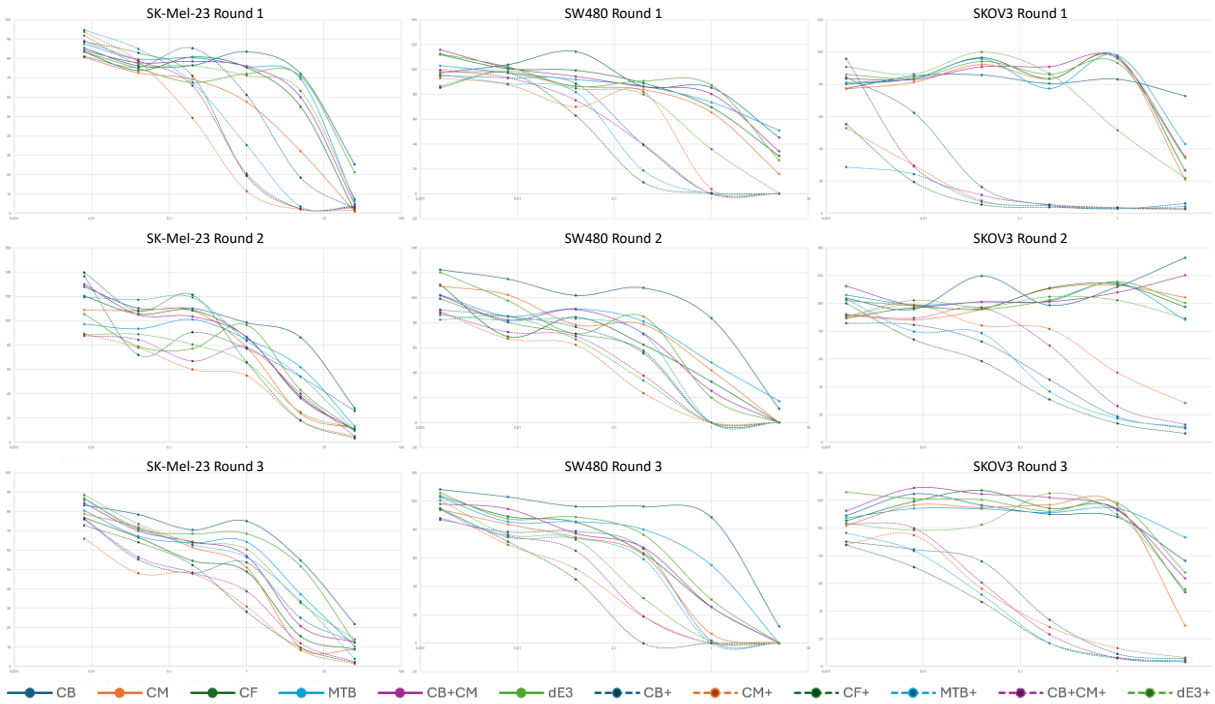

Figure S4 Viability curves of tumor cells in cocultures of TCE-armed oAd-infected tumor cells with and without PBMCs. Tumor cells were infected with serial dilutions of oAds. PBMCs were added 1 dpi and cell viability was measured via crystal violet staining 3 days after addition of PBMCs. PBMCs were added in an effector:target cell ratio of 3:1 for SKOV3 and SW480 and 6:1 for SK-Mel-23.CB - Ad5/3-CMV-BiTE-EGFR; CM - Ad5/3-CMV-scDb-cMET; CF - Ad5/3-CMV-scDb-cMET-scFv-EGFR; MTB - Ad5/3-CMV-scDb-cMET-T2A-BiTE-EGFR; CB+CM - Ad5/3-CMV-BiTE-EGFR + Ad5/3-CMV-scDb-cMET; dE3 - Ad5/3-ΔE3; "+" - with PBMCs.

Declaration of Authorship

I hereby declare that this thesis is my own work. I have only used the sources indicated and have not made unauthorized use of services of a third party. Where the work of others has been quoted or reproduced, the source is always given.

_____

Martin Alexander Boos

Heidelberg, 27.01.2025